Long Term Behavior of Arall Laminates

by

Ricardo Osiroff

Thesis submitted to the Faculty of the

Virginia Ploytechnic and State University

in partial fulfillment of the requirements for the degree of

Master of Science

in

Engineering Mechanics

APPROVED:

Wayne W. Stinchcomb, Chairman

Kenneth L. Reifsnider

Norman E. Dowling

June, 1988

Blacksburg, Virginia

LONG TERM BEHAVIOR OF ARALL LAMINATES

by

Ricardo Osiroff

Wayne W. Stinchcomb, Chairman

Engineering Mechanics

(ABSTRACT)

The behavior of ARALL (ARamid ALuminum Laminates) subjected to tension-tension cyclic loading was experimentally investigated as a first step towards the understanding of the fatigue damage mechanisms in Arall laminates, and the relationships between damage and stiffness change, remaining strength and life.

The quasi static and dynamic material response of unnotched Arall-2 coupons were measured. Damage evaluation techniques included stiffness monitoring, strain accumulation, C-scan, microscopy and residual strength measurement. The S/N curve was generated for maximum cyclic stresses ranging from 0.9 to 0.4 (R=0.1).

At high stress levels, the aluminum dominates the response while at low stress levels, the fiber plies are dominant. The damage sequence involves crack initiation in the aluminum plies, simultaneous crack growth and delamination, matrix cracking, fiber fracture and failure. Residual strength changes were measured for three stress levels and at three differents fractions of fatigue life, as determined from stiffness reduction. Viscoelastic effects were evaluated on the basis of the accumulated strains.

Three analytical models were considered. A shear lag model was used to predict the Characteristic Damage State, the regular pattern of cracks that develops in the aluminum plies. The Critical Element Model was proposed in order to perform residual strength and life predictions based on stiffnes and strength reduction curves for the different plies, critical and subcritical elements were identified. Viscoelastic lamination theory was used to evaluate time dependent effects and their relationship to fatigue phenomena.

ACKNOWLEDGEMENTS

The author gratefully aknowledges the direct and undirect support of this work, and wishes to express thanks to:

Committee chairman, Dr. Wayne Stinchcomb, for all the hours, the patience, the effort and the opportunity to engage in exciting research work.

Dr. Reifsnider and Dr. Dowling, for serving as committee members and for all the excellent advice throughout this investigation.

Alcoa Laboratories at Alcoa Center, Pennsylvania, for funding this work, and Rick Stiffler, for serving as monitor.

Dr. Wightman, at the Chemistry Department, for the surface analysis work and its interpretation.

, and , for their help with the analysis and computer codes they developed.

, and , for their assistance in the laboratory, and , for the SEM work.

, the author's parents, for their invaluable support and understanding.

Last, but not least, the author's wife, , for the thousand different ways she helps every day, and our two sons, and , for without them, there is no purpose.

TABLE OF CONTENTS

LIST OF ILLUSTRATIONS

LIST OF TABLES

CHAPTER 1

INTRODUCTION AND LITERATURE SURVEY

The bible warns us in chapter 22, verse 11 of the book of Deuteronomy "...thou shall not wear a mingled stuff, wool and linen together ...". Talmudic commentators have interpreted this admonition to mean that the mingling of different materials causes a degradation of properties and negates the order of the universe. Hence, it is in man's best interest to refrain from tampering with nature. This simple statement was expanded and led to a long list of dictates, banning mingling in all aspects of life.

In the thirty five hundred years since, man has mastered the art of mingling susbtances to obtain new and improved properties out of what nature has to offer. Indeed, modern life would be impossible without the advances man has made in the science of mingling.

One of the boldest steps in this direction was made at the Delft University of Technology [1]. The concept of adhesively bonded primary structures, first introduced by Fokker in 1948 was developed into a new family of structural composite materials, combining the strength and ductility of metals with the stiffness and excellent fatigue properties of fiber reinforced polymers [2].

From an endless number of possibilities regarding the choice of metal sheet, fibre, matrix, geometry and processing conditions; a commercial material system patented by the Delft University of Technology and manufactured by Alcoa emerged in 1981. Full scale components manufactured from ARALL or ARamid ALuminum Laminates have been in service since 1986.

Extensive investigations into the nature of this new breed of hybrid laminated composites have been performed by the developers, manufacturers, and the community of potential users all over the world. The growing interest in Arall laminates has yielded a rich body of information and fuels the ongoing research.

The present study aims to extend the knowledge of the fatigue response of Arall laminates and pursue its understanding. It represents a first step within the broader purpose of long term behavior characterization and modelling of Arall laminates.

1.1 ARALL LAMINATES

Arall laminates consist of alternating thin aluminum sheets bonded by aramid fiber reinforced adhesive film as shown in figure 1. Primarily developed for civil aircraft fatigue and fracture critical

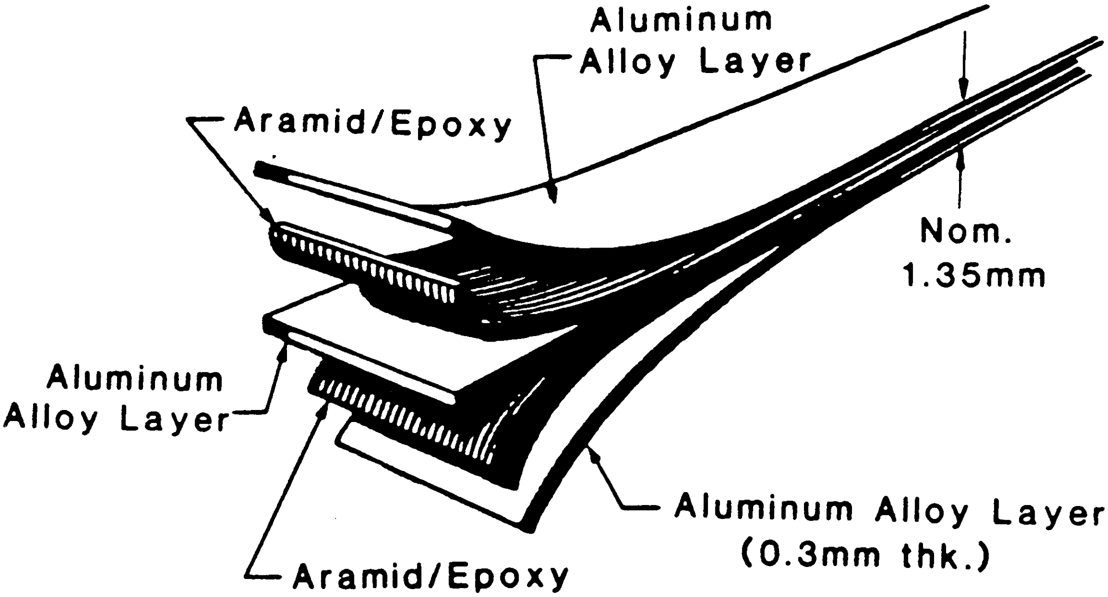

Figure 1. Illustration of the 3/2 Arall Laminate Layup [10]

structures, Arall laminates offer many advantages over monolithic aluminum and conventional fiber reinforced composites. The advantages include:

- lower density than conventional aluminum alloys
- retains the plasticity, formability, ease of manufacture and supportability of metals
- improved tensile fatigue response
- the outer metal layers provide resistance to impact damage, moisture barrier and lightning protection.
- better vibrational damping ability

All of these attributes contribute to a significant potential for structural weight reduction - the main driving force. Concerns are always present when a new structural material is introduced. Mohaghegh and coworkers at Boeing [3] compared Arall laminates to conventional monolithic aluminum and expressed their concern regarding the lower elastic moduli, lower strain to failure, notch sensitivity, transverse fatigue, bond durability and environmental effects on design properties.

Four Arall products are commercially available. Their description and characteristics are listed in Table 1. In 1985, Alcoa initiated a cooperative test program where numerous aerospace companies evaluated these products. Table 2 summarizes the quasi static mechanical properties of Arall 1 and Arall 2. It also includes a comparison with

Table 1. ARALL Laminate Commercial Product Forms [4]

GRADE	ALUMINUM[a]	PREPREG[b]	STRETCH[c]
ARALL -1	7075-T6	250°F cure	0.4%
ARALL -2	2024-T3	250°F cure	0.4% optional
ARALL -3	7475-T76	250°F cure	0.4%
ARALL -4	2024-T8	350°F cure	0.4% optional

(a) Bonding surfaces anodized and primed

(b) Approximately 50% by volume unidirectional aramid fibers

(c) Amount of prior prestraining

Table 2. Comparison of Mechanical Properties of Arall Grades, Aluminum and Carbon Fiber Composites [4]

		3/2 laminate 0.053 in thick		Alloy sheet 0.063 in thick		Carbon Fiber Composite[a]	
Property[b]	Test Dir.	Arall-1	Arall-2	7075-T6	2024-T3	Unidir.	Typical Struct.[c]
Tens. ult.	L	116	104	83	66	180	95
strength	LT	56	46	83	65	8	40
0.2% Ten.	L	93	52	74	52	NA	NA
Yld. Str.	LT	48	33	72	47	NA	NA
Ten. Elas.	L	9800	9300	10300	10500	21000	11000
Modulus	LT	7000	7100	10300	10500	1700	5000
Strain to	L	1.9	2.5	12	19	0.9	0.5
Failure %	LT	7.9	12.7	12	19	0.5	0.5
Poisson	L	0.33	0.32	0.33	0.33	0.31	0.48
Ratio,Ten.	LT	0.25	0.26	0.33	0.33	0.017	0.23
0.2% Comp.	L	54	38	73	44	180[d]	95[d]
Yld. Str.	LT	57	34	76	50	30[d]	42[d]
Comp. Ela.	L	10200	9700	10500	10700	21000	11000
Modulus	LT	7500	7600	10500	10700	1700	5000
0.2% Shear	L-LT	NA	17[e]	NA	NA	12[f]	37[f]
Yld. Str.	LT-L	NA	16.5[e]	NA	NA	NA	NA
Shear Mod.	L-LT	2400[e]	2500[e]	3900	4000	650	3100
	LT-L	NA	2300[e]	3900	4000	NA	NA
Density		2.29	2.29	2.78	2.78	1.55	1.55

(a) generic F180 graphite/epoxy, NASA
(b) Ksi, unless otherwise specified
(c) 42% 0-deg,50% +45 deg,8% 90 deg
(d) failure strength
(e) Iosipescu shear test
(f) in-plane shear ultimate

common aluminum sheet alloys and two carbon fiber layouts. Bucci and Mueller [4] discuss these and other properties, such as fracture toughness, static notch strength, environmental durability and more.

A significant analytical effort complements the quasi static mechanical characterization. Teply [5] presented analytical models at the micromechanical, laminate, and structural levels. A viscoelastic version of the periodic hexagonal array models the aramid/epoxy layers and an elastic-plastic lamination code was developed to predict lamina engineering properties, process dependence, and residual stresses. A modified WEK (Waddoup, Eisenman, Kaminski) model was applied to study notch sensitivity and residual strength. Finally, two finite element approaches were employed to model delaminations and their results were compared to experimental data [6].

Residual stresses have a pronounced effect on the performance of Arall laminates and command special attention. Due to curing, thermal residual stresses develop. The aluminum layers are in tension while the fiber layers are in compression, a disadvantageous situation since the fiber layers have poor compression properties. In order to overcome this shortcoming, Arall laminates may be stretched causing a reversal of the residual stress situation, figure 2. The effect is dramatic and of special significance in the fatigue behavior.

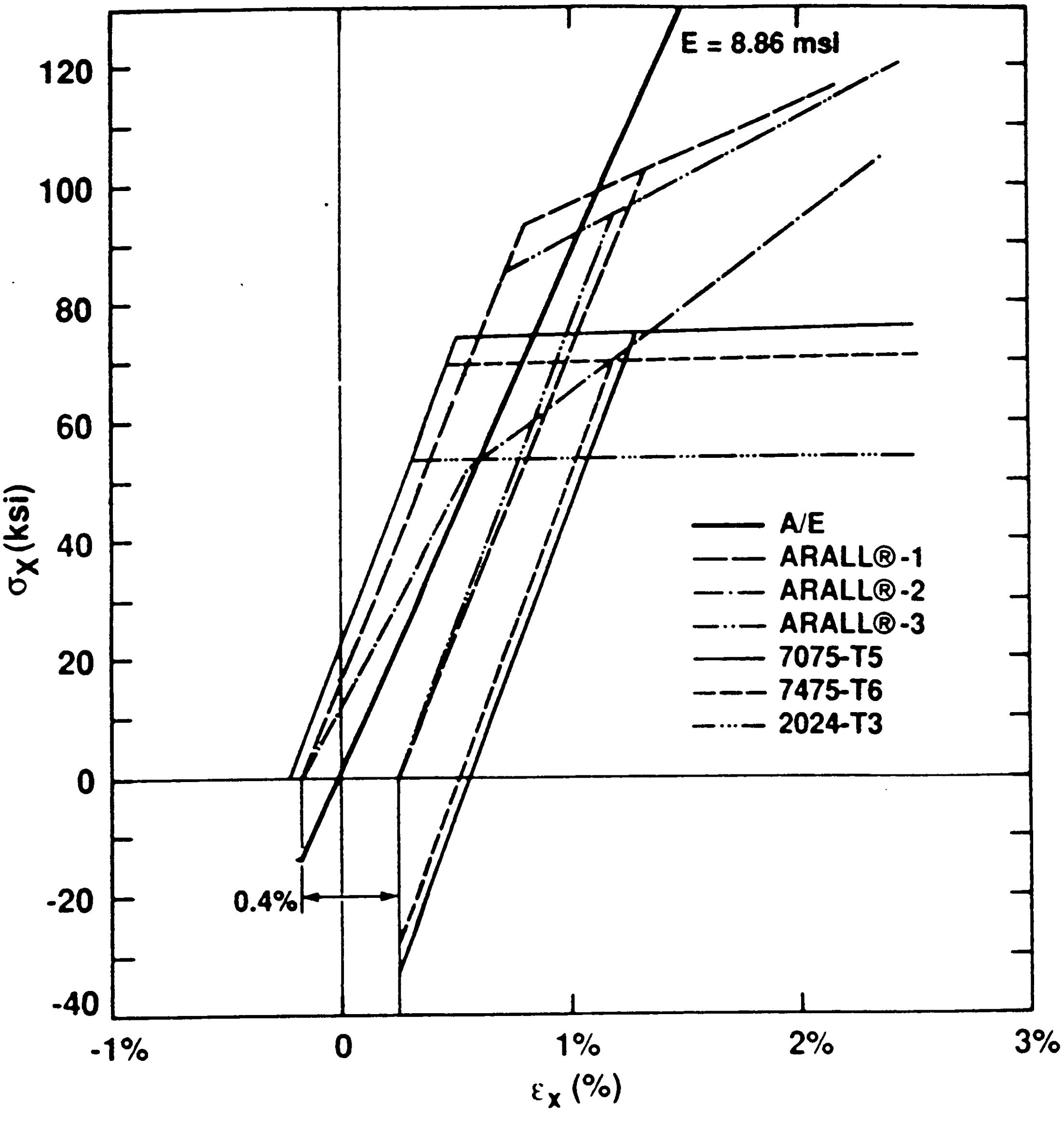

Figure 2. Residual Stresses after Stretching of Arall laminates [5]

1.2 FATIGUE RESPONSE

Arall laminates were developed primarily as a structural alternative to aluminum offering improved fatigue resistance. Extensive tensile fatigue testing has been done under constant load amplitude and simulated flight conditions. Available data include smooth and notched coupons, cracked specimens, fastened and bonded joints and combinations of environmental conditions. The beneficial contribution of the fiber layers is apparent in figure 3, where Arall-1 smooth specimen tensile fatigue behavior, measured in the cooperative test program, is compared to 7075-T6 aluminum sheet of comparable thickness.

The largest body of research in the area of fatigue behavior corresponds to notch sensitivity and crack growth in the outer aluminum layers for several notched configurations. Phillips [7] shows that the inner aluminum layer cracks grow slightly behind the outer layers, figure 4.

Figure 5 illustrates the advantages of Arall 1 over 7075-T6 aluminum and emphasizes the importance of the reversal of residual stresses by means of stretching. The improvement over monolithic aluminum is attributed to the mechanism of crack bridging, i.e. to the closing forces exerted by the fibers on the crack surfaces. Teply [5] and Marissen [8] have studied this mechanism extensively and conclude that the crack bridging effect due to uncracked aramid fibers in the

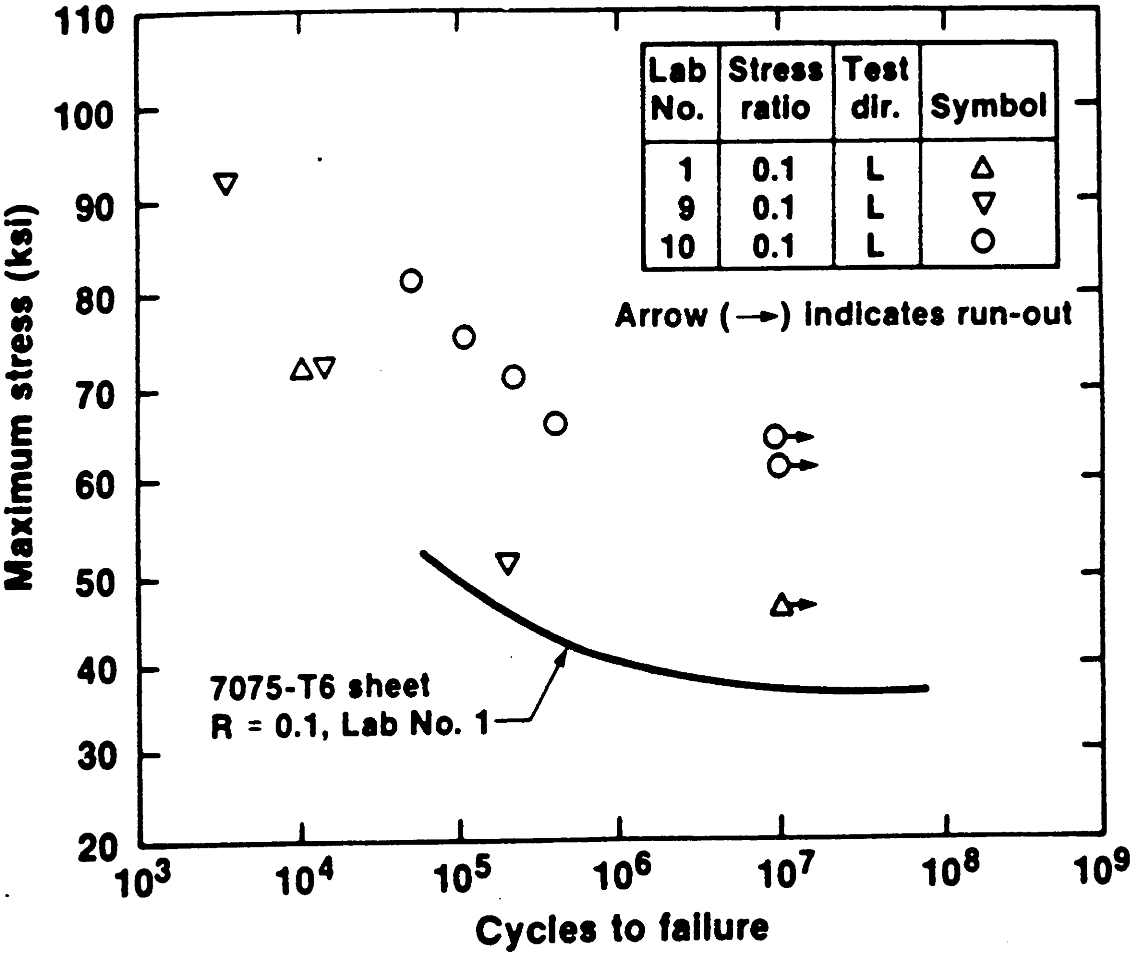

Figure 3. Smooth specimen Fatigue Behavior of Arall-1 Laminate vs. 7075-T6 Aluminum [61]

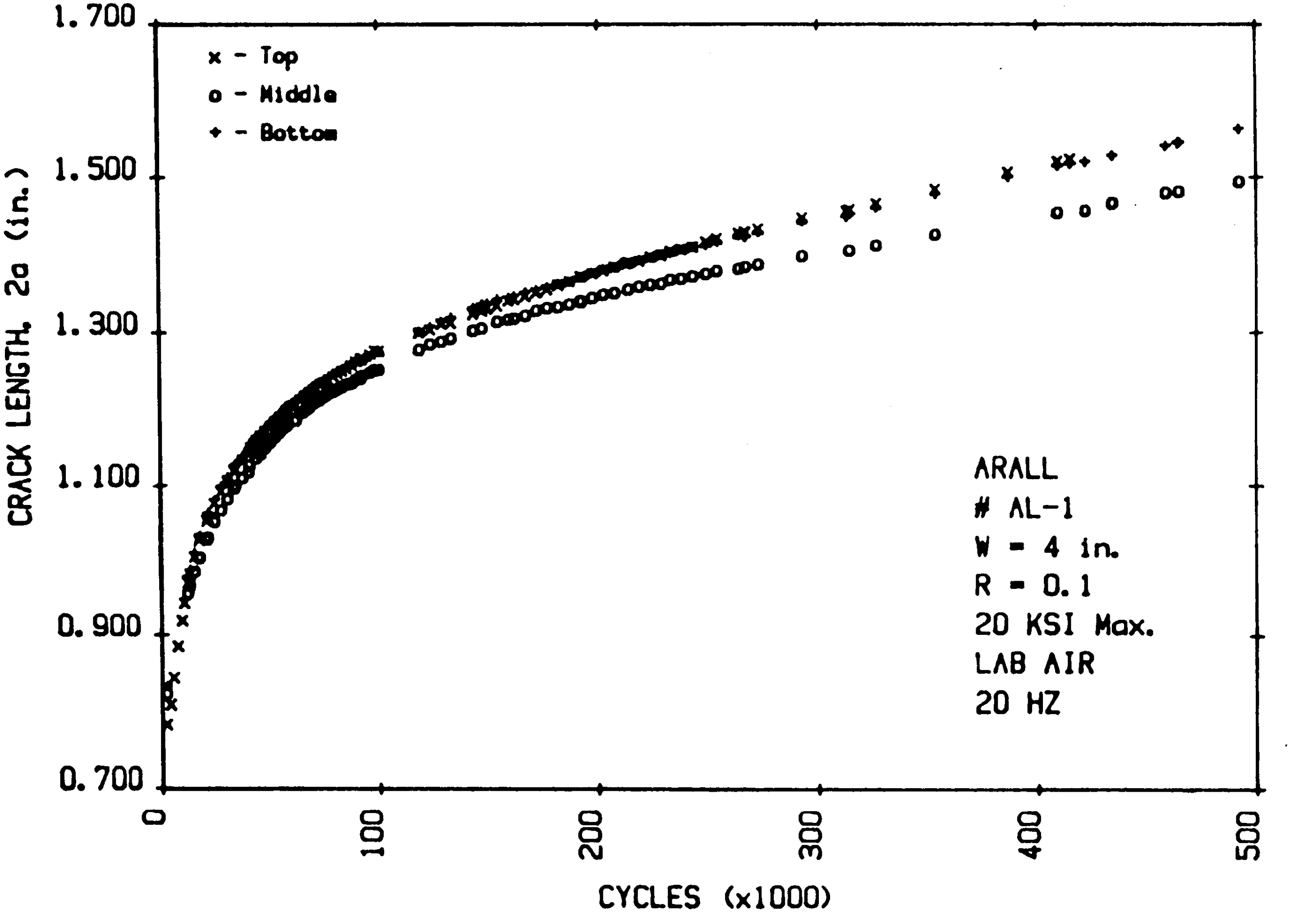

Figure 4. Fatigue Crack Growth in Aluminum Plies of Arall Laminate [7]

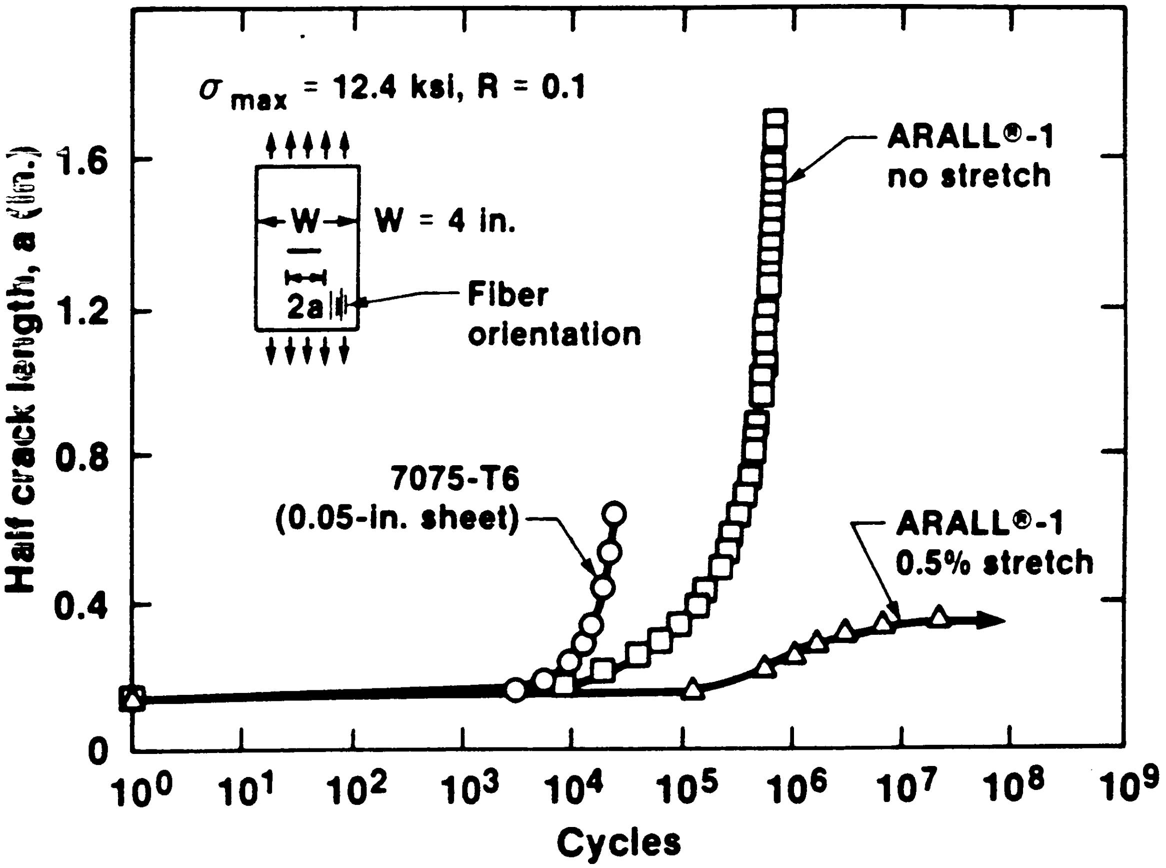

Figure 5. Fatigue Crack Growth of Stretched and Unstretched Arall-1 and 7075-T6 Aluminum [4]

wake of the crack can be intensified by favorable residual stresses.

Marissen presented a detailed model based on the hypothesis that crack growth is controlled by the stress intensity factors in the aluminum. These were calculated assuming that the crack-closing forces of the fibers may be considered external forces acting on the crack flanks. Delamination of the aluminum/epoxy adhesive interface during fatigue occurs simultaneously and its rate is dependent on the load carried by the fiber plies, which in turn is related to the crack length. Adhesive shear deformation and residual stresses were also considered. The damage mechanisms are illustrated in figure 6.

Marissen also developed a computer code that predicts the dynamic balance between crack growth and delamination rate based on analytical expressions for the stress intensity factor at the crack tip of the aluminum and energy release rate for delamination. Qualitative agreement with data is obtained although the accuracy is very conservative. Petit [9] reports crack growth rates of nearly an order of magnitude lower than those predicted using the Marissen's approach.

Ritchie et al. [10] also investigated the effect of crack tip shielding from crack bridging on fatigue crack propagation using some novel experimental techniques. The occurrence of crack bridging by the unbroken fibers in the wake of the crack was found to be the major contributor to the excellent crack growth resistance. Crack bridging by unbroken fibers is promoted by controlled delaminations, the progressive cohesive failure of the epoxy interface.

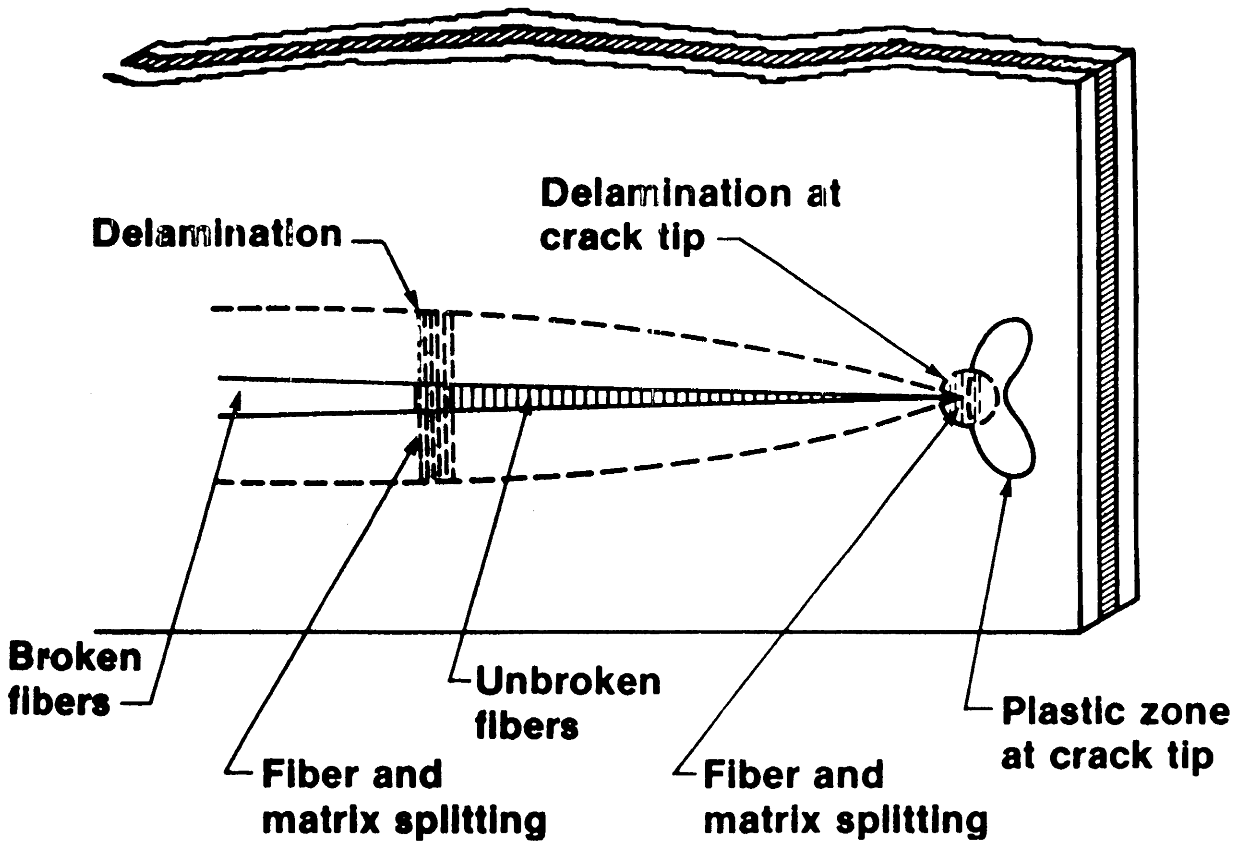

Figure 6. Fatigue Crack Damage Mechanisms [5]

Due to the unusual length of the bridging zone (between 3 to 5 mm), fatigue crack growth rates were found to be crack-size and history dependent and showed no unique correlation with the applied stress-intensity range.

In spite of the seemingly abundant experimental information and the sophisticated analytical efforts, the result of an extensive cooperative test program, there are wide gaps in the understanding of the long term behavior of Arall laminates. Most experimental investigations were and are oriented towards specific applications, making difficult the task of correlating among widely differing configurations, geometries, loading conditions and environments. The lack of internationally accepted standardized testing in many areas adds to the pitfalls of data interpretation. The most common approach has been to treat the fatigue response as a fracture mechanics problem with almost exclusive focus on the crack growth in the aluminum layers originating from different notched configurations.

Only partial and widely scattered information is available on unnotched geometry and the Arall grades other than Arall 1. No information at all is available on the fatigue process occuring in the fiber layers. So far, the question of performance (e.g. stiffness change and residual strength) of the laminates under cyclic loading has hardly been addressed [11. On the analytical frontier, a cumulative damage model is still missing.

Fatigue response investigation has always been characterized by experimental difficulties because of the extreme sensitivity to testing conditions and naturally occuring data scatter. Extensive testing of Arall laminates is still required to cope with these problems and achieve reasonable confidence. More over, Arall laminates should be regarded as composite laminates. The basic mechanisms of fatigue in composite materials and their analytical treatment differ from those of homogeneous materials. The viscoelastic nature of the epoxy matrix and the aramid fibers add another dimension to the problem.

Consequently, the study of initiation and propagation of a crack in the metal layers provides only partial answers to the questions of long term behavior.

Having reviewed and commented on the available information on Arall laminates, and having stated that Arall laminates should be treated as full fledge composite materials; the following section addresses the more general aspects of fatigue damage mechanisms in composites.

1.3 FATIGUE-INDUCED DAMAGE IN COMPOSITES

Fatigue damage in composites consists of combinations of matrix, fiber, interfacial cracks and debonds that form a very complex damage state [12]. The material system, stacking sequence, geometry, stress state and environment are interacting fatigue mechanisms that affect the engineering properties in many intricate ways. While present technology can be used to detect almost every type of damage, no general approach to representation is available. Damage interpretation and response prediction remain a frontier.

Different loading conditions have distinctive fatigue processes that cause changes in the local geometry and changes of local stress. A review of the mechanics of fatigue development in composite materials can be found in [13]. Investigators such as Schapery [14] and Christensen [15] address the nature of damage in a viscoelastic isotropic media and composites.

By far, the case of axial tension-tension fatigue has drawn the attention of the largest number of investigators. Because of its applicability to the present study, the fatigue response of unnotched laminates containing 0-degree and off-axis plies is discussed briefly. In this discussion, failure is defined as complete fracture.

In such a case, the first observed damage mode is matrix cracking in off-axis plies. The initiation of such cracks can be predicted from lamination plate theory and the Tsai-Hill failure theory [16]. The cracks extend through the thickness of the ply and grow in the fiber direction across the witdh of the specimen. This first change in local geometry leads to the first change in the local state of stress. A region carrying less load exists around the stress-free crack surfaces. Hence, in the vicinity of the crack, the uncracked plies carry an increased load creating a local change of stress. Through shear forces, load is reintroduced to the cracked plies.

During cyclic loading, a characteristic array of cracks in the off-axis plies develops achieving a uniform spacing. This pattern, named the Characteristic Damage State [17,18], is dependent on material properties, geometry,and stacking sequence. The ability of the constraining plies to transfer the load back to the cracked plies determines the distance over which the stress in those plies resumes its original value. The importance of matrix cracks, especially their influence on long term behavior, is in the internal stress redistribution they cause. A more detailed discussion of the shear lag analysis is presented in chapter 5.

Cracks in adjacent off-axis plies may couple through small scale interfacial debonding. In the case where the crack forms next to a 0-degree ply the situation is different. The crack tip acts as a stress raiser and facilitates fiber fracture in the 0-degree ply. Jamison [19] reported that in fact, fiber fractures concentrate next to matrix cracks, in and through the thickness of the ply plane.

The stress field around fiber fractures is similar to that around matrix cracks. The axial stress in the adjacent fibers is increased locally; and, through shear forces, the load is reintroduced to the broken fibers. Cracks in the 0-degree direction form next. Tensile stresses in the direction of the off-axis crack line are exerted by the constraining fibers of the off-axis ply on the 0-degree ply, creating the cracks. These cracks are initially located at the ply interface and eventually propagate through the thickness of the 0-degree plies resulting in longitudinal splitting.

A pattern of cross cracks is formed and they influence the strain energy release rate. Delaminations form at the crack intersections. Highsmith and Reifsnider examined the stress field around the intersection of two cracks in adjacent plies [21]. They concluded that significantly increased interlaminar normal and shear stresses develop at the intersection point. Talug [22] computed the three dimensional stress field near a crack tip using finite difference analysis. At the adjacent ply near the crack tip, all normal stresses are tensile. This region of highly localized and increased stress could provide the initiation point for fracture.

Depending on the laminate stacking sequence, delaminations may grow across the width and along the specimen or be restricted to small areas. Delamination growth is planar and self similar, O'Brien [23] relates its growth rate to the total (modes I,II and III) strain energy release rate by a power law.

High stress concentrations, usually of singular nature, with complex states of stress occur at the edges of a laminate, Pipes and Pagano [24], Wang [25]. Stacking sequence and loading conditions determine the magnitude and sign of the normal stresses. While transverse (intralaminar) stresses lead to crack initiation, interlaminar stresses lead to edge delaminations. This situation is especially severe in composite laminates subjected to cyclic fatigue loading, Reifsnider [26], Stinchcomb and Reifsnider [13], O'Brien [23]. Most recently, Shalev [27] presented a solution to the exact order of singularity based on Lekhnitskii's [28] complex variable stress potentials. An eigenfunction expansion method is used to determine the general solution and in turn, the eigenvalues are used to find the stress distribution.

Delaminations, irrespective of their origin, cause a reduction in axial stiffness and couple with other damage modes to reduce strength [30]. If the reduction is significant, the strength may reach the value of the applied load.

Highsmith et al. [32] observed that fiber-matrix interface degradation occurs in the 0-degree plies and plays an unknown role. Matrix tensile fracture, shear failure and sub-microcracking have been observed around broken fibers by Sundaresan and Henneke [73]. It has also been observed that the 0-degree fibers fractured surfaces are in a plane perpendicular to the tensile axial load. The fractured surfaces of off-axis fibers are at an angle with respect to the tensile axial load, indicating a mixed failure mode.

The critical event that governs final failure has not been identified yet. Accumulation of fiber fractures often dominate failure of composite laminates. Limited knowledge is available on the details of these microscopic events and how this mode of damage influences and is influenced by matrix related damage modes.

Jamison [65] has recently surveyed the significant accomplishments in the areas of modelling and characterization of fiber fracture. Jamison reports that efforts to develop an understanding of stress redistribution in the vicinity of broken fibers concentrate on the solution of the elasticity problem. The complexity of the problem has led the investigators to consider different degrees of material, geometry and damage inhomogeneity.

Rosen and Zweben [71] formulated the chain of bundles model and included fiber strength variability. Goree and Gross [65,66] simplified the problem by including only certain components of stress and, were thus able to include matrix yielding and splitting in their analysis. Phoenix and Harlow [68-70] formulated an exact solution for an idealized two-dimensional case. Batdorf [31,72] treated the stability of a Griffith-type flaw consisting of multiple adjacent fiber failures. Composite failure is then predicted upon the first occurrence of a critical "multiplet" at the applied stress.

Although the models differ in their rigor, a number of assumptions are shared by most investigators:

- Fiber fractures are random events with a probability described by a strength distribution function.
- Subsequent fiber fractures are influenced by existing breaks due to load redistribution.
- A critical number or arrangement of broken fibers is seen as the

triggering mechanism for cascading fiber fracture and composite failure.

- Given the microstructural scale involved, linear elastic fracture methodologies are inadequate.

With the exception of edge delaminations, the damage process just described, involves sequential changes in local geometry causing a local stress redistribution affecting negatively the damaged region. Additional changes contribute to further localization of damage until finally, fracture occurs.

1.4 EXPERIMENTAL OBSERVABLES AND ANALYTICAL METHODS

Ideally, the three dimensional state of strain in the material should be known through direct measurement or analysis. Together with knowledge of the stiffness and suitable analytical tools, the state of stress could be determined, thus allowing predictions of residual strength and life.

Available techniques of nondestructive testing interrogate the material and assess the damage state by measuring variations in material uniformity and/or material properties due to imperfections. A variety of non destructive methods have been developed or modified specifically for implementetion in composite materials because of the need to distinguish damage modes and in order to complement one another. A review of special interest techniques and the associated physical phenomena is found in [33]. These include surface replication, X-ray radiography, vibrothermography, ultrasonic A-scans and C-scans, acoustic emission, etc. The techniques used in this study are briefly introduced in chapter 2.

Special attention is given to the measurement of stiffnes since its reduction has been found to correlate well with damage and depends only on the material's condition.

O'Brien [34], presented applications of stiffness measurements for indirect assessment of damage growth for different configurations and loading conditions. Reifsnider and Stinchcomb [29] reviewed, described and investigated the concept of stiffness change as a nondestructive fatigue damage parameter. In general, they found that stiffness change can be quantitatively related to the fatigue life and residual strength of composite laminates through various models of observed micro-damage events and the damage patterns formed by those events.

All the damage events described in the previous section change the load carrying capability of neighboring regions, increasing the global engineering compliance of the laminate. The nature of each event and their collective response determines the extent of the changes in strength, stiffnes and life.

The first event is usually matrix cracking in the off-axis plies and the creation of a stable, saturated crack pattern. Highsmith and

Reifsnider used the shear lag analysis [30] to model the local stress field around an array of regularly spaced cracks. The stress and strain state was evaluated and, in turn, was used to predict global stiffness changes as a function of crack density during cyclic loading.

The next phase of damage includes matrix-fiber debonding and delaminations. The stiffness change due to edge delaminations was discussed by O'Brien [23], who related the fraction of delaminated width, a/b, with the current stiffness E in terms of the initial stiffness E_o and fully delaminated stiffness, E_d.

$$E = E_o + \frac{a}{b} (E_d - E_o) \qquad (1)$$

Internal delaminations occur in all regions of the laminate. Highsmith et al. [32] reported and predicted stiffness reductions of up to 25 percent due to such delaminations. Since internal delaminations cannot be easily avoided by design, the impact on performance is of great importance.

Fiber fracture frequently causes a large local stress concentration. It has been suggested [35] that near the threshold of fracture, a sufficient number of fibers break with sufficient frequency to cause a global change of stiffness.

During cyclic loading some or all of the above damage modes occur, resulting in a corresponding degradation of stiffness. Every mode is associated with a specific and distinct stage in a typical damage vs life fraction curve, such as shown in figure 7.

As damage develops strength is changed. Hahn and Kim [36] suggested that for a constant amplitude fatigue test, the strain to failure is the same as in a quasi static test. The elastic modulus decreases until, at failure, it is equal to the applied stress divided by the failure strain. This reduction may be achieved in the last few cycles and should be carefully measured. Fracture occurs when strength is reduced to the applied stress level.

Many ongoing investigations have the purpose of understanding the exact relationship between damage state, stiffness, residual strength and fatigue life, and the development of appropriate models. Rotem [37] described a lamina based analysis. The fracture mechanics approach was chosen by Wilkins et. al [38], Chou [39], and Wang and Slomiana [40]. Hashin and Rotem [41] and Poursartip [42] proposed phenomenological theories. Chariewicz and Daniel [43] presented a cumulative damage model based on residual strength and the concept of equal damage curves.

Reifsnider and co-workwers [44] take a hybrid approach; a stiffness based cumulative damage model is used to predict residual strength and life. Subcritical and critical elements within the laminate are identified. The former are involved in fatigue damage development, while the latter are responsible for the eventual failure. Stiffness changes and models of the damage events are used to

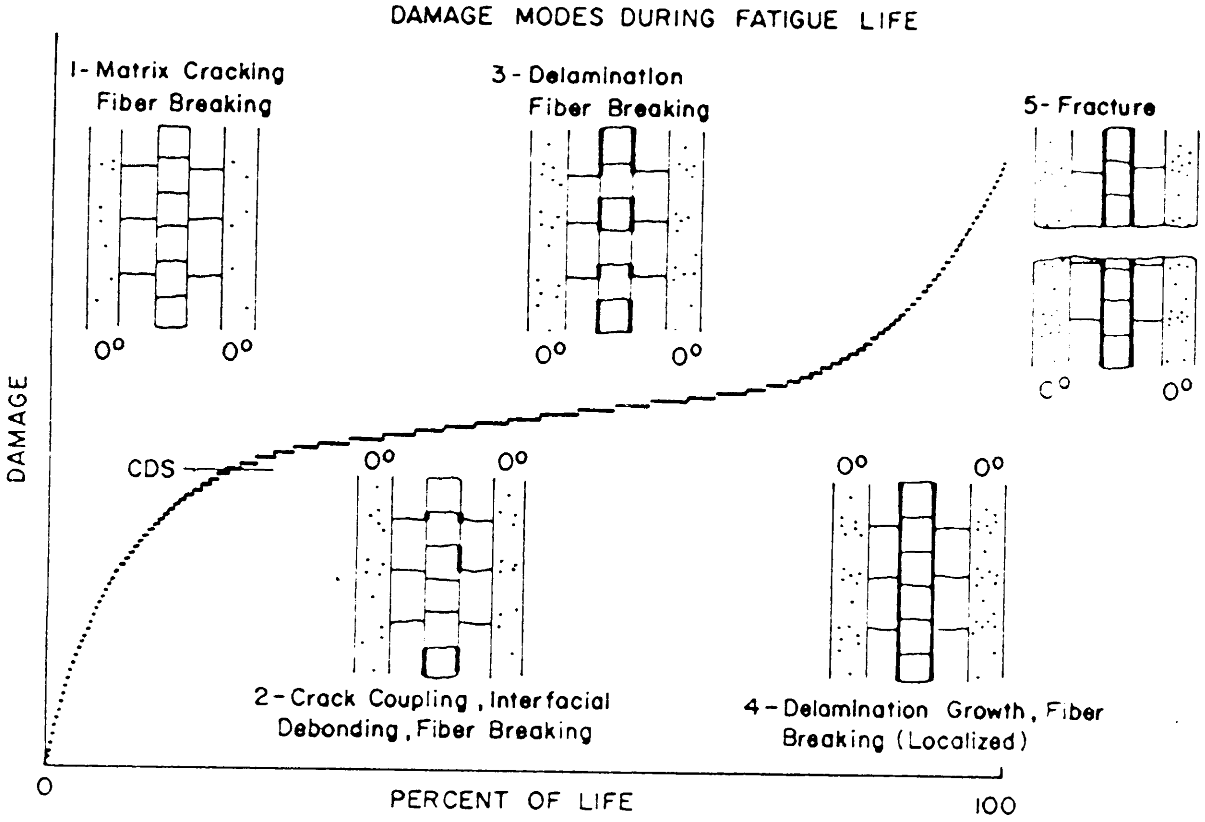

Figure 7. Damage Modes During Fatigue Loading of Composite Laminates [44]

estimate stress redistribution. Residual strength is evaluated with the aid of a failure theory. Details of this model and the applicability to Arall laminates are presented in chapter 5.

The characterization and analytical modeling of viscoelastic composite materials are at the heart of an extensive research program at VPI&SU. Brinson [45], Griffith [46], Dillard [47], Hiel [48] and Tuttle [49] have succesively contributed to the understanding of the time dependent effects taking place in fiber reinforced laminates. Most recently, Gramoll [50] has summarized the basic formulation and assumptions of a viscoelastic lamination theory where all four elastic coefficients of the orthotropic ply compliance matrix are assumed to be time dependent. Gramoll's predictions for the time dependent compliance of aramid/epoxy composites under constant load, are used in this study to estimate the amount of creep deformation in Arall laminates.

1.5 OBJECTIVES

The primary objective of this investigation was to develop an understanding of the long-term behavior of Arall laminates subjected to cyclic mechanical loads. Unnotched specimens of Arall-2 laminates (unstretched grade) were tested under quasi-static and cyclic tensile loading. Destructive and non destructive techniques were used to evaluate the state of the material. The effects of mechanical loading on stiffness, strength and life were recorded and documented. Time dependent deformation was measured. Critical and subcritical elements were identified.

Preliminary considerations for modeling are presented. A shear lag analysis is proposed to predict the characteristic damage state in the outer aluminum layers. Stiffness and strength reduction data are the input of the critical element model that predicts remaining strength and fatigue life. The case of tension-tension cyclic loading is discussed. A model for the viscoelastic characterization of composite laminates is presented. The probable interaction of fatigue and time dependent processes is discussed.

This study represents the first step in the long-term characterization of Arall laminates based on mechanistic cumulative damage concepts and philosophies developed at VPI&SU. The experimental and analytical effort is directed towards the implementation of a Critical Element Model for the prediction of residual stength and life under arbitrary loading conditions and environments.

A complete understanding of damage mechanisms and their effects on response of Arall laminates is essential to the development and use of accurate models to predict performance. Such models can then be used to engineer the optimum materials to meet the performance requirements of specific structural applications.

CHAPTER 2

MATERIALS AND METHODS

2.1 ARALL 2 LAMINATES

The specimens tested in this study were cut from one large panel of unstretched Arall 2 laminate material, panel #604995. Arall 2 laminates consist of alternating layers of 2024-T3 aluminum sheet and uniaxial aramid epoxy prepreg. The aluminum sheet is 0.012 inches (0.3 mm) thick and the prepreg is approximately 0.008 inches (0.2 mm) thick. Consolidation is obtained by processing at 250°F and applying 100 psi pressure in an autoclave. Laminating sequences typically range from 2 to 5 layers of aluminum, in this study a 3/2 configuration is investigated. The two layers of aramid reinforced epoxy (denoted K/E) - prepreg SP366 - are manufactured by 3M specially and solely for this purpose. A conceptual view of Arall 2 was shown in figure 1.

Typical mechanical properties of Arall 2 laminates are listed in Table 2. Although fatigue data for Arall 1 laminates is profuse, it is not available for Arall 2 except in the form of crack growth for different notched geometries. Processing parameters do influence material properties but such a task is outside the scope of the persent investigation.

The different components of Arall laminates may dominate the behavior of the hybrid material depending on loading conditions and other circumstances. A short review of quasi static and dynamic properties of these components follows.

2.1.1 2024-T3 ALUMINUM

Data on Aluminum grade 2024-T3 is extensive and readily available, reference [51] offers detailed information. The effects of temperature, rolling direction, thickness, etc. on mechanical properties are discussed in depth.

Of particular interest to this investigation is the fatigue response at room temperature. Figure 8 shows fatigue data at different stress ratios for unnotched 2024-T3. Best fit S/N curves are approximated by the equivalent equation,

$$\text{Log } N_f = 11.1 - 3.97 * \log(S_{eq} - 15.8) \qquad (2)$$

where the equivalent stress is defined as,

$$S_{eq} = S_{max}(1-R)^{.56} \qquad (3)$$

and R is the stress ratio, S_{max} is the maximum applied stress.

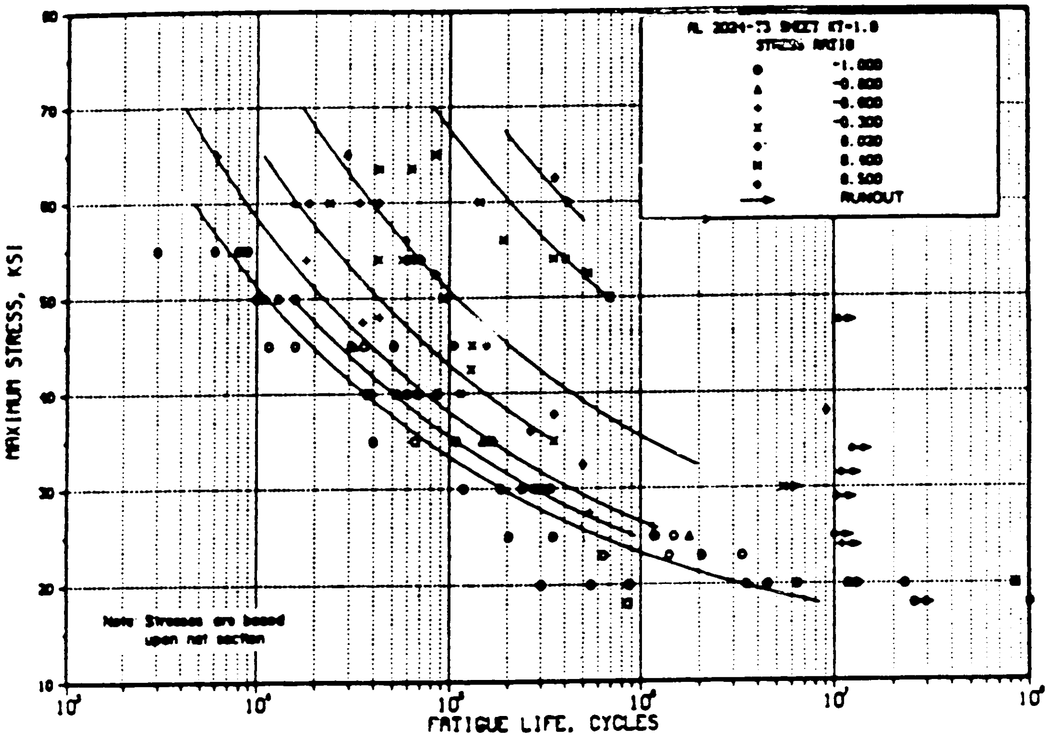

Figure 8. Best-fit S/N Curves for Unnotched 2024-T3 Aluminum Sheet, Longitudinal Direction [51]

2.1.2 ARAMID/EPOXY

Kevlar 49 aramid fibers and AF-163-2 epoxy adhesive (3M) are used by 3M to manufacture prepreg SP-366 used in Arall 2 laminates.

The mechanical response of Kevlar fibers (Dupont) and Kevlar reinforced epoxy composites has been extensively studied [58] although fatigue data are rare. Table 3 presents the room temperature static data for Kevlar 49 fibers and figure 9 shows the tensile fatigue behavior of a typical K/E unidirectional laminate vs. 2024-T3 aluminum.

In addition to the ample information supplied by the manufacturer, the report by Ho, Schapery and Harbert [52] is of particular importance, stressing the environmental and time dependent effects at the fiber and laminate levels. Figure 10 presents the stress-strain response of a single fiber tested at 75°F and 50% RH. The bilinear curve exhibits a distinct increase in slope (stiffening) at large strains attributed to fiber straightening.

A modified epoxy matrix (250°F cure) is used in the prepregging process of SP 366. Two layers of unsupported structural adhesive film AF-163-2 (3M) are pressed on both sides of a fiber layer to produce a unique unidirectional prepreg with improved adhesive performence. A summary of the epoxy matrix properties is presented in Table 4. Large deformations and nonlinearity were measured by Cooper [53] for this adhesive, as shown in figure 11.

Table 3. Room Temperature Static Data for Kevlar 49 Fibers [58]

Property	U.S. Customary	S.I.
Axial Modulus	18×10^6 lb/in^2	124 GPa
Transverse Modulus[a]	1×10^6 lb/in^2	6.9 GPa
Axial Shear Modulus[a]	0.4×10^6 lb/in^2	2.8 GPa
Axial Poisson Ratio[a]	0.36	0.36
Transverse Shear Modulus[a]	0.4×10^6 lb/in^2	2.8 GPa
Axial Tensile Strength[b]	525×10^3 lb/in^2	3.62 GPa
Strain to Fracture[b]	2.9%	2.9%
Axial Thermal Expansion[a] Coefficient	-2.9×10^{-6} in/in°F	-5.2×10^{-6} m/m°C
Transverse Thermal[a] Expansion Coefficient	23×10^{-6} in/in°F	41.4×10^{-6} m/m°C
Density	0.052 lb/in^3	1.44 g/cm^3

(a) Determined from unidirectional composite data

(b) Resin impregnated Strand Test (ASTM D-2343)

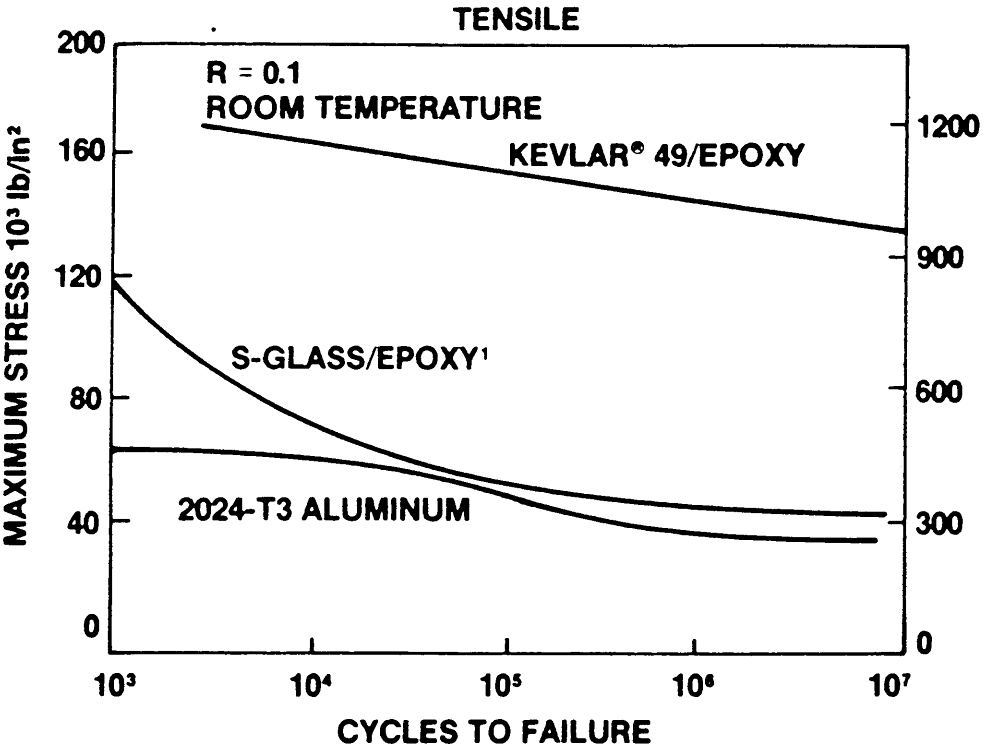

Figure 9. Fatigue Behavior of Unidirectional Kevlar/Epoxy and Aluminum [58]

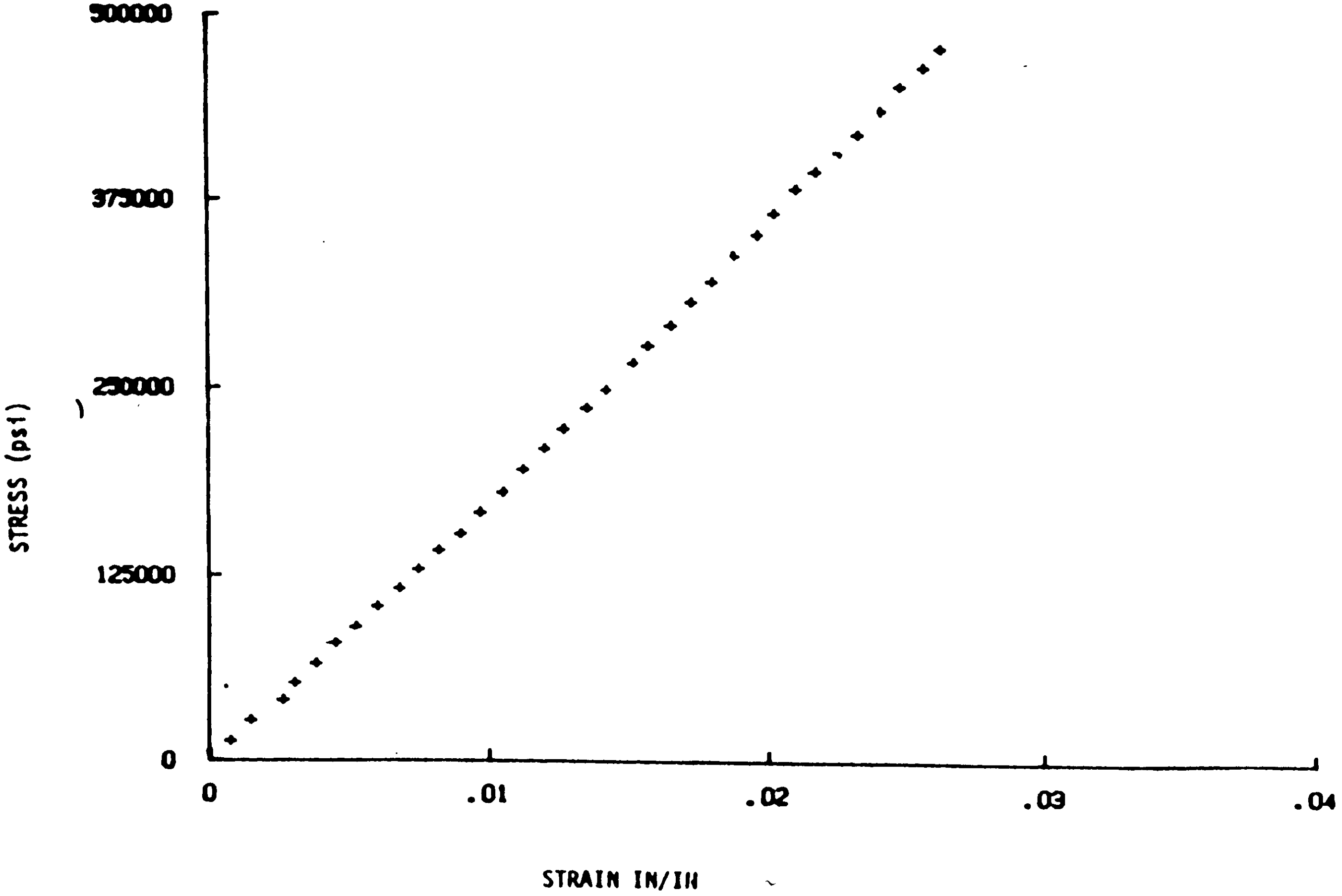

Figure 10. Stress vs. Strain for a Single Kevlar Fiber at 75°F and 50% RH Environment [52]

Table 4. Room Temperature Thermo-Mechanical Properties of Structural Adhesive Film AF-163-2 [62]

Property	Conditions	U.S. Customary (SI)
Glass Transition Temperature	Dry	108°C (226°F)
	Wet	82°C (180°F)
Tensile Strength	75°F	7000 psi (48.7 MPa)
	180°F	3000 psi (20.9 MPa)
Tensile Modulus	75°F	1.6×10^5 psi (1.1 GPa)
	180°F	6×10^4 psi (0.42 GPa)
Poisson Ratio	75°F	0.34
Shear Modulus[a]	75°F	6.4×10^4 psi (0.44 GPa)
	180°F	2.6×10^4 psi (0.18 GPa)
Shear Strength[a]	75°F	6950 psi (48.3 MPa)
	180°F	5780 psi (40.2 MPa)
Fracture Toughness[b] G_{Ic}	75°F	21-25 in-lb/in ^{2}

(a) Thick adherent, 2024-T3 aluminum, 0.25 in thick, FPL etched

(b) 2024-T3 aluminum, 0.5 in thick, phosphoric acid anodize

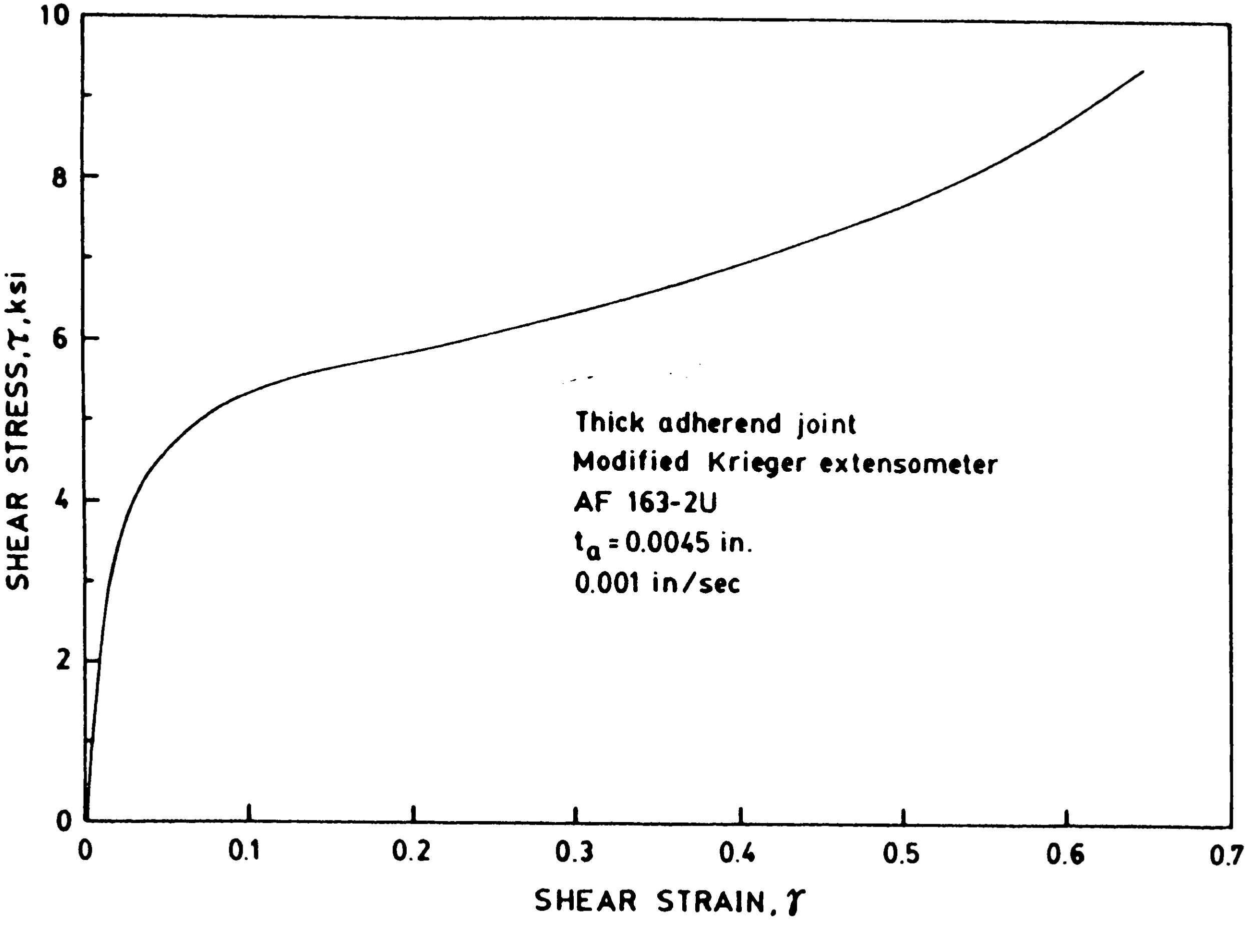

Figure 11. Shear Stress vs. Strain for AF-163-U [53]

A very complete thermomechanical characterization of the unidirectional composite prepared from this prepreg was performed by Pindera et al. [54]. A summary of the thermomechanical properties of the cured unidirectional K/E prepreg is presented in Table 5. The nonlinear behavior of the aramid fibers is apparently responsible for the stiffening behavior of the monotonic tensile loading of the unidirectional laminate at 0°, figure 12. The laminate also stiffens due to cyclic loading, as shown in figure 13.

2.2 MECHANICAL TESTING

2.2.1 APPARATUS AND PROCEDURE

All specimens were cut from panel #604995 using mechanical shears. Previously, the panel was C-scanned (subpanel PA2-4995-6 is shown in figure 15) to assure good and consistent quality. Areas showing porosity, delaminations or prepreg seams were discarded. It should be noted that 20% to 30% of the panel was discarded in this manner even though the panel was accepted by the manufacturer in its entirety. Preliminary tests of the discarded material show a decrease in ultimate tensile strength and elastic modulus of approximately 3%. The presence of defects may be much more damaging during fatigue and off-axis tests.

Because of equipment availability considerations, two specimen dimensions were used: 10"*1.5" and 8"*1.5", where the longest dimension is in the fiber direction. Monotonic and fatigue test results of both geometries do not indicate measurable differences.

Monotonic and fatigue tests were performed on a 20 kip MTS servo-hydraulic, closed loop testing machine, equipped with hydraulic, wedge action grips. Strains were measured with a one inch gage length MTS extensometer. As shown in figure 14, the extensometer's knife edges are mounted on v-notched aluminum tabs bonded to the specimen with a compliant silicone adhesive. The extensometer is held in place by four rubber bands.

The use of strain gages was discontinued after several adhesive failures occured due to the large strains. The development of cracks across the face of the specimen during fatigue testing makes the use of strain gages impractical and erroneus. The one inch gage also offers a much better description of the average global strains compared to the local nature of the strain gage measurement.

A very low gripping pressure was used for all tests. Fatigue specimens were gripped with 800 psi pressure with good results; i.e. no significant damage or failures were induced by the grips. Monotonic specimens were gripped at 300 psi and a layer of sandpaper was placed between the grip surface and the specimen to avoid grip-induced damage and premature failure.

Table 5. Mechanical and Thermal Characteristics of Unidirectional Aramid/Epoxy, SP366 (3M), 55% Fiber Volume Fraction [54]

	Tension Properties	Compression Properties
Longitudinal		
Elastic Modulus, E_{11}	8.86[a](10.4) Msi	8.94 Msi
Poisson Ratio, ν_{12}	0.435	0.233
Failure Stress, σ_{11}^{ult}	165.5 Ksi	28.6 Ksi
Failure Strain, ε_{11}^{ult}	1.79 %	0.58 %
Transverse		
Elastic Modulus, E_{22}	0.6 Msi	0.75 Msi
Failure Stress, σ_{22}^{ult}	3.96 Ksi	13.5 Ksi
Failure Strain, ε_{22}^{ult}	0.85 %	2.83 %

Shear Properties

In-plane		Out-of-plane	
Shear Modulus, G_{12}	0.224 Msi	Shear Modulus, G_{23}	0.217 Msi
Failure Stress, τ_{12}	6.75 Ksi	Failure Stress, τ_{23}	3.93 Ksi
Failure Strain, γ_{12}	> 5 %	Failure Strain, γ_{23}	2.57 %

Thermal Expansion Properties

Longitudinal ($-50^{O}F < T < 125^{O}F$), α_{11}	-0.9×10^{-6} in/in/^{O}F
Transverse ($-50^{O}F < T < 185^{O}F$), α_{22}	41.7×10^{-6} in/in/^{O}F

(a) initial and final values as determined from σ-ε data

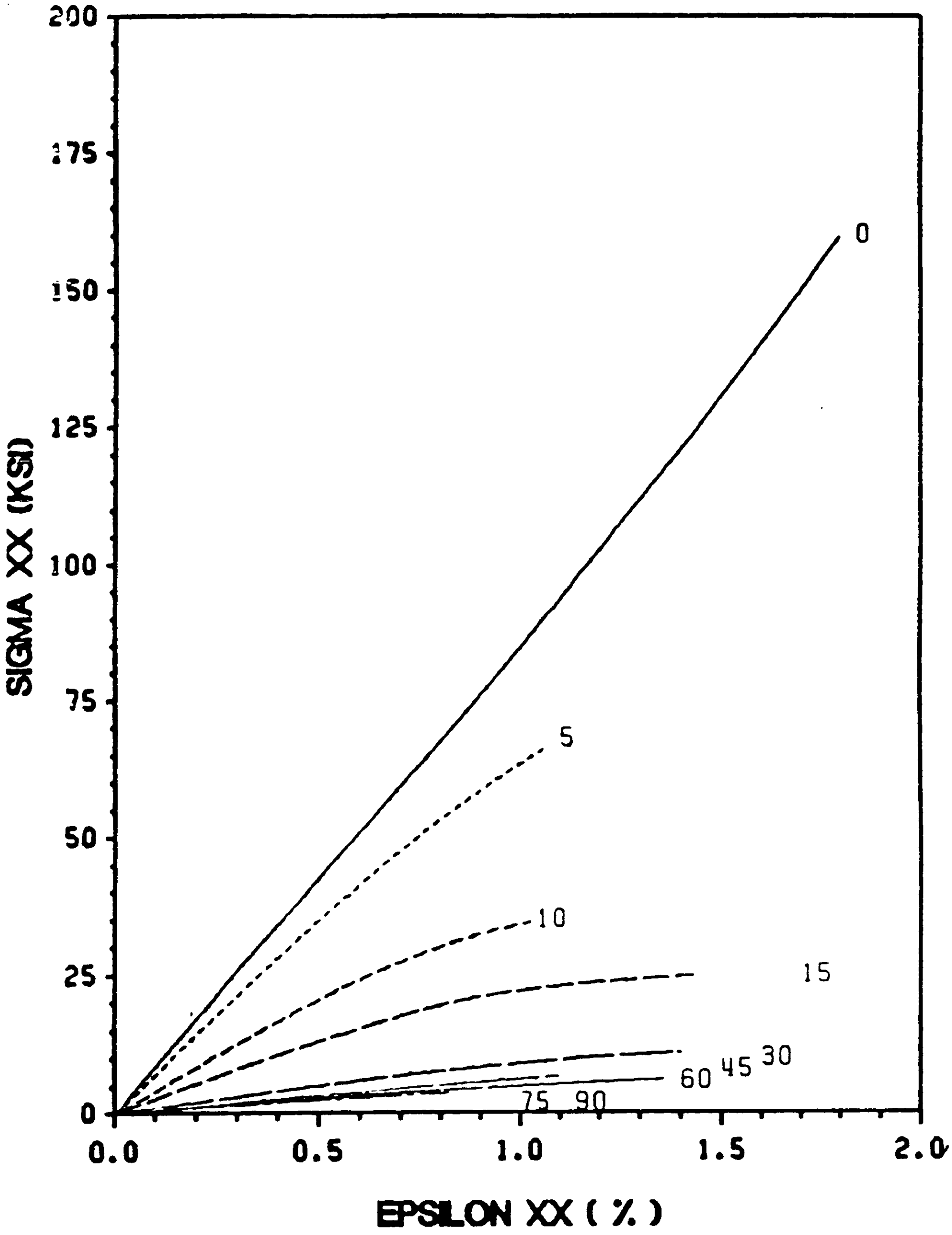

Figure 12. Unidirectional Kevlar/Epoxy Laminate Monotonic Response at Different Angles [54]

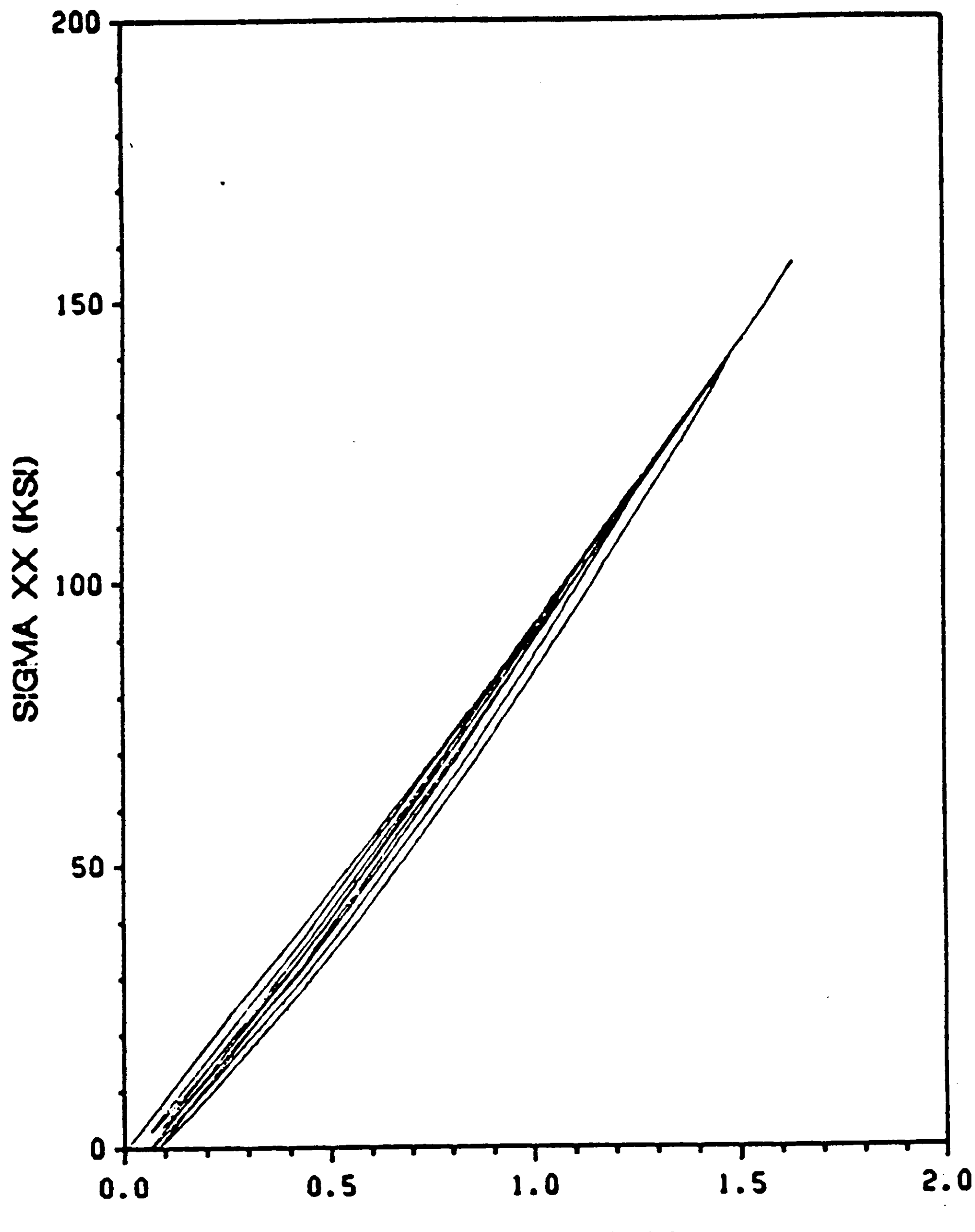

Figure 13. Unidirectional Kevlar/Epoxy Tensile Response to Cyclic Loading [54]

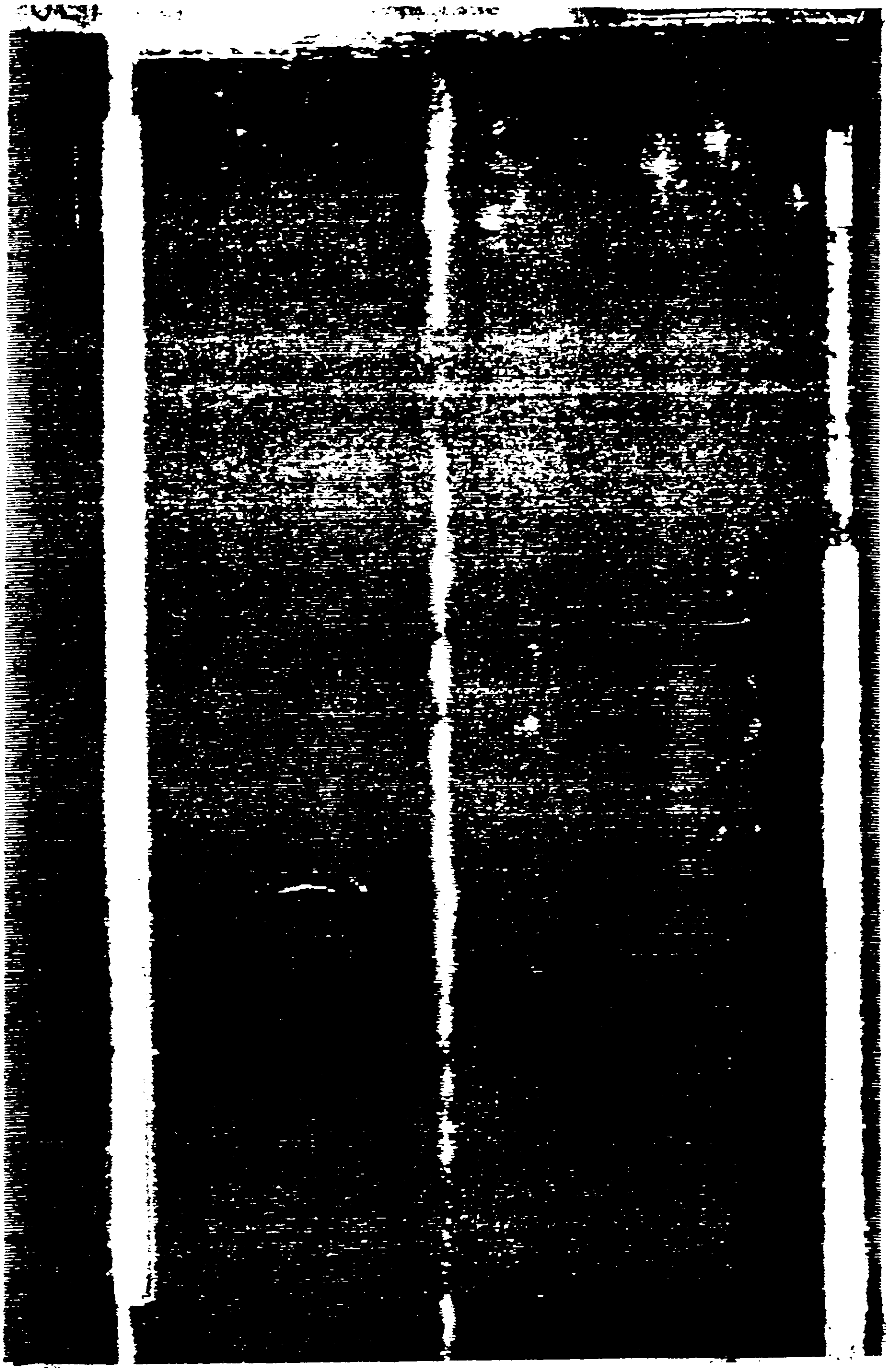

Figure 14. C Scan of Subpanel PA2-4995-6, 5 MHz

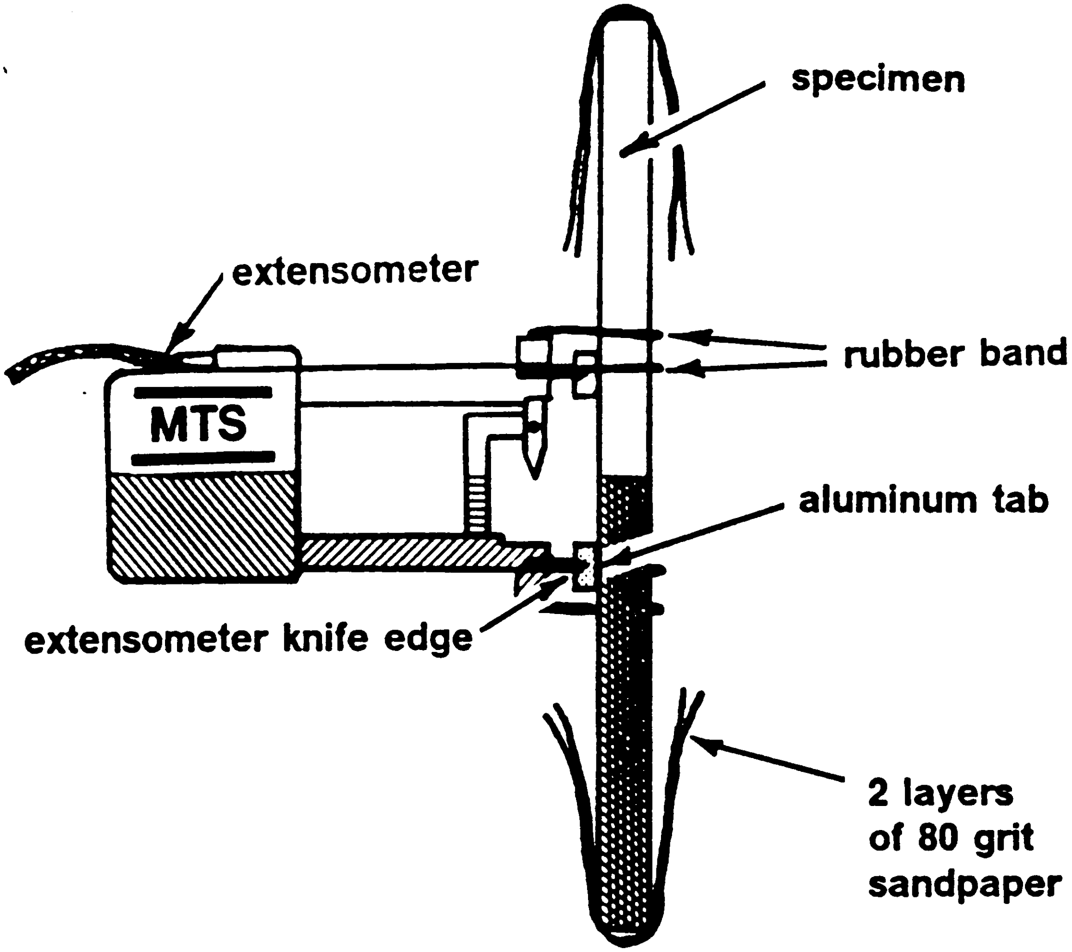

Figure 15. Extensometer Attached to a Specimen With Aluminum Tabs and Rubber Bands [63]

All fatigue tests were conducted in load control, at 10 Hz and R=.1 (R=S_{min}/S_{max}) using a sinusoidal wave. S_{max} and S_{min} are the maximum and minimum nominal applied stresses respectively. Monotonic loading tests were performed in load control at a rate of 20 lb/sec.

2.2.2 QUASI STATIC AND FATIGUE TESTS

Quasi static tests were conducted to determine initial material properties and residual tensile strength.

Table 6 lists the quasi static and fatigue testing program. Specimens were tested at varying maximum cyclic stresss, from S=0.9 to S=0.4 times the monotonic tensile strength. The stress level S is defined as S_{max}/S_u, where S_u is the ultimate tensile strength of the laminate in the fiber direction. At each of the seven stress levels, three specimens were tested. At S=0.4, the tests were concluded after the specimens survived one million cycles. The specimens were then tested for residual tensile strength.

2.2.3 RESIDUAL STRENGTH

On the basis of the S/N curve, three stress levels of engineering interest resulting in lives of 10^5 to $>10^6$ cycles were chosen. Residual tensile strength was tested at three different stages in life as determined from stiffness mesurements (see chapter 2.3). The quasi static strength measurements, coupled with the changes in stiffness were used to determine the effect of damage on the performance of a specimen. Each test was repeated three times as indicated in the testing program shown in Table 7.

2.3 NONDESTRUCTIVE EVALUATION

Nondestructive methods were employed to examine the state of the material, ideally without affecting the strength, stiffness or life of the specimen. Techniques which are common in the investigation of composite materials response are microscopy, ultrasonic C-scan, acoustic emission, radiography, stiffness, sectioning, replication, modified ultrasonic pulse-echo, vibrotermography, etc. Regrettably, penetrant enhanced radiography, a technique widely used by many investigators, had to be discarded because of the large absorption of X-rays by the aluminum compared to the relative transparency of the K/E layers. In the future, acoustic microscopy might supply the same (if not better) information.

Complimentary methods were combined to obtain information pertaining to the damage. Stiffness reduction was the method chosen to represent the degradation of performance during fatigue cycling. A short description of the methods employed follows.

Table 6. Quasi Static and Fatigue Testing Program

Stress Level, S[a]	Specimen # 1	Specimen # 2	Specimen # 3
Quasi static	SA2Q-1-7	SA2Q-2-7	SA2Q-2-5
0.9	SA2F-1-5	SA2F-2-3	SA2F-1-9
0.8	SA2F-1-11	SA2F-1-1	SA2F-2-2
0.7	SA2F-1-8	SA2F-1-2	SA2F-2-6
0.6	SA2F-2-1	SA2F-1-10	SA2F-1-4
0.5	SA2F-1-12	SA2F-2-8	SA2F-1-6
0.45	SA2F-4-7	SA2F-4-8	SA2F-4-3
0.4	SA2F-4-6	SA2F-6-6	SA2F-4-10

(a) $S = S_{max} / S_{ult}$, S_{ult} as determined from quasi static tests

Table 7. Residual Strength Testing Program

Stress Level, S	Condition	Specimen
0.5	Short, $E(n)^{a} = E_o$ 15000 cycles	SA2R-7-5 SA2R-7-1 SA2R-7-6
	Medium, up to $E(n) = 0.7$	SA2R-6-5 SA2R-6-4 SA2R-6-10
	Long, $E(n) \leq 0.6$	SA2R-5-8 SA2R-5-10 SA2R-5-6
0.45	Short, $E(n) = E_o$ 30000 cycles	SA2R-7-7 SA2R-7-2 SA2R-7-3
	Medium, up to $E(n) = 0.7$	SA2R-6-3 SA2R-6-2 SA2R-6-9
	Long, up to $E(n) =$ const.	SA2R-5-2 SA2R-5-9 SA2R-5-4
0.4	Short, $E(n) = E_o$ 60000 cycles	SA2R-2-4 SA2R-5-3 SA2R-5-1
	Medium, up to $E(n) = 0.7$	SA2R-5-7 SA2R-6-8 SA2R-5-5
	Long, up to 10^6 cycles	SA2F-6-6 SA2F-4-1 SA2F-4-6

(a) $E(n)$ is the reduced unloading stiffness at life fraction n.

2.3.1 MICROSCOPY

Light microscopy and scanning electron microscopy were used to observe the details of the laminate's edge and interfaces.

The panels, as received from the manufacturer, were observed to have an initial curvature in the fiber direction. A metallographic microscope was employed to determine the thicknesses of the plies from the view of a polished edge.

Scanning electron microscopy was employed in order to confirm the results from the light microscope and in an attempt to discover a distinct resin-rich interface between the aluminum and fiber reinforced layers.

2.3.2 SURFACE ANALYSIS

Electron spectroscopy for chemical analysis (ESCA), a surface analysis technique was used to determine the location of the delaminations developing around the cracks that form at the edges of the specimen and grow inward.

ESCA or X-ray photoelectron spectroscopy - XPS, involves analysis at high resolution of electrons which are photoejected from the top 5 nanometers of a solid surface on irradiation with X-rays. A schematic diagram is shown in figure 16.

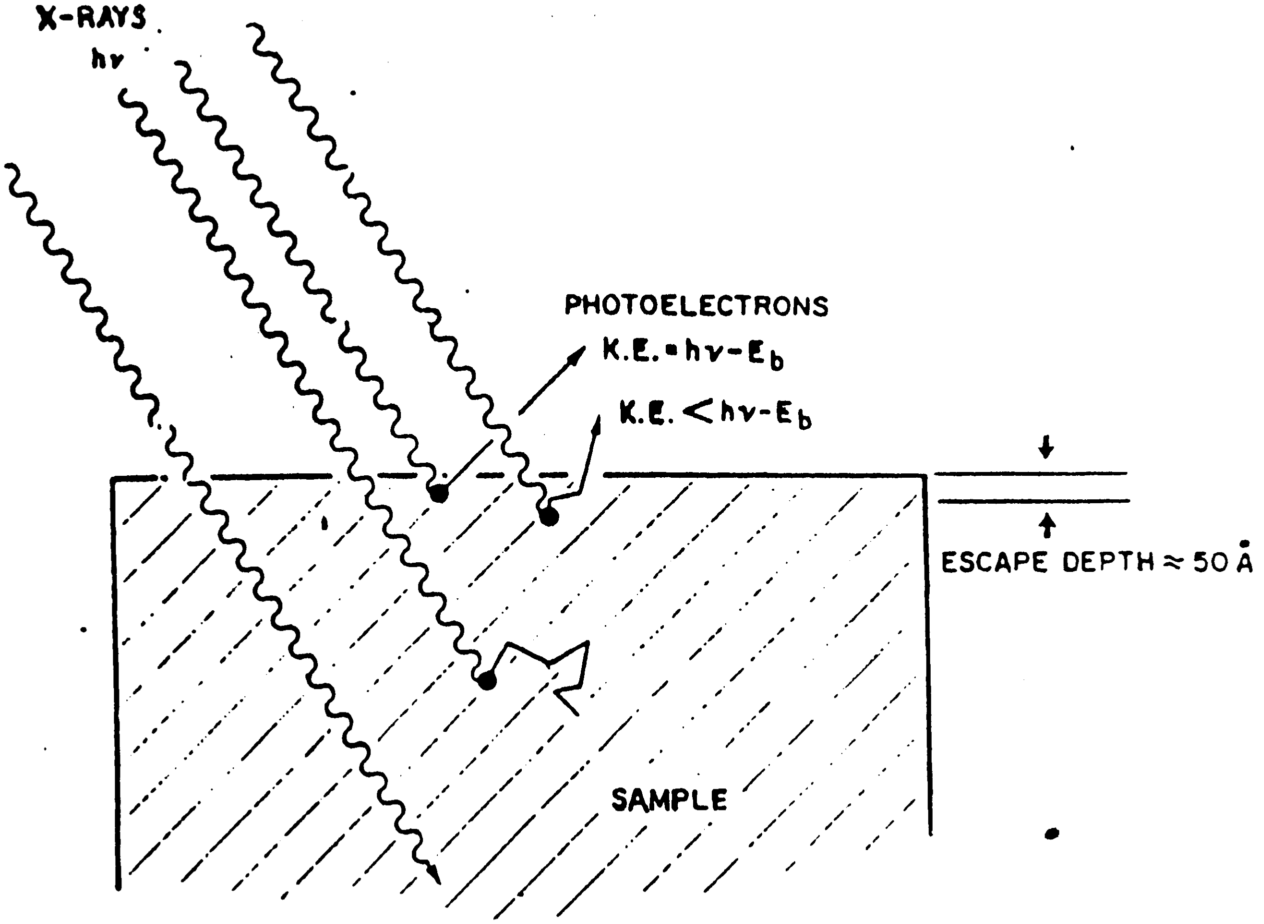

Figure 16. Schematic Diagram of ESCA Sampling Depth

The energy balance equation is,

$$h\nu = KE + BE + \Phi \qquad (4)$$

The energy of the incident beam is $h\nu$, KE is the kinetic energy of the photoelectron, BE is the binding energy of the photoelectron and Φ is is the work function of the spectrometer. The technique is used to measure BE with high precision. The value of BE is characteristic of the element to which a given electron is bound. Furthermore, the technique can detect small changes in BE which occur due to to differences in chemical bonding between atoms - a "chemical shift" - and such shifts are listed in the literature. Thus, ESCA is an excellent surface technique for bonding state and element identification.

2.3.3 PHOTOGRAPHY

The development and location of cracks was documented with the aid of photography. The shiny surface of the aluminum made it difficult to observe the cracks. This obstacle was overcomed by the use of oblique lighting that enhanced the lips of the cracks, suitable magnification and the use of slide film. A clear picture of the crack pattern is obtained in this manner.

The number of cracks per unit length is compared to the characteristic damage state predicted for this laminate.

2.3.4 ULTRASONIC C-SCAN

The ultrasonic C-scan is one of the more frequently used non destructive methods for inspection of composite materials. It is particularly useful in detecting defects in the plane of the plate and locating regions of relative good and bad quality, as was done for these specimens. No quantification of damage/quality was made.

This technique uses high frequency sound waves emitted by an ultrasonic transducer and received back after passing through the specimen inmersed in a tank of water that acts as a coupling medium. All of the wave characteristics carry information (amplitude, frequency, shapes, etc.) but usually the attenuation in the amplitude of the signal is used. The attenuation of the original signal is associated with discontinuities, and the different attenuation at different spots is related to defects in the plane of the layered composite such as delaminations, voids, etc. The nature of the test is such that it integrates the damage through the thickness of the specimen, losing some of the information.

Ultrasonic C-scans were performed to determine acceptable areas in the received panel for specimen preparation (as shown in figure 15) and to determine the extent of through-the-width growth of edge delaminations in residual strength specimens.

2.3.5 STIFFNESS MONITORING

Changes in stiffnes were monitored to follow the development of damage during cyclic loading, these changes correlate well with data from other techniques which measure damage in composite materials such as the ultrasonic C-scans described above [29,30,32].

Secant and unloading elastic moduli were measured during all cyclic tests using the strain data from the extensometer and load readings from the MTS load cell. The secant modulus is defined as,

$$E_{sec} = \frac{\sigma_{max} - \sigma_{min}}{\varepsilon_{max} - \varepsilon_{min}}$$

and the unloading modulus is determined from the initial slope of the unloading stress-strain curve.

A predetermined reduction in unloading stiffness was used as the criterion to end the cyclic loading of residual strength specimens. Stress-strain curves were plotted during all cyclic tests at regular intervals.

2.3.6 STRAIN ACCUMULATION

The strain accumulated during cyclic loading at zero, minimum, mean and maximum loading is presented. If a creep test is considered to be a static fatigue test, then the accumulated strain is analogous to creep strain. It includes the initial elastic and plastic deformations, and subsequent dynamic strains due to cyclic loading. The accumulated strain is correlated to stiffness changes, creep compliance and strain-to-failure data for K/E.

CHAPTER 3

EXPERIMENTAL RESULTS

3.1 MECHANICAL PROPERTIES

3.1.1 ARALL 2 QUASI STATIC PROPERTIES

The results of the monotonic tensile tests performed on specimens cut from the as-received panel #604995 are summarized in table 8, and three of the σ-ε curves are shown in figure 17. The reported values on this table include:

- Ultimate tensile strength
- Yielding stress, 0.2% offset
- Knee stress, located at the interception of the linear slopes
- Ultimate strain (at fracture)
- Yielding strain, 0.2% offset
- Knee strain, as defined above
- Initial elastic axial modulus
- Secondary elastic axial modulus

Table 8. Arall 2 Quasi Static Properties

Spec. #	SA2Q-1-7	SA2Q-2-7	SA2Q-2-5	AVERAGE
UTS (Ksi)	102.7	104.1	103.9	103.6
Yield Stress[a] (Ksi)	53.8	54.3	54.5	54.2
Knee Stress[b] (Ksi)	45.5	46.0	46.1	46
Ultimate strain %	2.40	2.48	2.40	2.43
Yield Strain %	0.78	0.78	0.77	0.78
Knee Strain %	0.48	0.48	0.48	0.48
Initial[c] Elastic Axial Modulus (Msi)	9.28	9.38	9.34	9.33
Secondary[d] Elastic Axial Modulus (Msi)	3.03	2.95	3.07	3.02

(a) 0.2 % offset

(b) intersection of slopes in bilinear σ-ε curve

(c) initial slope of σ-ε curve

(d) secondary slope of σ-ε curve

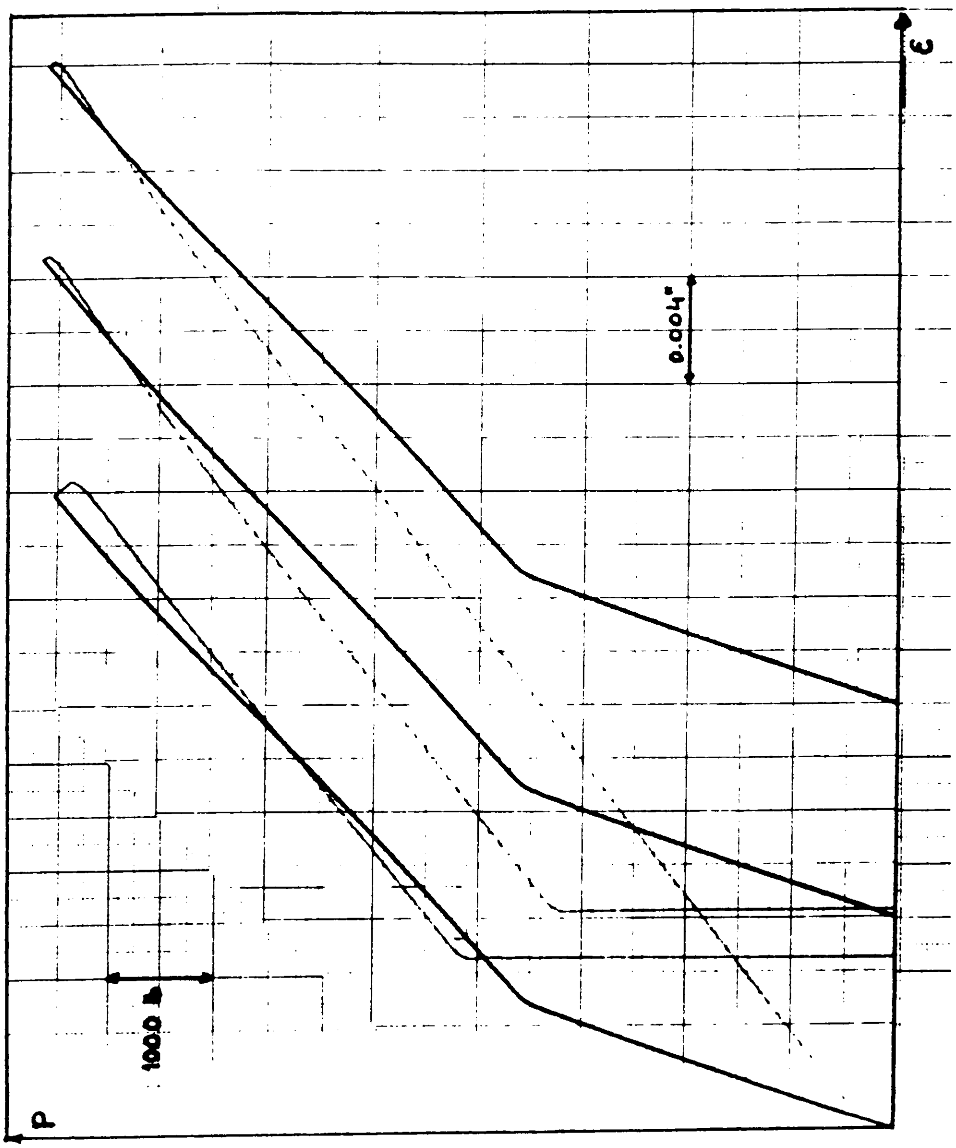

Figure 17. Arall 2 Quasi Static Load-Strain Curves

3.1.2 ARALL 2 FATIGUE RESPONSE

The results of the cyclic loading testing program are presented in table 9. The same data are presented as a Smax/Su vs. log N_f (N_f-cycles to failure) in figure 18.

Using the average number of cycles to failure, a fit of the form

$$S_{max}/S_u = C - A*(\log N_f)^B \qquad (5)$$

is found to describe well the S/N curve, as shown in figure 18.

A, B and C are material parameters with the following values,

A=-9.5773 B=-2.0065 C=0.16338

and the coefficient of variance is 0.036. This approximation yields a life of 2.5 million cycles at Smax/Su=0.4.

3.1.3 RESIDUAL TENSILE STRENGTH

The stress ratios chosen for residual tensile strength measurements were: S=0.5 resulting in lives of 10^5cycles, S=0.45 resulting in lives of 650000 cycles, and S=0.4 resulting in lives of over one million cycles. At each stress level residual strength was determined at E(n)=1 and E(n)=0.7, where n is the fraction of fatigue life (henceforth denoted life fraction), and E(n) is the unloading stiffness at n. In addition residual strength tests were conducted at one other stage of fatigue life, different for each stress level.

Table 9. Fatigue Testing Program Results

Stress Level, S	Specimen #	Fatigue Life (Cycles)	Mean Life (Cycles)
0.9	SA2F-1-5	3530	
	SA2F-2-3	3590	
	SA2F-1-9	3960	3690
0.8	SA2F-1-11	7960	
	SA2F-1-1	7860	
	SA2F-2-2	8780	8200
0.7	SA2F-1-8	21800	
	SA2F-1-2	17500	
	SA2F-2-6	17270	18860
0.6	SA2F-2-1	49710	
	SA2F-1-10	47160	
	SA2F-1-4	59180	52020
0.5	SA2F-1-12	106560	
	SA2F-2-8	103650	
	SA2F-1-6	95490	101900
0.45	SA2F-4-7	663960	
	SA2F-4-8	778890	
	SA2F-4-3	490550	644500
0.4	SA2F-4-6	$> 10^6$	
	SA2F-6-6	$> 10^6$	
	SA2F-4-10	$> 10^6$	NA

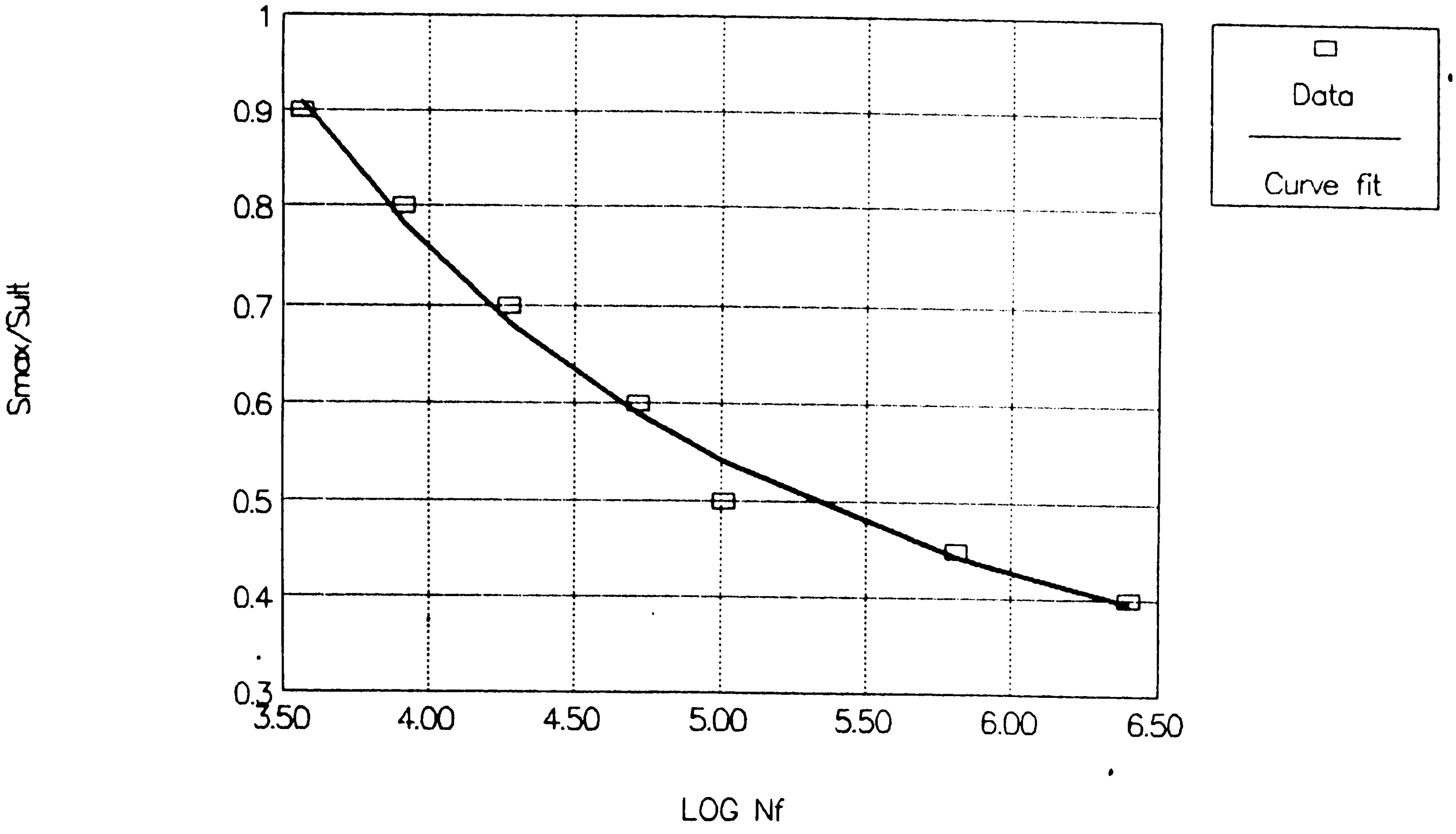

Figure 18. Fatigue Data and Best-fit S/N curve for Arall 2 Laminates, R=0.1, 10 Nz

- At S=0.5 : for n >0.9
- At S=0.45: for E(n) ≅ constant, after the drop in stiffness
- At S=0.4 : after 10^6 cycles

At each stress level and life fraction, three specimens were tested. A compilation of data similar to that presented for quasi static tests is shown in tables 10 to 12 for comparison purposes. Residual strength - $\sigma(n)$ - is plotted vs. stiffness fraction in figure 19. A simple power law with leading coefficient correlates the normalized residual strength with the normalized stiffness fraction.

$$\frac{\sigma(n)}{\sigma_{ult}} = 0.48067 + 0.46779 * \left(\frac{E(n)}{E_o} \right)^{2.7661} \qquad (6)$$

and the coefficient of variance is 0.0689.

The fracture plane of virgin specimens is relatively regular with little or no fiber pull out. This is in contrast to the usual situation encountered in uniaxial fiber reinforced composite specimens, where the fracture surface is ragged and the fibers literally explode. Residual strength specimens with delaminations may fracture on different planes in each aluminum ply and the fibers occasionally pull out.

Table 10. Residual Strength Testing Program
Results at S = 0.5

Short, 15000 cycles	SA2R-7-5	SA2R-7-1	SA2R-7-6	AVERAGE
Residual Strength (Ksi)	97.7	102.6	96.5	98.8
Knee Stress (Ksi)	52.7	52.9	53.4	53.0
Ultimate Strain, %	2.0	2.2	1.98	2.06
Knee Strain, %	0.525	0.55	0.55	0.54
Init. Modulus (Msi)	9.69	9.53	9.62	9.61
Secondary Mod. (Msi)	3.09	3.10	3.02	3.07

Medium, E(n) = .7	SA2R-6-5	SA2R-6-4	SA2R-6-10	AVERAGE
Residual Strength (Ksi)	70.8	69.1	76.5	72.2
Knee Stress (Ksi)	53.9	55.6	56.0	55.2
Ultimate Strain, %	1.30	1.15	1.45	1.30
Knee Strain, %	0.75	0.73	0.75	0.74
Init. Modulus (Msi)	6.86	7.05	6.76	6.89
Secondary Mod. (Msi)	3.05	3.18	2.99	3.07

Long, E(n) < 0.6	SA2R-5-8	SA2R-5-10	SA2R-5-6	AVERAGE
Residual Strength (Ksi)	66.89	58.46	66.26	63.87
Knee Stress (Ksi)	53.2	51.6	54.6	53.1
Ultimate Strain, %	1.33	1.20	1.48	1.33
Knee Strain, %	0.90	0.93	1.05	0.96
Init. Modulus (Msi)	5.37	5.63	5.25	5.42
Secondary Mod. (Msi)	3.17	2.55	2.92	2.88

Table 11. Residual Strength Testing Program
Results at S = 0.45

Short, 30000 cycles	SA2R-7-7	SA2R-7-2	SA2R-7-3	AVERAGE
Residual Strength (Ksi)	103	96.4	99.3	99.6
Knee Stress (Ksi)	45.7	47.7	46.5	46.6
Ultimate Strain, %	2.35	2.10	2.18	2.21
Knee Strain, %	0.53	0.45	0.48	0.48
Init. Mod. (Msi)	9.42	9.38	9.53	9.45
Secondary Mod. (Msi)	3.09	3.09	3.10	3.09

Medium, E(n) = .7	SA2R-6-3	SA2R-6-2	SA2R-6-9	AVERAGE
Residual Strength (Ksi)	69.1	68.6	71.9	69.9
Knee Stress (Ksi)	53.2	49.8	51.6	51.5
Ultimate Strain, %	1.25	1.38	1.43	1.35
Knee Strain, %	0.70	0.73	0.75	0.73
Init. Modulus (Msi)	6.65	6.83	7.09	6.86
Secondary Mod. (Msi)	2.92	2.92	2.93	2.92

Long, E(n) = const.	SA2R-5-2	SA2R-5-9	SA2R-5-4	AVERAGE
Residual Strength (Ksi)	52.7	62.3	62.6	59.2
Knee Stress (Ksi)	NA	NA	NA	NA
Ultimate Strain, %	1.73	1.65	1.63	1.67
Knee Strain, %	NA	NA	NA	NA
Init. Modulus (Msi)	3.81	4.27	4.03	4.03
Secondary Mod. (Msi)	2.76	3.45	3.21	3.14

Table 12. Residual Strength Testing Program
Results at S = 0.4

Short, 60000 cycles	SA2R-2-4	SA2R-5-3	SA2R-5-1	AVERAGE
Residual Strength (Ksi)	97.7	96.9	100	98.2
Knee stress (Ksi)	45.5	43.6	43.4	44.2
Ultimate Strain, %	2.13	2.15	2.25	2.18
Knee Strain, %	0.45	0.50	0.45	0.47
Init. Modulus (Msi)	9.45	9.30	9.46	9.40
Secondary Mod. (Msi)	3.08	3.12	3.19	3.13

Medium, E(n) = .7	SA2R-5-7	SA2R-6-8	SA2R-5-5	AVERAGE
Residual Strength (Ksi)	61.1	61.6	59.1	60.6
Knee Stress (Ksi)	42.5	45.2	46.0	44.5
Ultimate Strain, %	1.35	1.20	1.15	1.23
Knee Strain, %	0.73	0.65	0.75	0.71
Init. Modulus (Msi)	6.44	6.75	6.67	6.62
Secondary Mod. (Msi)	3.00	3.19	3.05	3.08

Long, > 10^6 cycles.	SA2F-6-6	SA2F-4-10	SA2R-4-6	AVERAGE
Residual Strength (Ksi)	50.3	51.3	53.2	51.6
Knee Stress (Ksi)	NA	NA	NA	NA
Ultimate Strain, %	1.20	1.90	1.85	1.65
Knee Strain, %	NA	NA	NA	NA
Init. Modulus (Msi)	NA	3.28	3.28	3.28
Secondary Mod. (Msi)	NA	NA	NA	NA

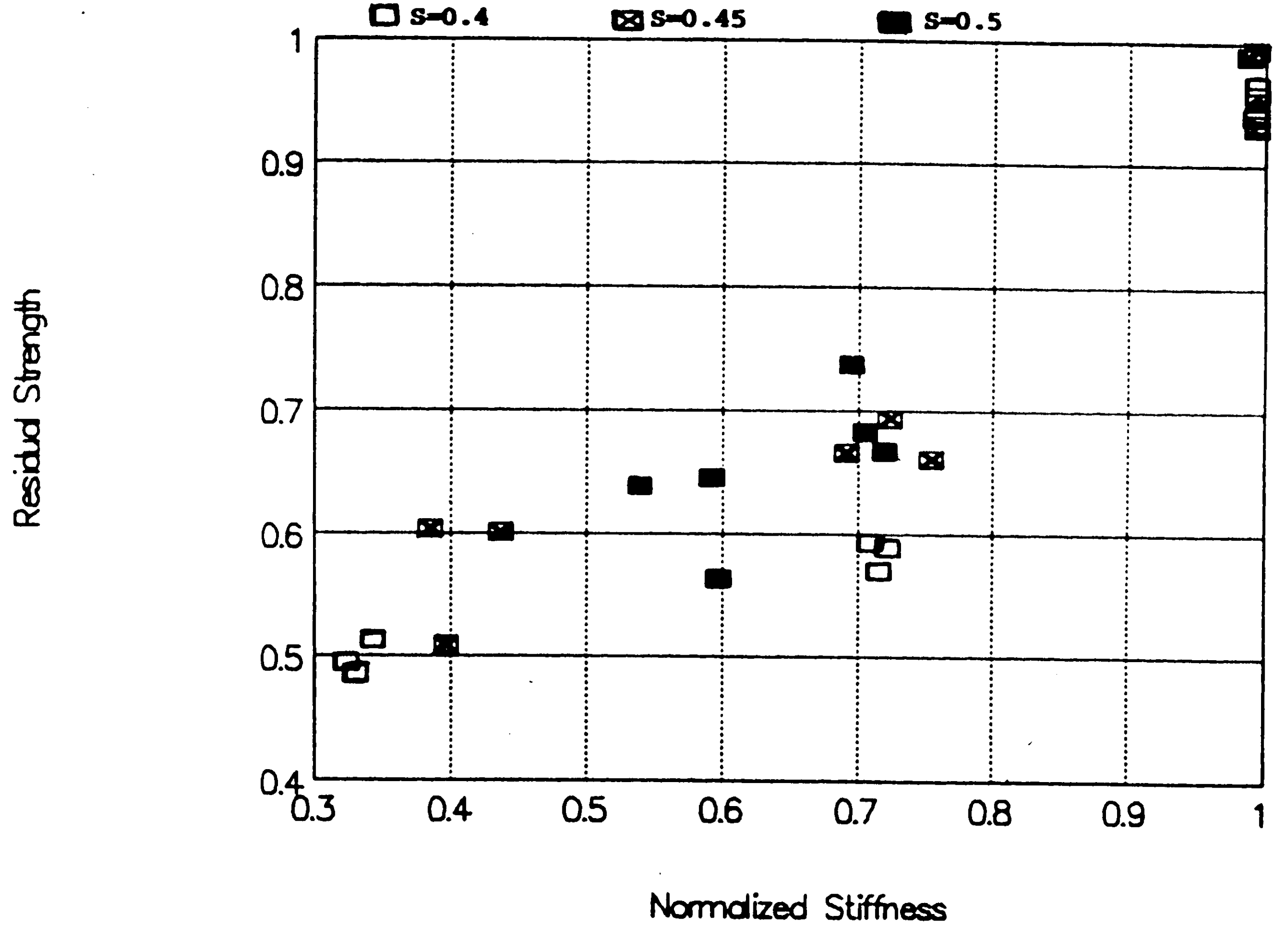

Figure 19. Normalized Residual Strength vs. Stiffness

3.2 NONDESTRUCTIVE EVALUATION

3.2.1 MICROSCOPY

The magnified edge of a polished specimen (fiber direction) is shown in figure 20. The aluminum layers appear as bright surfaces while the K/E layers appear dark. By calibrating with respect to the known thickness of the aluminum layers and the total thickness of the laminate, the calculated thicknesses of the K/E layers are 0.0075 inch and 0.0085 inch. This difference of 12% in the thickness of supposedly identical plies creates an asymmetric geometry with respect to the midplane that results in the observed bending of the laminate due to residual thermal stresses.

A scanning electron microscope picture of a similar edge, shown in figure 21, confirms this finding. This picture offers no definite proof of the existence of a significant resin-rich interface between the aluminum and fiber-rich areas. Ritchie [10] showed an optical micrograph of the cross section of the prepreg plies sandwiched between aluminum plies, figure 22. An irregular resin-rich region of approximately one fiber diameter in thickness exists close to the prepreg/aluminum interface.

Figure 20. Metallographic Picture of the Edge of an As-received Panel

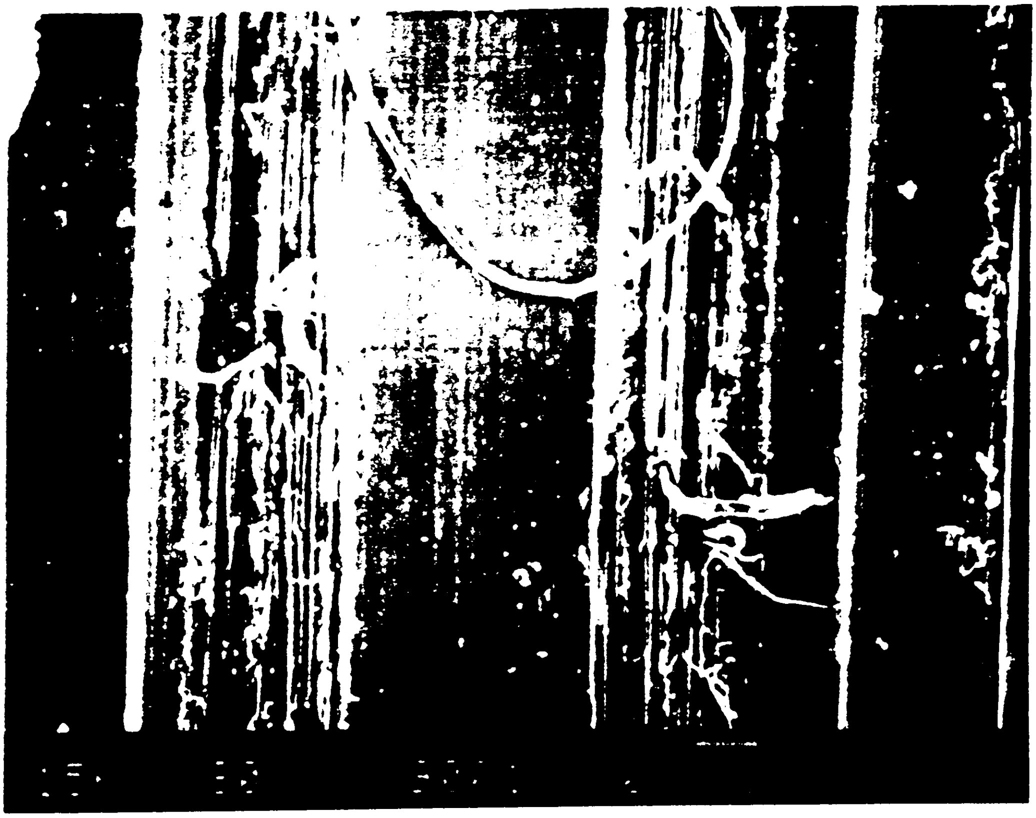

Figure 21. Scanning Electron Microscop Picture of the Edge of an As-received Panel

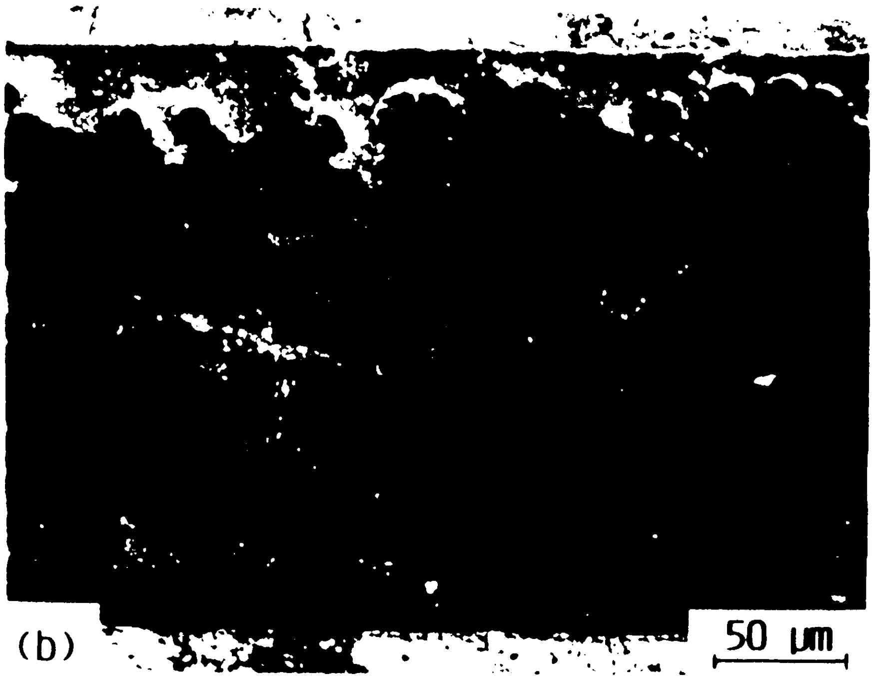

Figure 22. Optical Micrograph of a Prepreg Layer Between Aluminum Layers Showing Resin-rich Interface [10]

3.2.2 SURFACE ANALYSIS

Delaminated areas were analyzed using the ESCA technique. The surfaces of the "aluminum" surface and "K/E" surface were scanned in narrow and broad bands, figures 23 and 24. The elements and relative quantities present on both sides of the delamination are identical and correspond to an epoxy surface. This suggests that the crack growing in the aluminum layer causes the delamination to grow inside the resin-rich interface causing cohesive and not adhesive failure. Table 13 summarizes the elements and concentrations found in both sides.

3.2.3 PHOTOGRAPHY

Figures 25 to 30 show magnified and enhanced pictures of the crack patterns as they developed in residual strength specimens cycled to the prescribed life fraction, except for short-life-fraction specimens which did not show any cracks.

Cracks initiate at the edges of the specimen and grow in a direction perpendicular to the load. With progressive cycles, more cracks develop creating a distinct crack pattern. Eventually two cracks growing from opposite edges may join or interact in such a way to change the initial direction. Although the cracks attain different lengths, a uniform spacing is evident in most cases, indicating that at significant stiffness reductions (30% reduction and greater), a

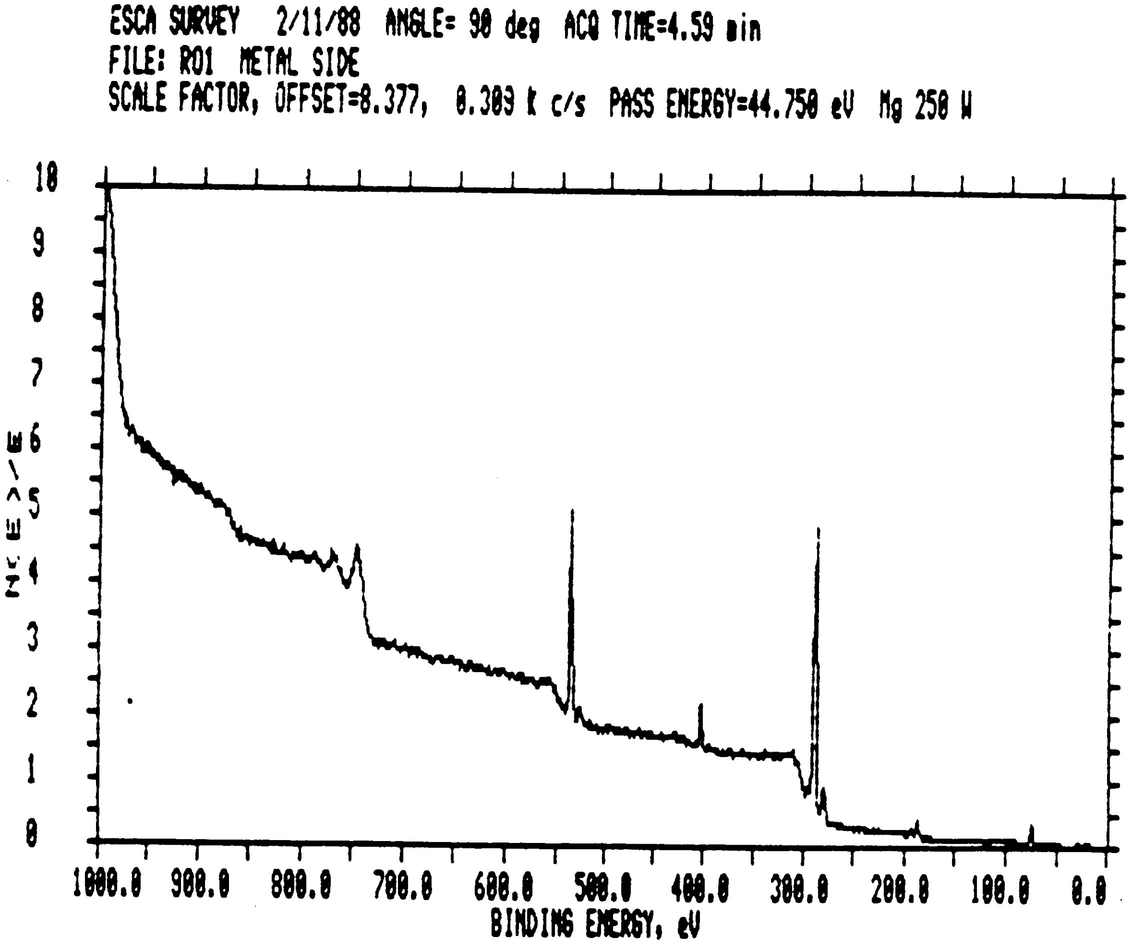

Figure 23. ESCA Survey of the Aluminum Side of a Delaminated Fatigue Specimen

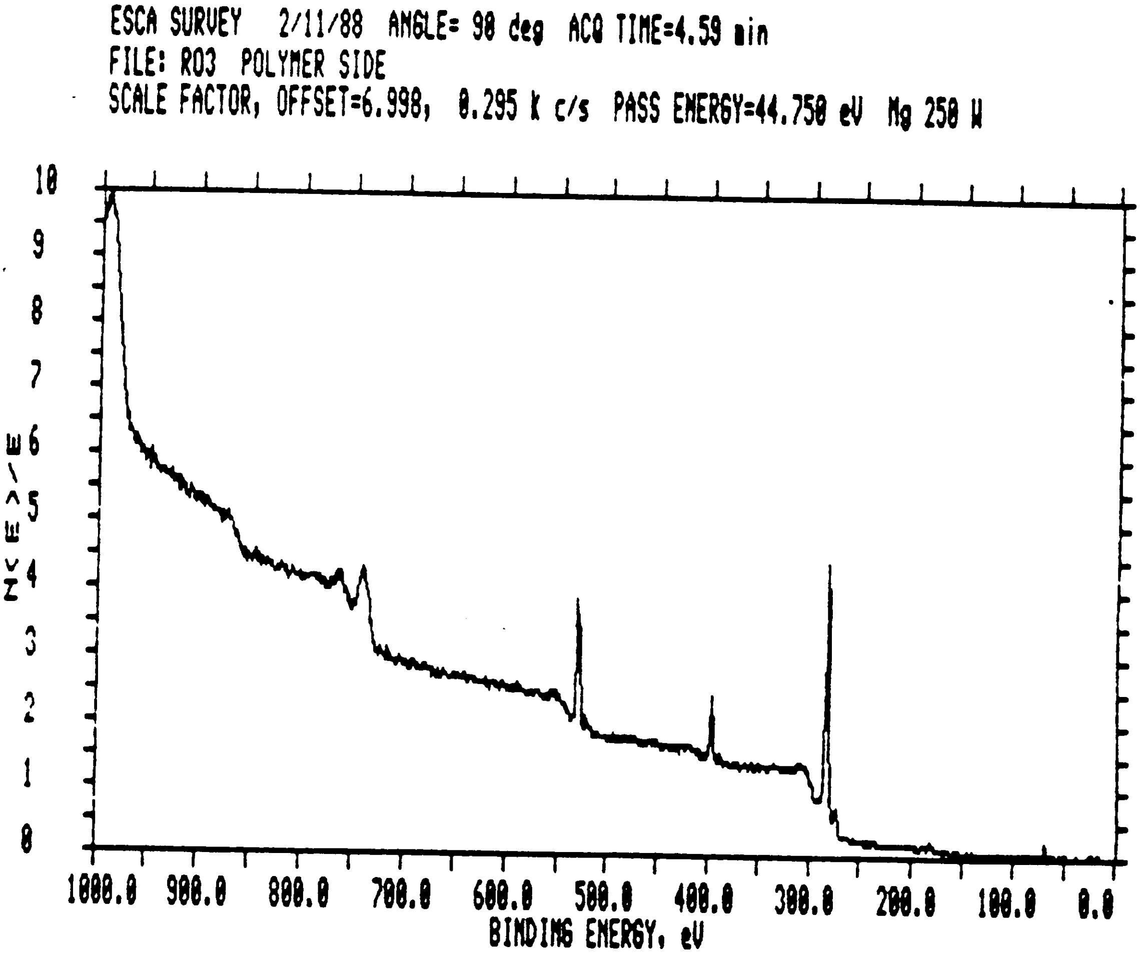

Figure 24. ESCA Survey of the Prepreg Side of a Delaminated Fatigue Specimen

Table 13. ESCA Surface Analysis of Delaminated Arall 2

Element	Sensitivity Factor	Aluminum Side Concentration, %	Aramid/Epoxy Side Concentration, %
C 1	0.250	77.17	76.42
O 1	0.660	16.42	14.01
Al 1	0.185	0.00	0.00
Br 1	0.830	1.02	0.59
N 1	0.420	5.39	8.98

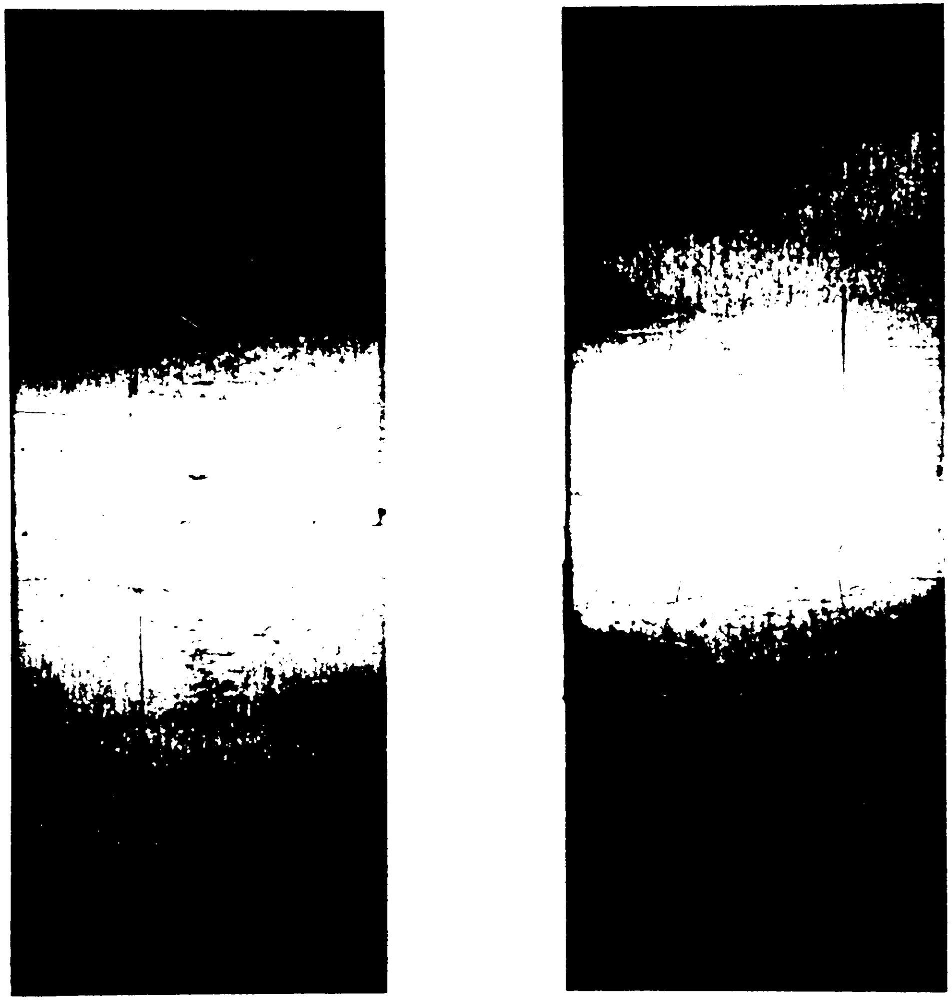

Figure 25. Cracked Residual Strength Specimens Tested at $S = 0.5$, Medium Life

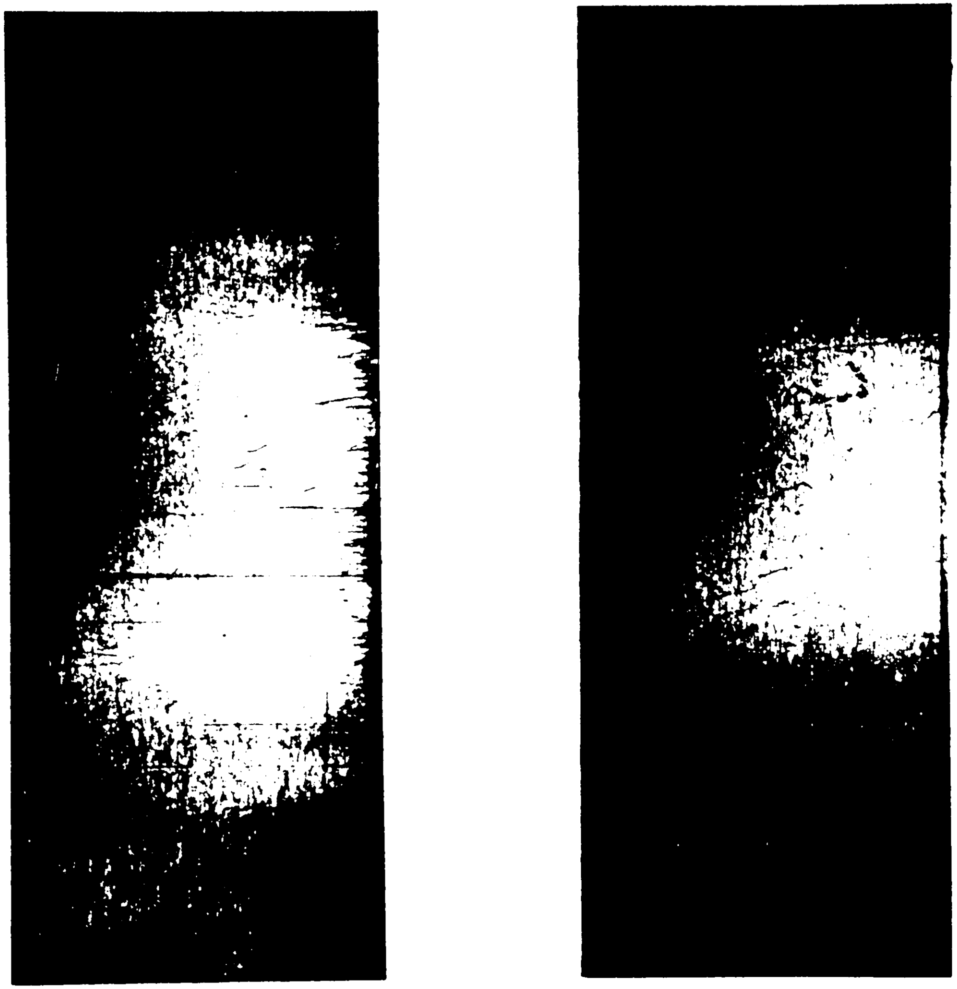

Figure 26. Cracked Residual Strength Specimens Tested at S = 0.5, Long Life

Figure 27. Cracked Residual Strength Specimens Tested at $S = 0.45$, Medium Life

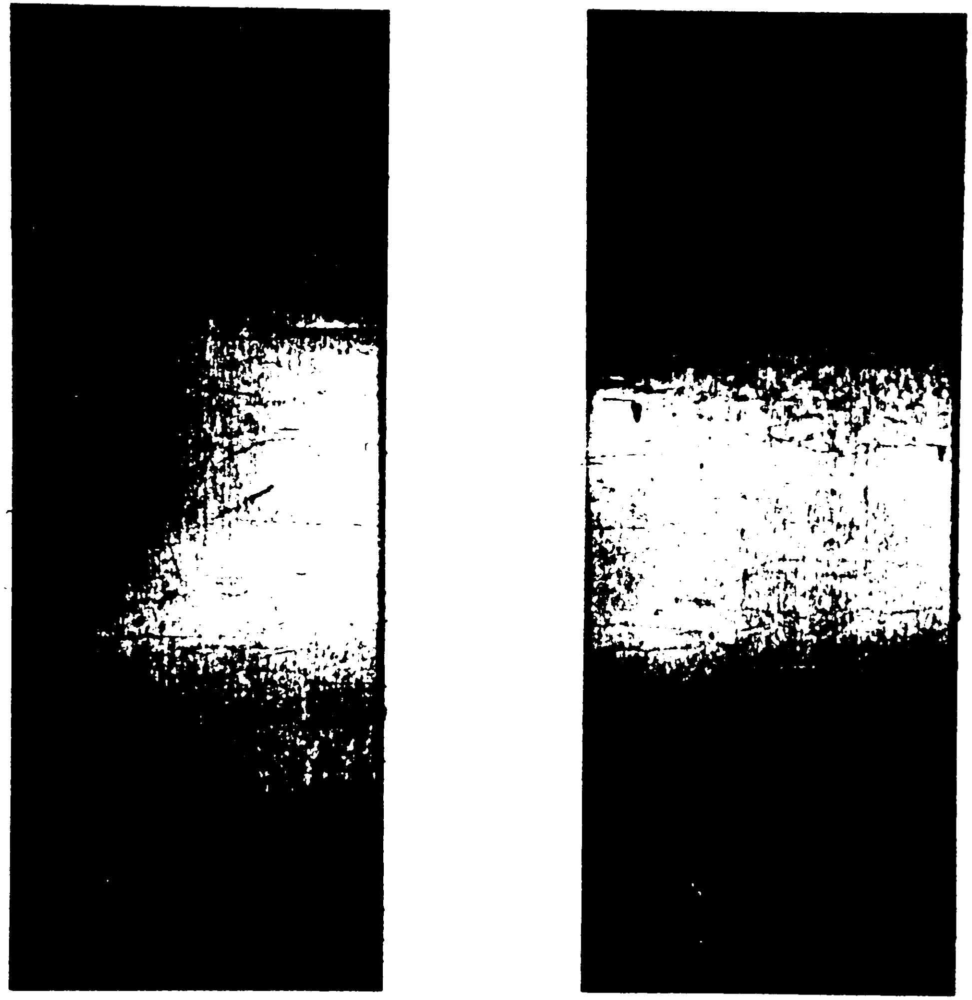

Figure 28. Cracked Residual Strength Specimens Tested at $S = 0.45$, Long Life

Figure 29. Cracked Residual Strength Specimens Tested at $S = 0.4$, Medium Life

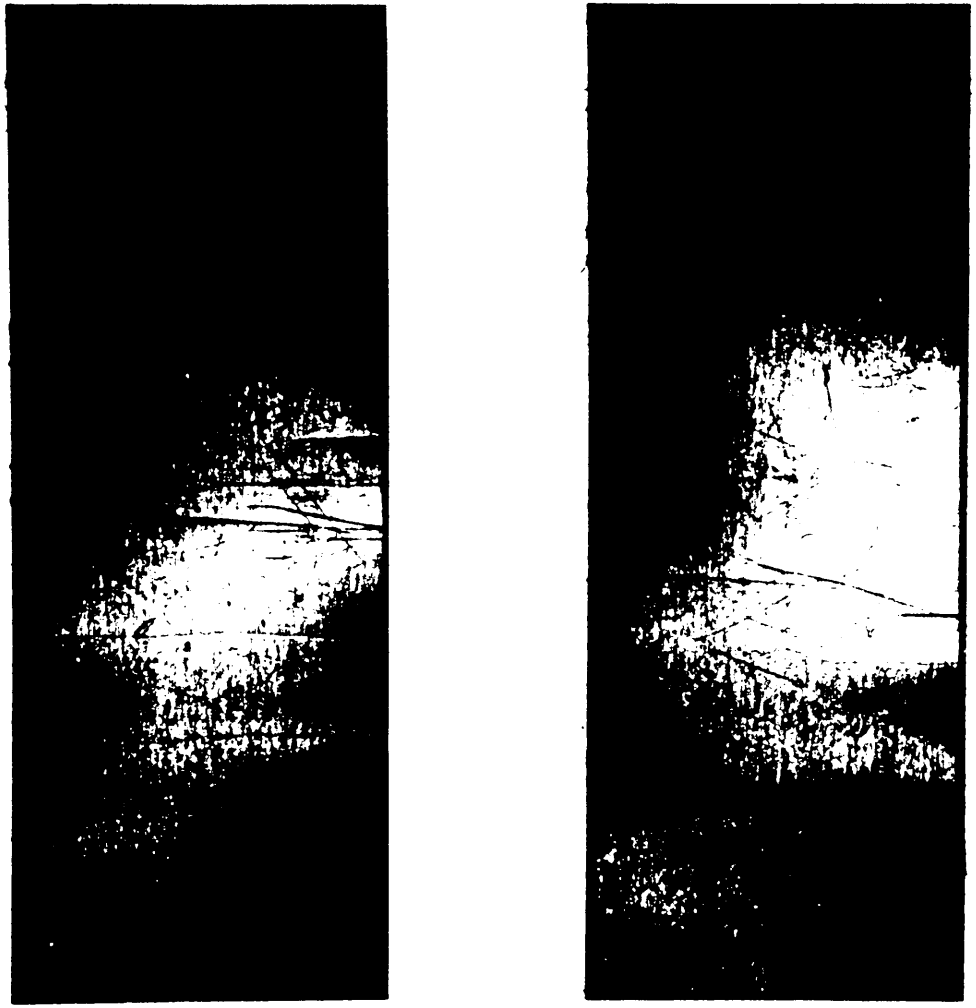

Figure 30. Cracked Residual Strength Specimens Tested at $S = 0.4$, after 10^6 cycles

Table 14. Cracks per 4 Inch Length in Residual Strength Specimens of Arall 2

S[a]	Spec.	Edge #[b]				Spec. Average	Avg. per Stress Level	Avg. Spacing (inch)
		1	2	3	4			
0.4	SA2R-6-8	10	12	10	12	11		
Med.	SA2R-5-7	9	8	13	11	10.25		
	SA2R-5-5	12	10	13	8	10.75	10.67	0.375
0.4	SA2R-4-6	11	12	14	11	12		
Long	SA2R-4-10	11	9	12	10	10.5		
	SA2R-6-6	12	12	8	11	10.75	11.08	0.361
0.45	SA2R-6-3	11	11	12	12	11.5		
Med.	SA2R-6-9	11	14	11	12	12		
	SA2R-6-2	12	11	10	11	11	11.5	0.348
0.45	SA2R-5-2	13	12	14	12	12.75		
Long	SA2R-5-4	13	12	12	16	13.25		
	SA2R-5-9	12	13	12	13	12.5	12.83	0.312
0.5	SA2R-6-10	6	15	16	14	12.75		
Med.	SA2R-6-5	7	15	16	12	12.5		
	SA2R-6-4	13	16	15	15	14.75	13.33	0.3
0.5	SA2R-5-10	7	14	14	5	10		
Long	SA2R-5-6	12	8	13	12	11.25	10.63	0.376

(a) Stress level, S_{max}/S_{ult}

(b) Four edges per specimen, arbitrarily numbered.

characteristic damage state or condition becomes stable. Table 14 summarizes the number of cracks per unit length initiating at the edges and indicates the average number of cracks and crack spacing for different stress levels and life fractions. The overall average spacing is 0.345 inches and the coefficient of variance is 0.093.

3.2.4 ULTRASONIC C-SCANS

Figures 31 to 33 show ultrasonic C-scan pictures of residual strength specimens. The dark tones indicate defects and the gray scale is proportional to the attenuation. There is excellent qualitative repeatability among specimens tested at the same stress level and life fraction, and reasonable repetition for different stress levels but similar life fraction. It should be noted that at S=0.5, the long-life-fraction specimens are less delaminated than at S=0.45 or S=0.4, as shown in figure 34.

The integrative nature of this technique makes it difficult to investigate single defects, especially for the long-life-fraction specimens which appear to be severely delaminated. The short-life-fraction specimens appear to be free of defects, while the 30%-stiffness-reduction specimens are moderately damaged. The latter offer the most qualitative information. Delaminations of elliptical shape initiating at the edges have developed, as predicted by Marissen [8].

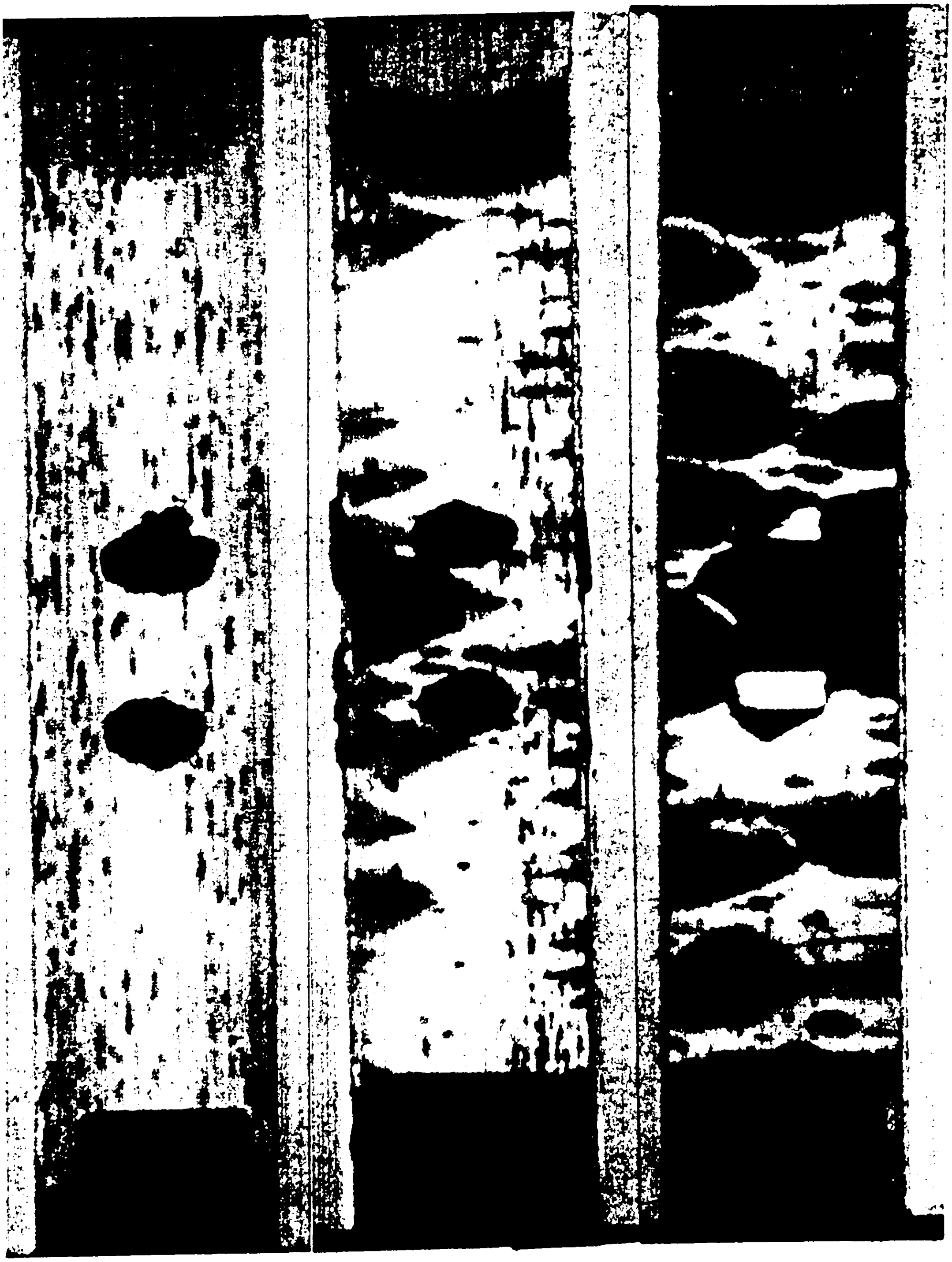

Short Life Medium Life Long Life

Figure 31. C Scans of Residual Strength Specimens at S=0.5

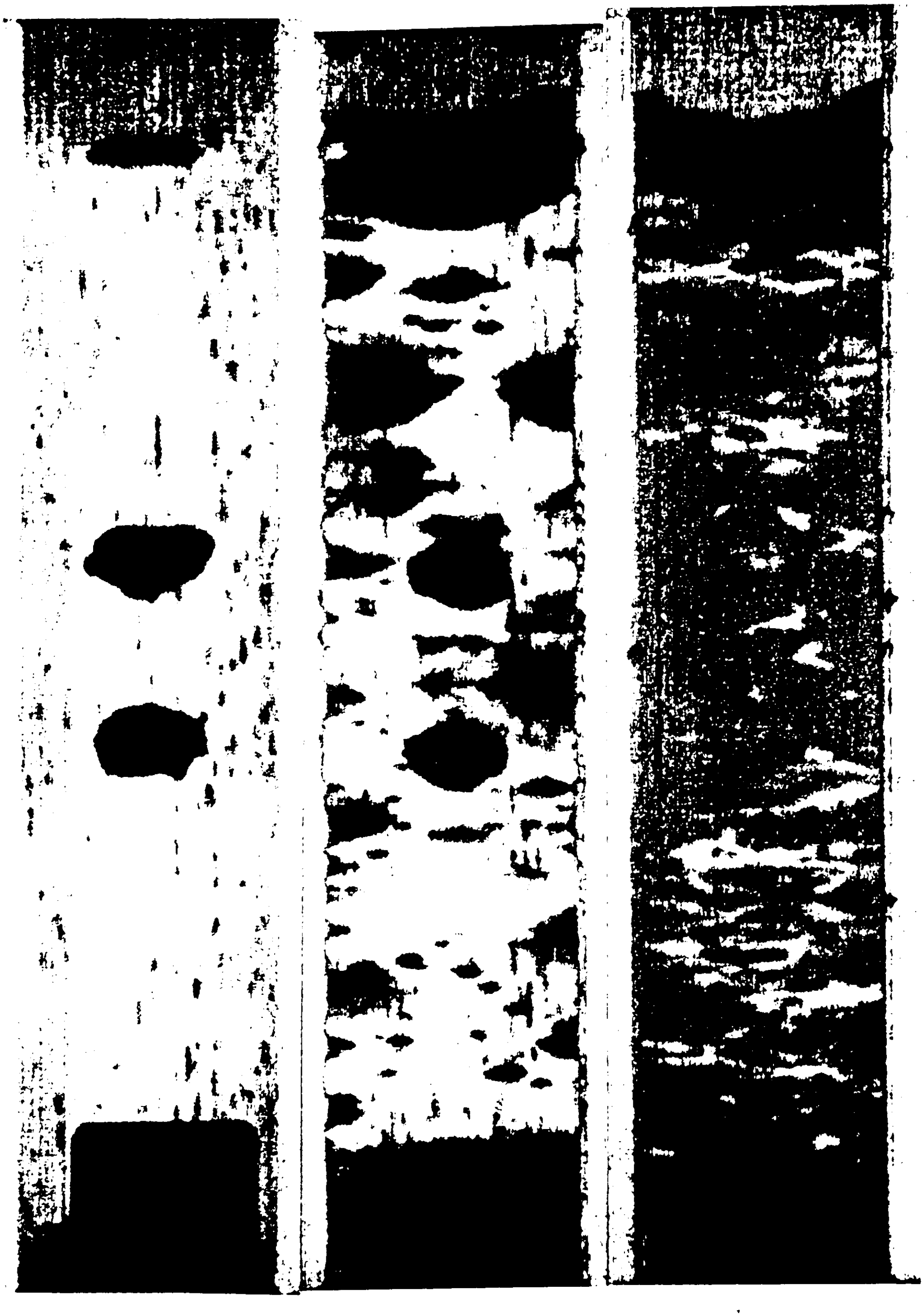

Short Life Medium Life Long Life

Figure 32. C Scans of Residual Strength Specimens @ S=0.45

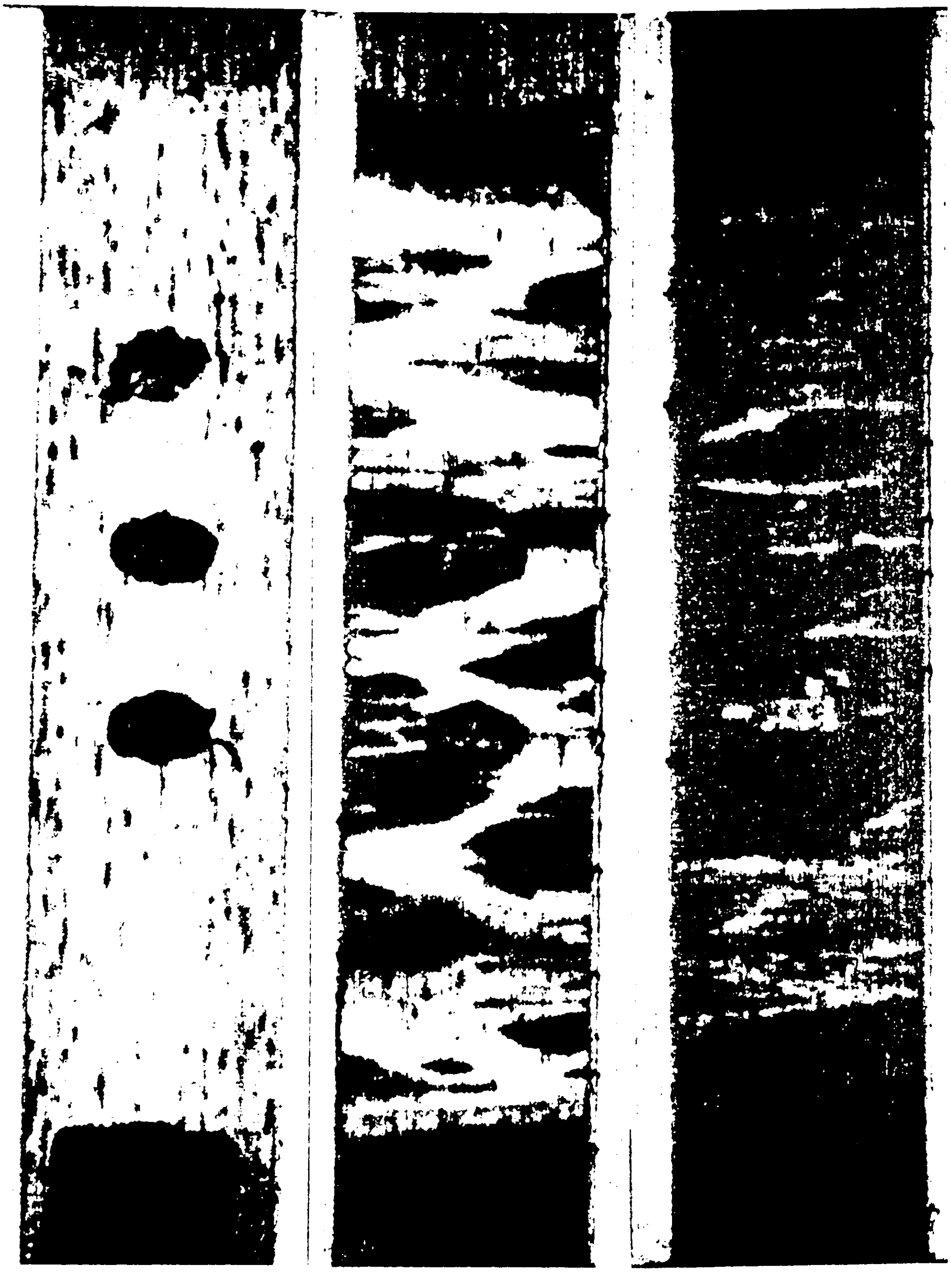

Short Life Medium Life Long Life

Figure 33. C Scans of Residual Strength Specimens at S=0.4

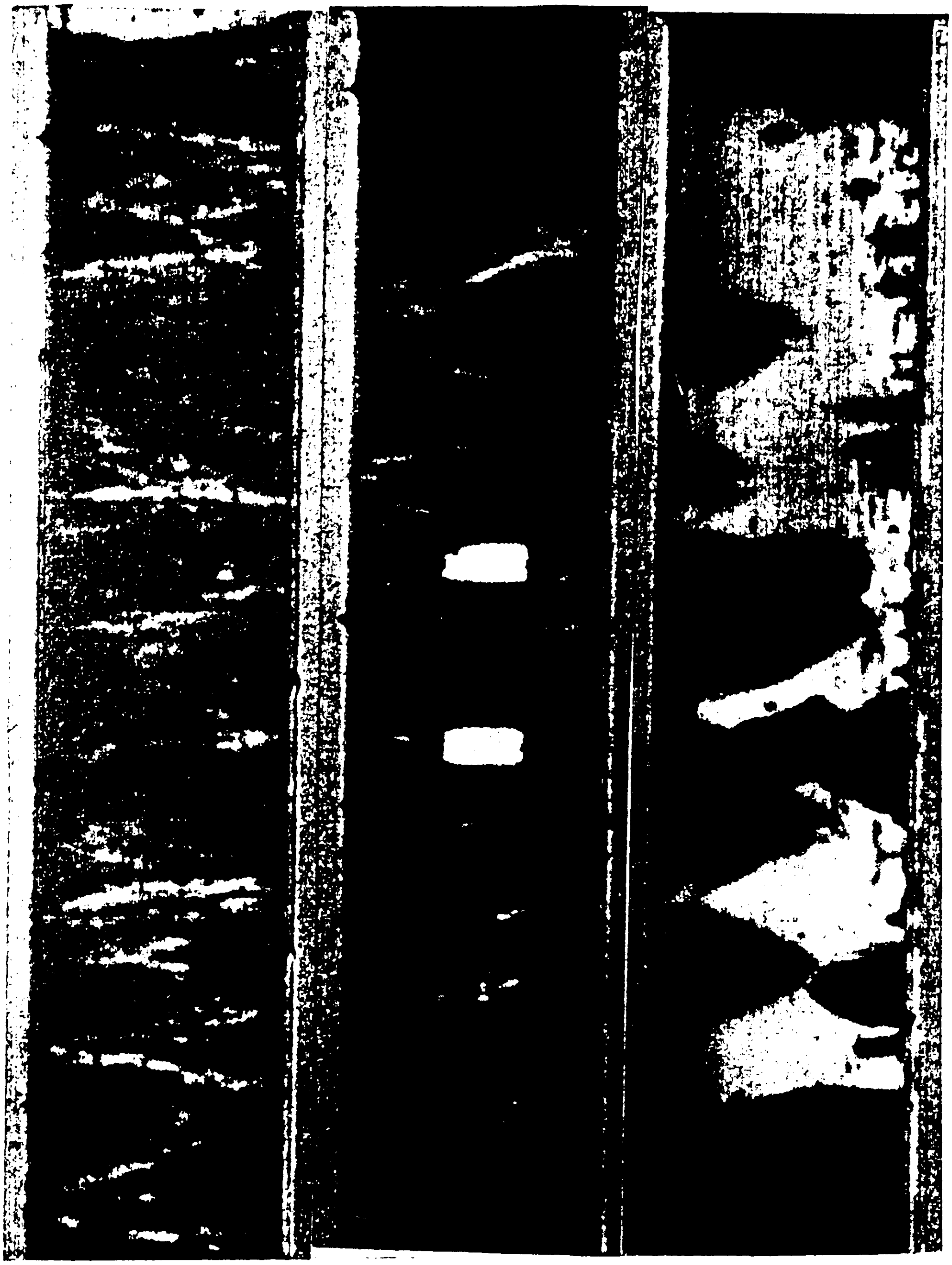

S = 0.4　　S = 0.45　　S = 0.5

Figure 34. C Scans of Long Life Specimens

3.2.5 STIFFNESS MONITORING

Secant and unloading moduli were monitored for all fatigue and residual strength specimens. Strains were recorded at zero, minimum, mean and maximum loads numerous times throughout each test. Stress-strain curves were plotted as shown in figure 35. Secant modulus is evaluated using the strains at minimum and maximum loads on the loading curve. Unloading modulus is evaluated using the maximum and mean loads on the unloading curve.

A comparison of secant and unloading moduli values for specimen SA2F-2-1, cycled at S=0.6, is shown in figure 36. The effect of strain hardening is evident at the early stages of life. After damage develops and the stiffness is reduced, the curves are similar in shape and value. Figure 37 shows the same data where the stiffness is reduced by its initial value; the same trends are present, but the value of the reduced unloading modulus is always below one. The amount of strain hardening (change in initial elastic modulus) and plastic (irrecoverable after unloading) deformation are listed in table 15 for all stress levels. The trend is of increasing hardening for higher load and amount of plastic deformation.

Unless otherwise specified, the reduced unloading modulus is always reported henceforth (and refered to as stiffness), since it seems to represent normalized stiffness changes due to damage and is not affected by strain hardening effects. Johnson [55] investigated

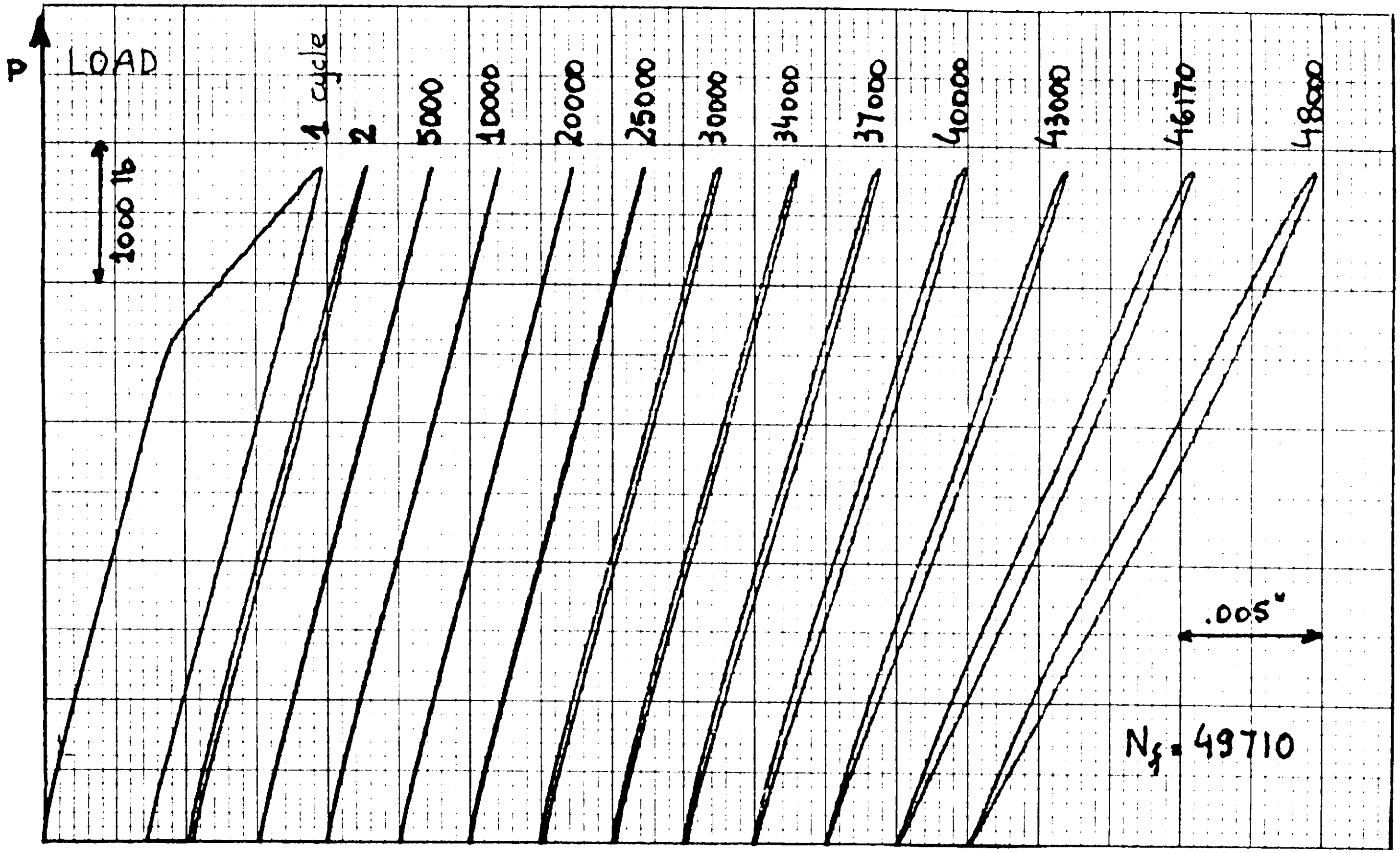

Figure 35. Family of Load-Strain Curves for SA2F-2-1 (S=0.6)

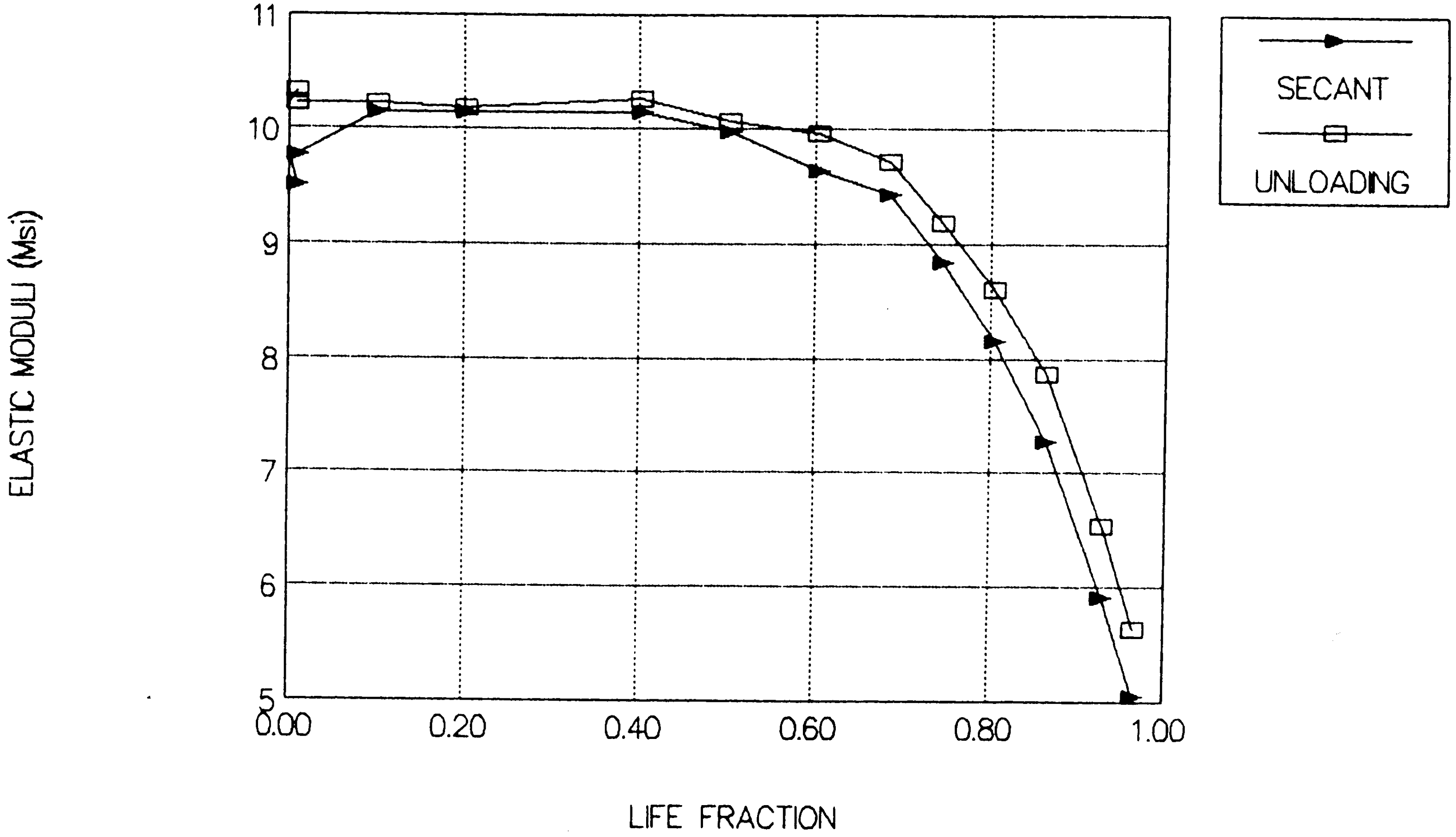

Figure 36. Secant and Unloading Moduli vs. Life Fraction for SA2F-2-1 (S=0.6)

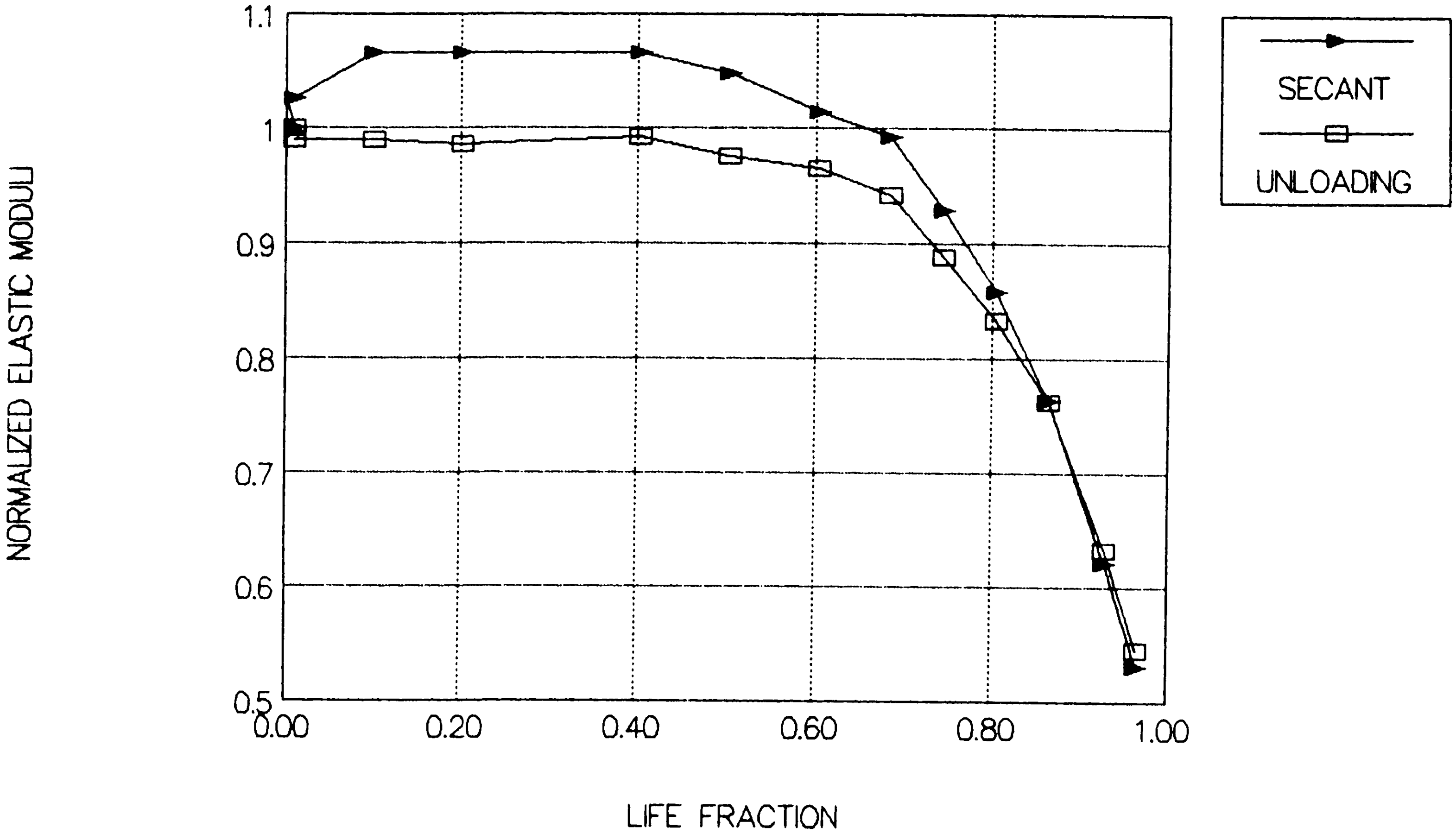

Figure 37. Normalized Secant and Unloading Moduli

vs. Life Fraction for SA2F-2-1 (S=0.6)

Table 15. Plastic Deformation and Strain Hardening in Fatigue Specimens of Arall 2

S[a]	Specimen	Initial[b] Mod(Msi)	Max. Secant[c] Mod. (Msi)	Average[d] % Strain Hardening	Average[e] Initial $\Delta\varepsilon_{pl}$
0.9	SA2F-1-5	9.31	9.99		
	SA2F-2-3	9.23	9.92		
	SA2F-1-9	9.03	9.76	7.62	0.01
0.8	SA2F-1-11	9.61	10.31		
	SA2F-1-1	9.23	10.07		
	SA2F-2-2	9.24	10.16	8.78	0.0085
0.7	SA2F-1-8	9.27	10.09		
	SA2F-1-2	9.26	9.89		
	SA2F-2-6	9.15	9.77	7.48	0.00625
0.6	SA2F-2-1	9.51	10.15		
	SA2F-1-10	9.40	9.96		
	SA2F-1-4	9.77	10.15	5.53	0.00383
0.5	SA2F-1-12	9.43	9.73		
	SA2F-2-8	9.39	10.02		
	SA2F-1-6	9.06	9.59	5.25	0.00167
0.45	SA2F-4-7	9.35	9.73		
	SA2F-4-8	9.57	9.95		
	SA2F-4-3	9.36	9.83	4.35	0.00042
0.4	SA2F-4-6	9.46	9.58		
	SA2F-4-10	9.75	9.90		
	SA2F-6-6	9.68	9.71	1.04	0.00

(a) S, stress level (b) From initial slope at first cycle

(c) based on $(\varepsilon_{max}-\varepsilon_{min})$ (d) Average percent for stress level

(e) Average plastic deformation on first cycle the fatigue damage mechanisms in metal matrix composites and reported the same phenomena.

An identical set of normalized stiffness data for specimen SA2F-4-3 (S=0.45) is shown vs. log cycles and life fraction in figures 38 and 39. Obviously, the representation of log cycles magnifies the early stages of life and dwarfs the latter events, creating the illusion of very rapid changes in response, or sudden death. Life fraction is closer to reality and allows for a better comparison of trends among specimens with different lives. For that reason, life fraction was chosen as the normalized time coordinate. In the case of S=0.4, where no failure occurs, life was arbitrarily defined as 2.5 million cycles (fitted from S/N curve parameters).

Excellent repeatability in the data is demonstrated in figure 40, where the reduced stiffness curves of three specimens tested at the same stress level (S=0.5) are presented. A set of typical curves for stress levels varying from 0.9 to 0.4 is depicted in figure 41.

Stiffness of specimens cycled at the higher stress levels, S=0.9 and S=0.8, remains constant until near the end of life. Failure occurs within relatively few cycles, and is preceeded by cracks in the outer aluminum layers forming at the edges and rapidly growing across the width of the specimen.

At intermediate stress levels, S=0.7 and 0.6, crack growth is slower and a sufficient number of stiffness measurements can be recorded to represent these events. A sharp drop in stiffness precedes

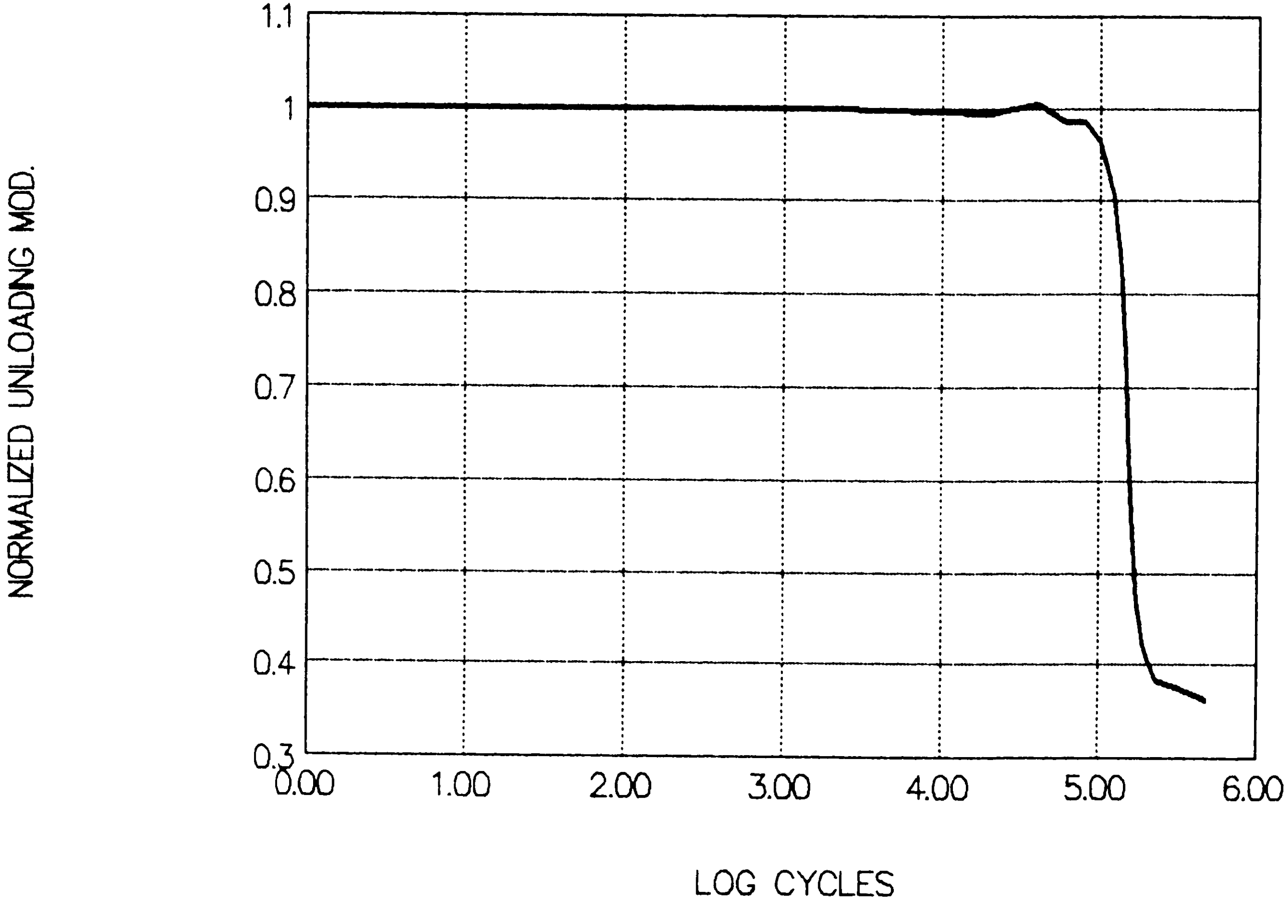

Figure 38. Normalized Stiffness vs. Log cycles, SA2F-4-3 (S=0.45)

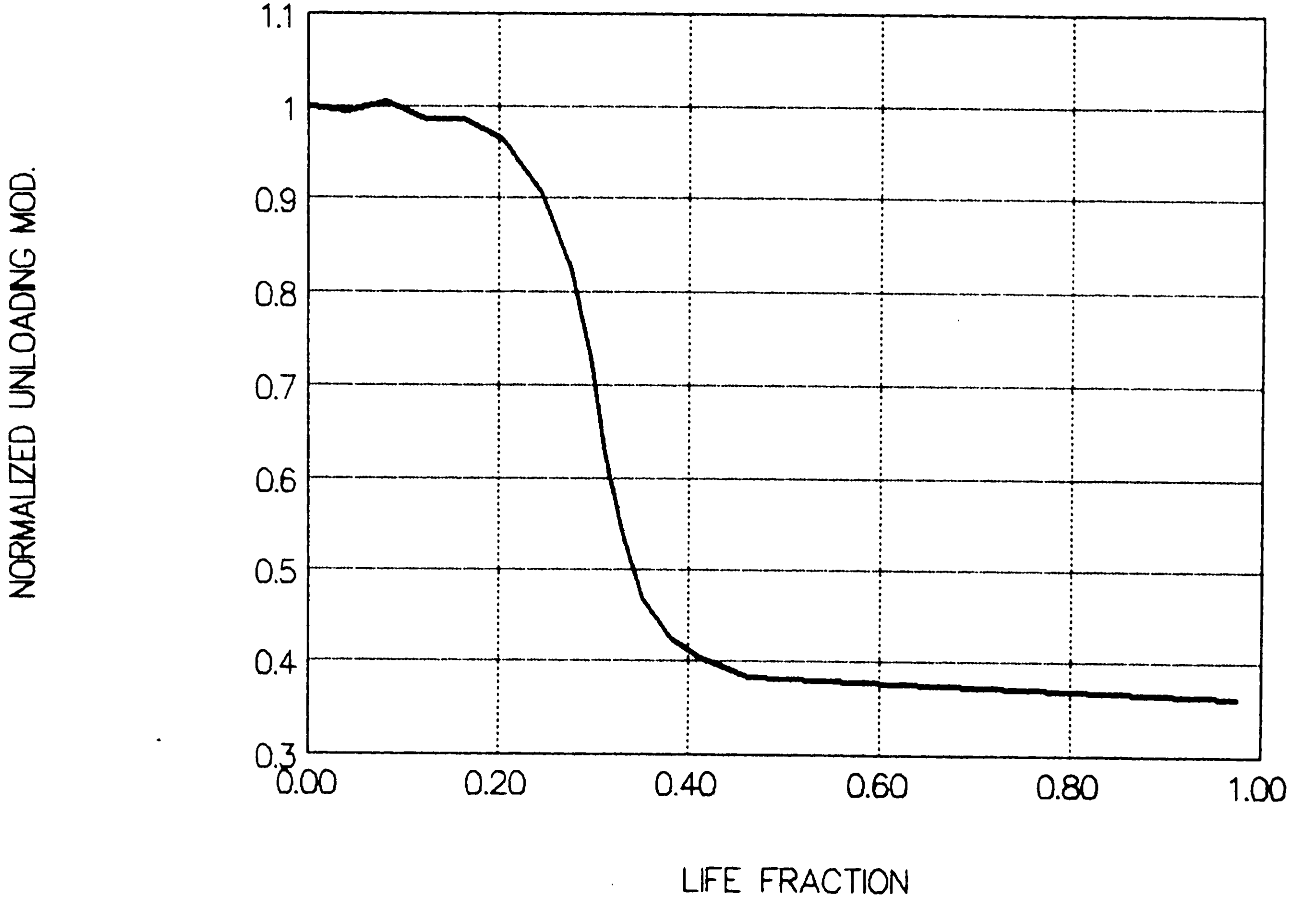

Figure 39. Norm. Stiffness - Life Fraction, SA2F-4-3 (S=0.45)

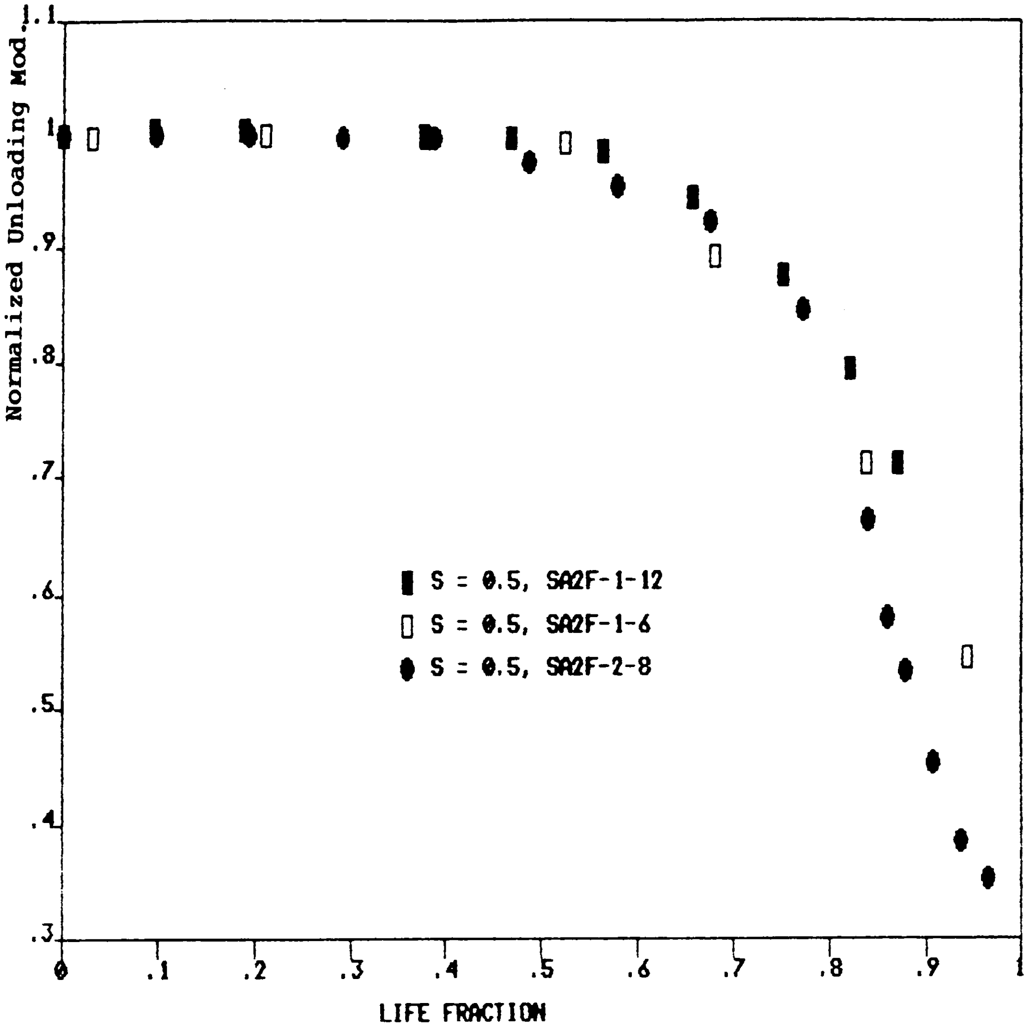

Figure 40. Norm. Stiffness - Life Fraction for

Three Specimens Tested at S = 0.45

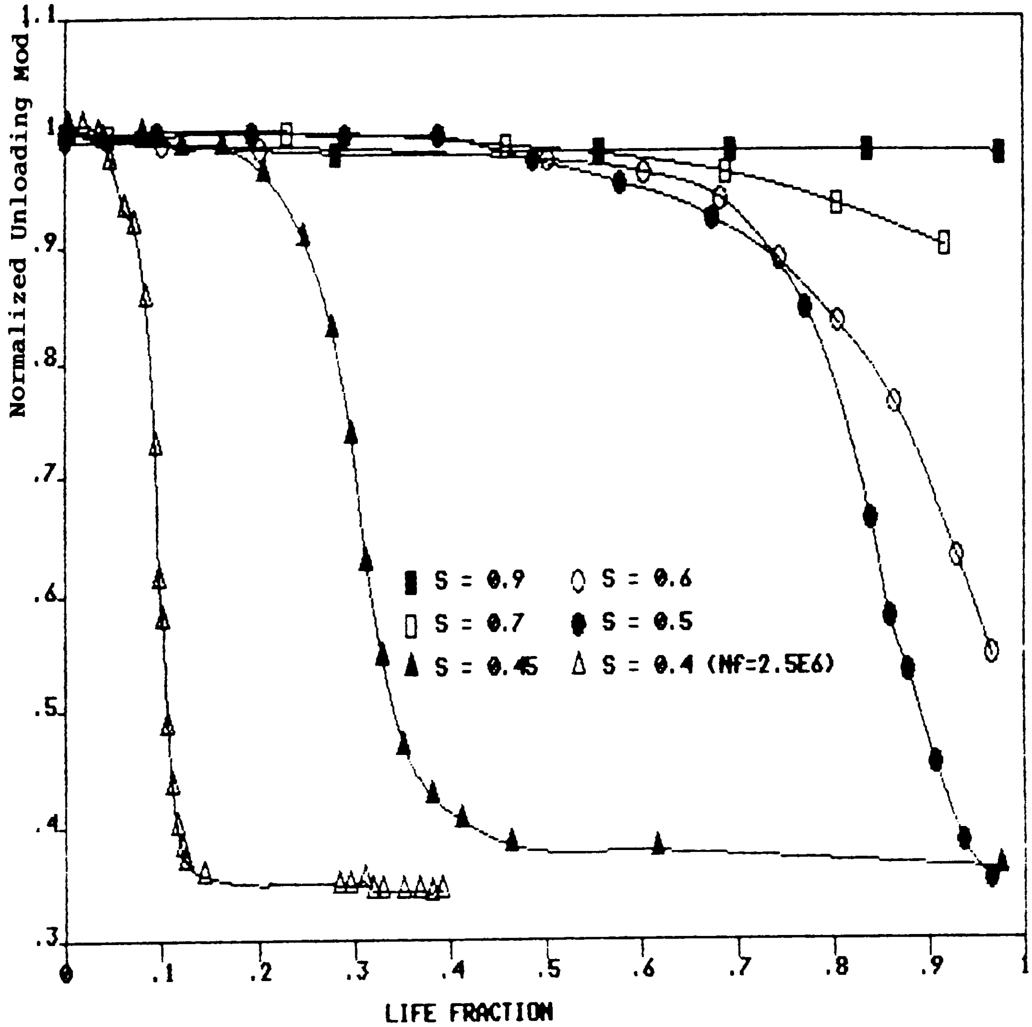

Figure 41. Normalized Stiffness vs. Life Fraction for

S = 0.4 to S = 0.9

the final failure, which occurs shortly before the cracks in the aluminum layers reach across the width of the specimen.

At S=0.5, the stiffness degradation rate decreases near the end of life. The specimens fail shortly after the cracks in the aluminum plies have propagated across the width of the specimen.

At S=0.45 and less, the residual stiffness reaches a stable value after a period of rapid deterioration corresponding to cracks developing in the aluminum layers and reaching a stable pattern. This secondary stable stiffnes is reduced very slowly for S=0.45 until final failure occurs due to fracture of the K/E layers. Stiffness remains essentially constant at S=0.4.

3.2.6 STRAIN ACCUMULATION

In order to explore the possibility of correlating damage, as measured from stiffness reduction, as well as the evaluation of time dependent effects, the strain accumulated at zero, minimum, mean and maximum load were recorded. The most significant measurements are:

- Strain accumulated at zero load, which reflects the sum of plastic deformation, anelasic and creep strains.
- Strain accumulated at maximum load which represents the additional elastic and plastic strains.

Zero and maximum load strain accumulation for specimen SA2F-4-3 (S=0.45) are shown in figure 42.

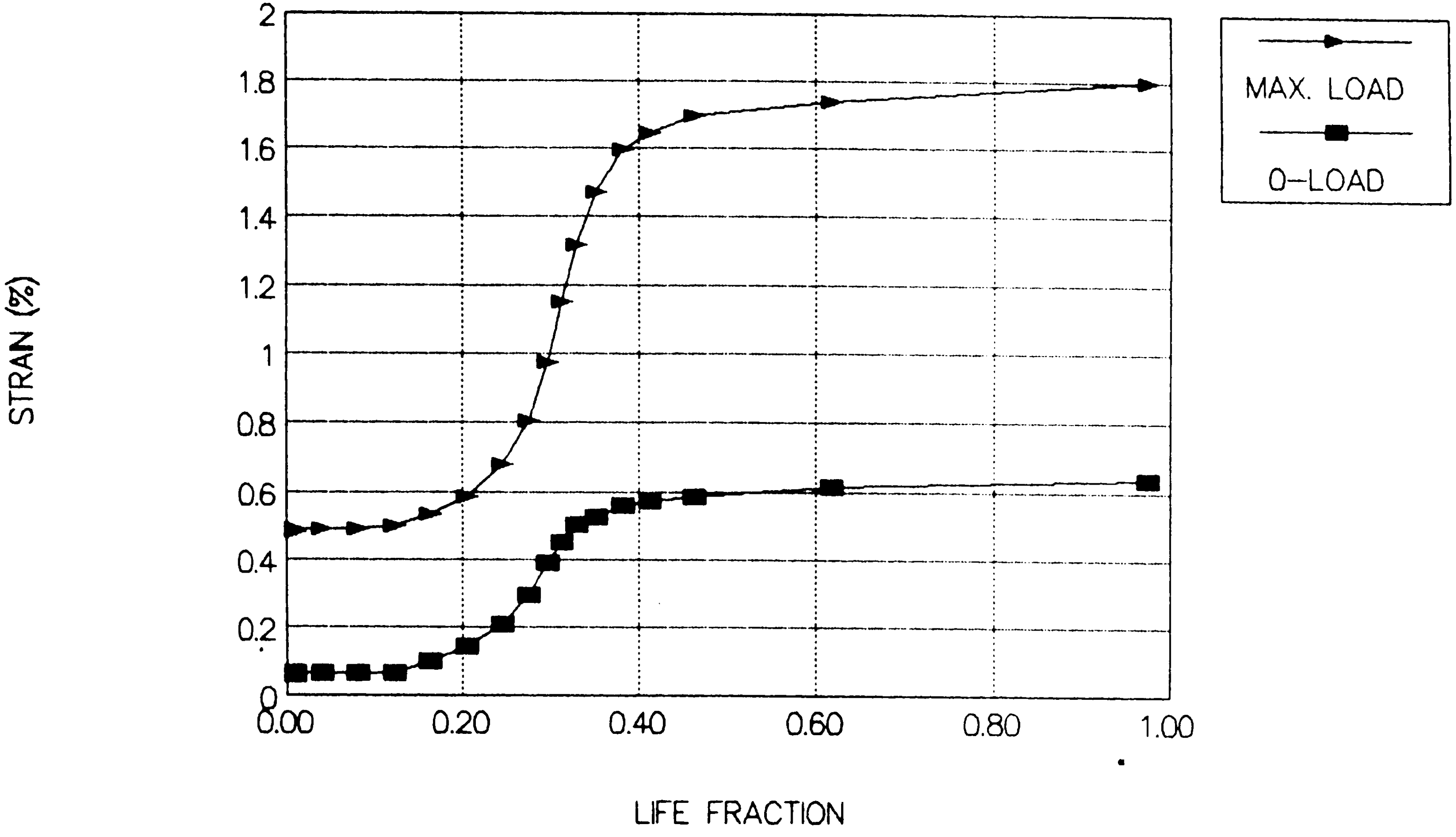

Figure 42. Max.-load and 0-load Strain vs. Life Fraction

for SA2F-4-3, S = 0.45

The total maximum-load strains for specimens tested at S=0.9 to 0.4 are presented in figure 43. The data are extrapolated in dotted lines, from the last data point to n=1. The maximum measured and extrapolated total strains are listed in table 16. Large reductions in stiffness may occur during the last few cycles. The listed extrapolated strains are only a conservative estimate.

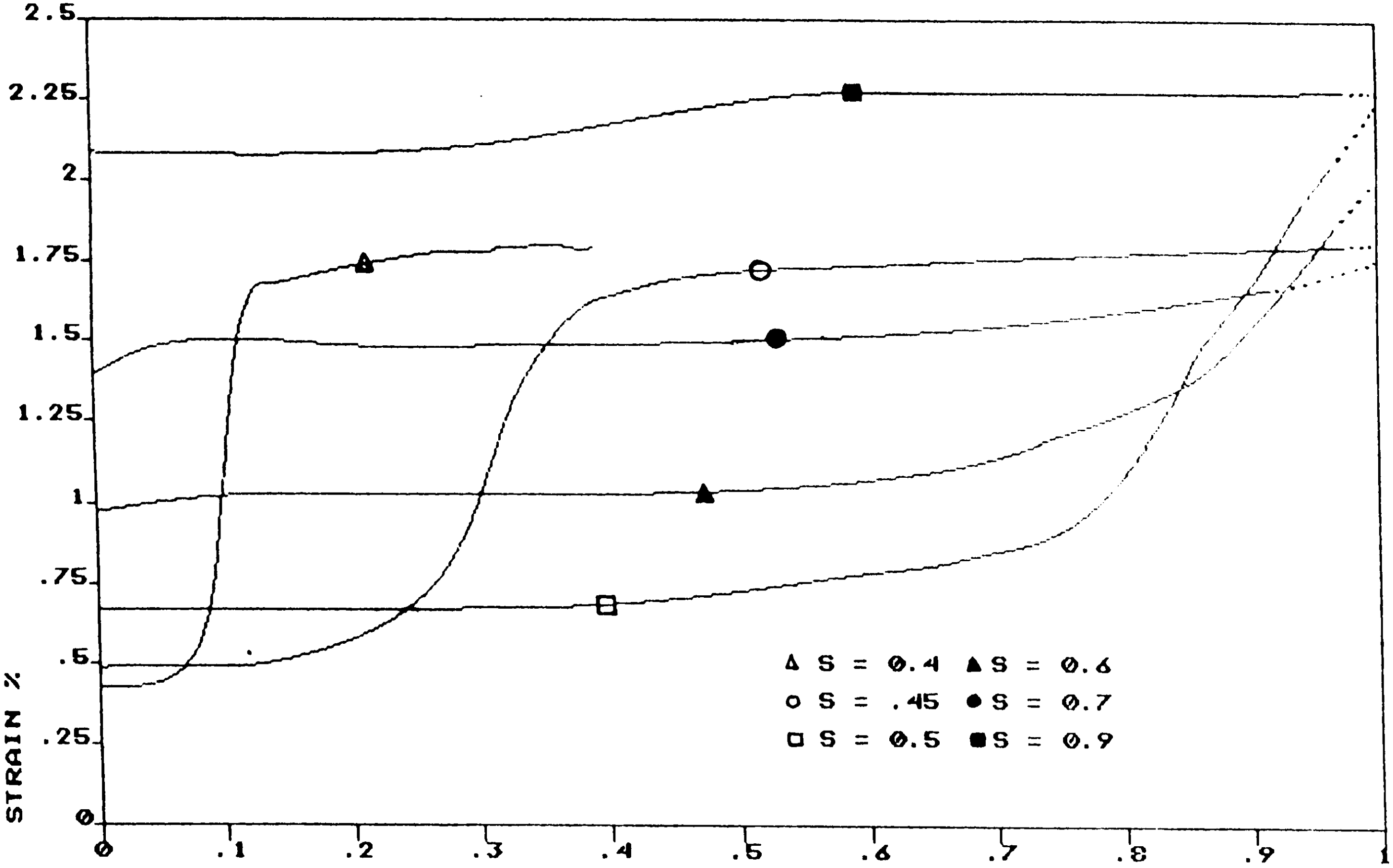

Figure 43. Max.-load Strain vs. Life Fraction for

S = 0.4 to S = 0.9

Table 16. Percent Strain Accumulation During Cyclic Loading

	First Cycle (Unloading) Strain		Last Measured Cycle (Unloading) Strain			Extrapolated Strain @ n=1
S	0-Load	Max load	n^a	0-Load	Max. Load	Max. Load
0.9	1.098	2.085	0.97	1.363	2.279	2.28
0.8	0.812	1.74	0.89	1.017	1.834	NA
0.7	0.642	1.391	0.92	0.909	1.665	1.77
0.6	0.363	0.975	0.97	0.643	1.856	2.06
0.5	0.148	0.666	0.96	0.556	2.047	2.21
0.45	0.018	0.481	0.97	0.556	1.802	1.81
0.4	0.002	0.43	NA	0.508	1.792	NA

(a) n- life fraction

CHAPTER 4

DISCUSSION

A more detailed and general discussion of the findings reported in chapter 3 is presented in this chapter. An effort is made to interweave the results from all experimental techniques, in order to offer a comprehensive phenomenological description of the damage process occuring in tension-tension fatigue of Arall 2 laminates. Where relevant, hypotheses not yet fully supported by the available data are ventured. Similarly, comments and observations made during the experimental program are reported.

4.1 QUASI STATIC TESTS

Quasi static stress-strain curves for virgin specimens and specimen cycled at stress levels of S=0.4, 0.45 and 0.5 are shown in figures 44, 45 and 46. Looking at the details on these pictures, and the data summarized in chapter 3, the following observations can be made.

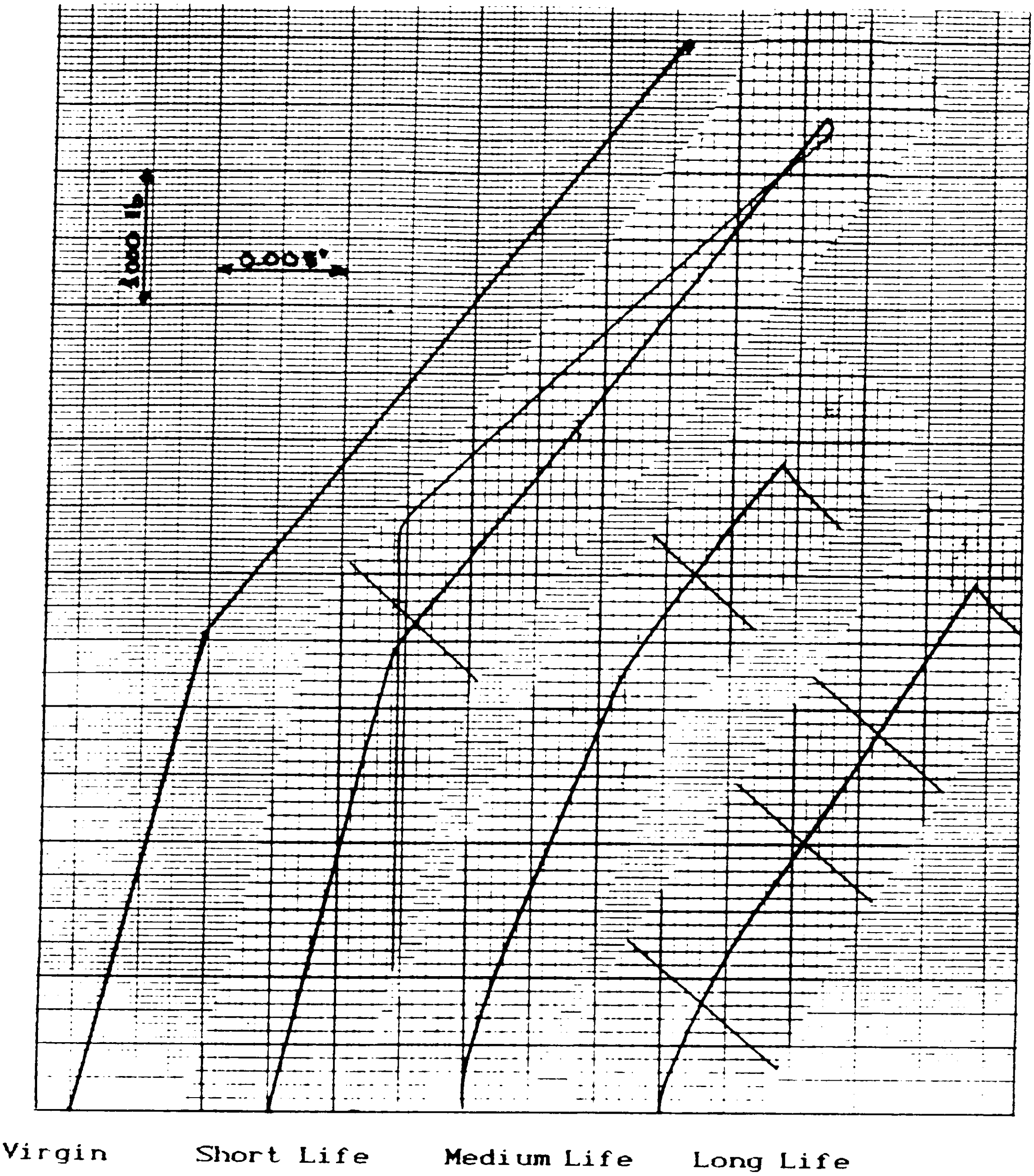

Figure 44. Quasi Static Load-Strain Curves for S = 0.4

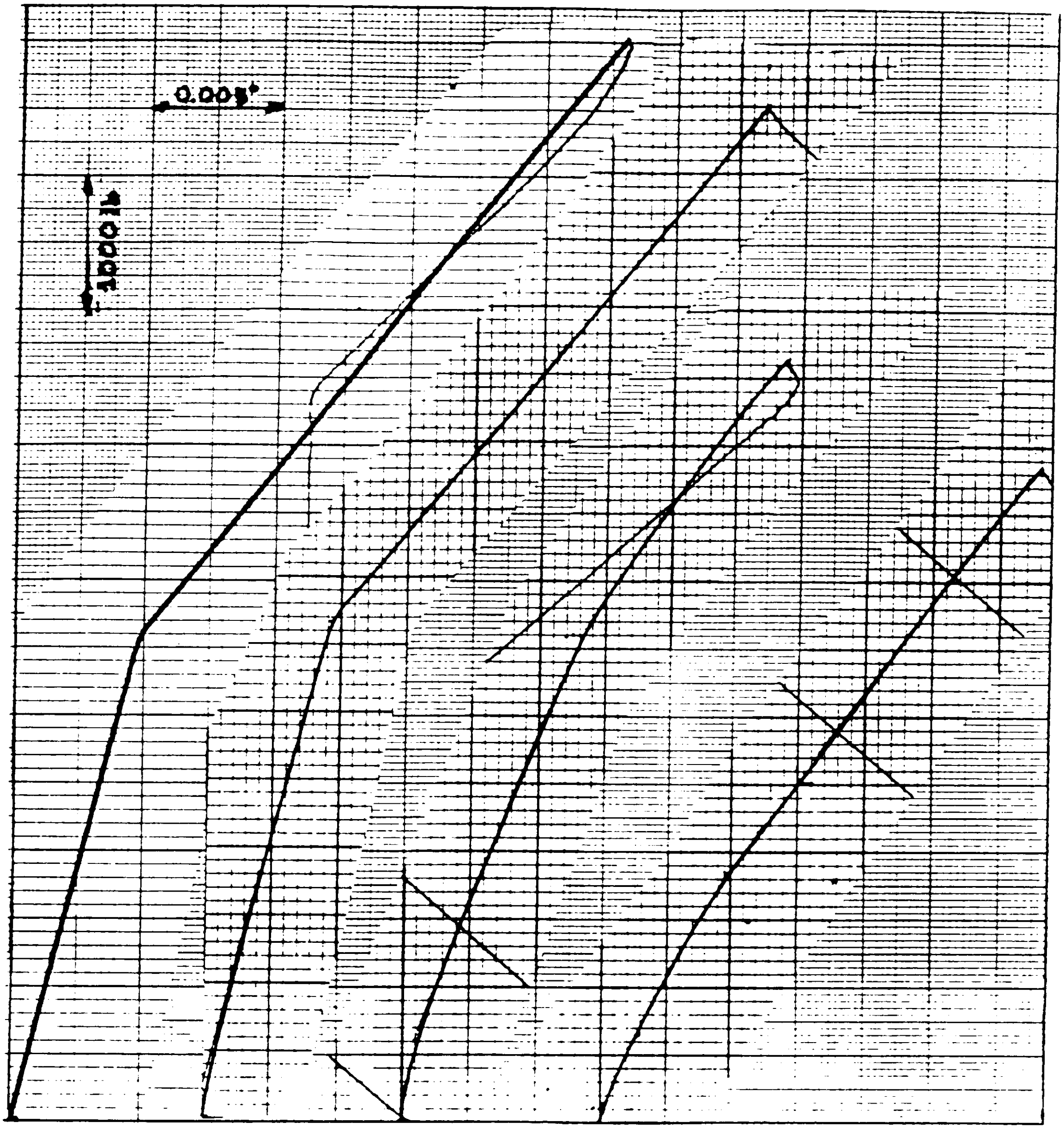

Figure 45. Quasi Static Load-Strain Curves for S = 0.45

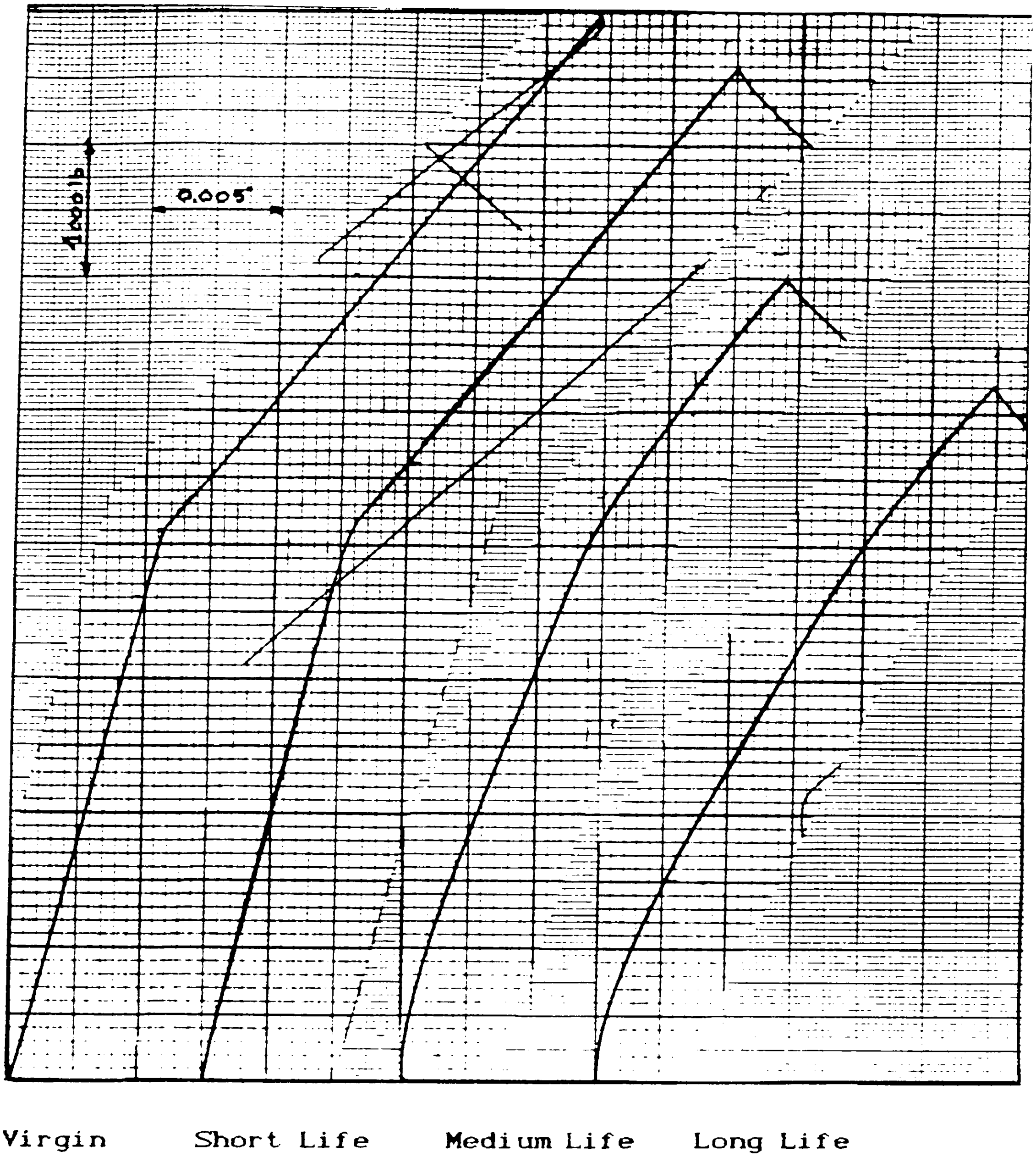

Figure 46. Quasi Static Load-Strain Curves for S = 0.5

- The ultimate tensile strength - 104 Ksi - corresponds to the sum of the individual contributions of the components at the fracture strain, as shown in (7a).

$$UTS = \frac{t_{Al}}{t_{tot}} \times \sigma_{Al}^{\varepsilon=.024} + \frac{t_{K/E}}{t_{tot}} \times \sigma_{K/E}^{ult} =$$

$$UTS_{Arall} = \frac{.036}{.052} \times 60 + \frac{.016}{.052} \times 200 = 103 \text{ Ksi} \qquad (7a)$$

- During cyclic loading, the initial elastic modulus increases to the unloading value when no damage is present and then decreases in magnitude with progressive damage in the form of cracks and delaminations.

- The secondary elastic modulus values of 2.92 to 3.14 Msi correspond essentially to the contribution of the K/E layers. Assuming total delamination and stiffenning of the fiber plies due to cyclic loading to the value of 10.4 Msi (as measured by Pindera and coworkers [54] for monotonic loading), the predicted secondary stiffness is given by (7b).

$$E_s = \frac{t_{K/E}}{t_{tot}} * E_{K/E} = \frac{.016}{.052} * 10.4 = 3.2 \text{ Msi} \qquad (7b)$$

which is an upper bound on the value of E_s since $E_{K/E} \leq 10.4$ Msi.

- The normalized residual strength, the actual value divided by the virgin strength, decreases for all cyclic stress levels. The normalized residual strength correlates very well with the normalized residual stiffness as shown in figure 19 and equation (6).

At short life fractions there is a small reduction in strength (up to 5%), although no change in stiffness is measured and there is no evidence of damage in the C-scans. It is possible that early damage consists of matrix cracks, not detectable by the C-scan or, that localized damage starting at the edges is not detected by the extensometer positioned at the center of the specimen.

At intermediate life ($E(n)=0.7$), strength is reduced from 30% for $S=0.5$ to 42% for $S=0.4$. The cracks in the aluminum plies have a double effect. They reduce the ability of the aluminum plies to carry load and create local stress concentrations that reduce the strength of the fiber reinforced plies.

Sun and Jen [64] isolated the effect of off-axis plies cracks (analogous to the aluminum plies in Arall laminates) on the laminate strength by introducing a thick adhesive layer between the 0-degree plies and off-axis plies. The presence of the adhesive arrested the cracks from propagating into the 0-degree plies and reduced the stress concentration on the 0-degree plies. The difference in strength was found to be in the order of 30% for the graphite-epoxy composite they investigated.

At long lives delamination is almost complete (except for $S=0.5$)

and strength decreases further, depending on stress level. At S=0.45 strength was measured after the degradation of the aluminum plies was complete and a constant secondary stiffness was achieved. The measured laminate residual strength (59.2 Ksi) corresponds to the strength of the fiber plies. Normalizing the laminate residual strength by the area ratio of fiber plies to total crossectional area, yields a strength value of 192 Ksi. At S=0.4 residual strength was measured after 10^6 cycles (51.6 Ksi) while the constant secondary stiffness was achieved after 250000 cycles. The same normalization yields a value of 168 Ksi, or 13% less than the previous case due to further damage to the fiber plies.

- The ultimate strain (at fracture), accumulated strains during cyclic loading and their sum are listed in Table 17. At short and long lives, the total strain is similar to that of the virgin specimens and matches the maximum elongation of the fibers.

At short lives there is no evidence of damage from the C-scans and stiffness measurements. The small drop in residual strength corresponds to the slight difference in total strain. At long lives the specimens are completely delaminated, failure is determined by the fiber plies. At intermediate lives, cracks in the aluminum plies develop while the plies are still bonded to the fiber plies. The presence of cracks causes large local stress concentrations which lead to premature failure.

Table 17. Total Strain % at Fracture of Residual Strength Specimens of Arall 2

S	Initial Plastic ε @ 0-Load	Accumulated Strain @ 0 load	Ultimate Strain @ Fracture	Total Strain	Average
0.4	0	0.006	2.13	2.13	
Short	0	0.004	2.15	2.15	
	0	0.005	2.25	2.30	2.20
0.4	0.002	0.285	1.35	1.63	
Med.	0.002	0.269	1.20	1.47	
	0.001	0.217	1.15	1.37	1.49
0.4	0.002	0.506	1.85	2.36	
Long	0.004	0.539	1.90	2.44	2.40
0.45	0.068	0.011	2.35	2.43	
Short	0.053	0.004	2.10	2.16	
	0.054	0.006	2.18	2.24	2.28
0.45	0.028	0.468	1.25	1.75	
Med.	0.026	0.304	1.38	1.71	
	0.024	0.277	1.43	1.73	1.73
0.45	0.083	0.598	1.73	2.41	
Long	0.044	0.614	1.65	2.31	
	0.040	0.400	1.63	2.07	2.26
0.5	0.197	0.012	2.00	2.21	
Short	0.168	0.007	2.20	2.38	
	0.207	0.007	1.98	2.19	2.26
0.5	0.148	0.288	1.30	1.74	
Med.	0.120	0.270	1.15	1.54	
	0.150	0.324	1.45	1.92	1.73
0.5	0.172	0.353	1.33	1.85	
Long	0.191	0.469	1.20	1.86	
	0.164	0.546	1.48	2.19	1.97

Equation (8) defines the ratio of the maximum applied load S_{max}, and the crossectional area of the K/E layers divided by the ultimate strength of the fiber plies as SR. The values of SR are listed in table 18 assuming that the ultimate stress of the fiber plies is 200 Ksi instead of 165.5 Ksi as reported by Pindera [54].

$$SR = \frac{S_{max}}{\text{Area K/E}} * \frac{1}{\sigma_{ult}^{K/E}} \qquad (8)$$

A value of 200 Ksi is consistent with the calculations of Teply [5], the stresses predicted using figures 2 and 48 and the previous discussion of residual strength results. Sun and Jen [64] measured the effect of the number of plies on the strength of a unidirectional graphite-epoxy composite. By measuring the strength of $[0]_2$, $[0]_4$ and $[0]_6$ configurations, they extrapolate and conclude that strength is dependent on the number of plies and that a single ply is approximately 20% stronger than the $[0]_6$ configuration, which is consistent with the assumption stated above.

Due to the lack of any data regarding the fatigue behavior of the SP-366 composite, equation (9) is used to fit the fiber manufacturer's fatigue data [58] for K/E unidirectional composite (R=0.1) as a first order approximation.

$$\frac{S_{max}}{S_{ult}} = -0.45489 + 1.6969*(\log N_f)^{-0.202} \qquad (9)$$

The ratio SR indicates that there is a transition point at S=0.6 where SR has a value of less than one. Only at stress levels less than 0.6 are the fiber plies able to carry the maximum load by themselves. Keeping this fact in mind and using equation (9) to evaluate and approximate the remaining life after complete degradation of the aluminum plies, the following observations were made.

- At S=0.5 a severe reduction in the load carrying capabilities of the aluminum layers will lead to quick failure of the Arall laminate. It was observed thatshortly after the outer aluminum layers were cracked across the width, the specimens failed. The remaining life for the K/E plies is 6500 cycles, a small fraction of the total life.
- At S=0.45 there exists the possibility of the K/E layers carrying all of the load for a significant number of cycles. Indeed, the stiffness curves and the residual strength data (chapter 3) suggest that after the aluminum layers have been completely degraded and delaminated, the specimen still carries the load at a reduced - slowly decreasing - stiffness. The remaining life predicted by (9) is 169000 cycles, in the same order of magnitude as the observed remaining life, 387000 cycles.
- At S=0.4 no cyclic failures were recorded. Equation (9) yields an estimate of 35 million cycles for the remaining life, i.e. the cyclic load causing complete degradation of the aluminum plies is only a small fraction of the potential of the fiber plies.

4.2 FATIGUE RESPONSE

4.2.1 THE S/N CURVE

The fatigue response of K/E and that of 2024-T3 aluminum have been superimposed on the S/N curve for Arall 2 on figure 47. In order to do so, the strains at maximum and minimum load were used to evaluate the stresses and stress ratios in the K/E and aluminum layers for each stress level, using figure 48. These stresses were then normalized by the ultimate strength of each component. The fiber ply response is plotted according to (9) and the aluminum ply response is plotted according to (10).

$$\log N_f = 11.1 - 3.97 * \log (S_{max} * (1-R)^{.56}) - 15.8) \qquad (10)$$

Where N_f, S_{max} and R are the life, maximum stress and stress ratio respectively, in the aluminum plies.

Clearly, at high stress levels, S>0.5, the fatigue response of Arall 2 is governed by the aluminum layers, their failure leads to immediate failure of the laminate. At the low stress levels, S≤0.45, the failure of the aluminum layers transfers more load to the K/E layers, whose response controls laminate failure. At 0.6 > S > 0.5 a transition zone occurs. The initial normalized stresses in each component are listed in table 18 for all S values. Columns 4 and 6

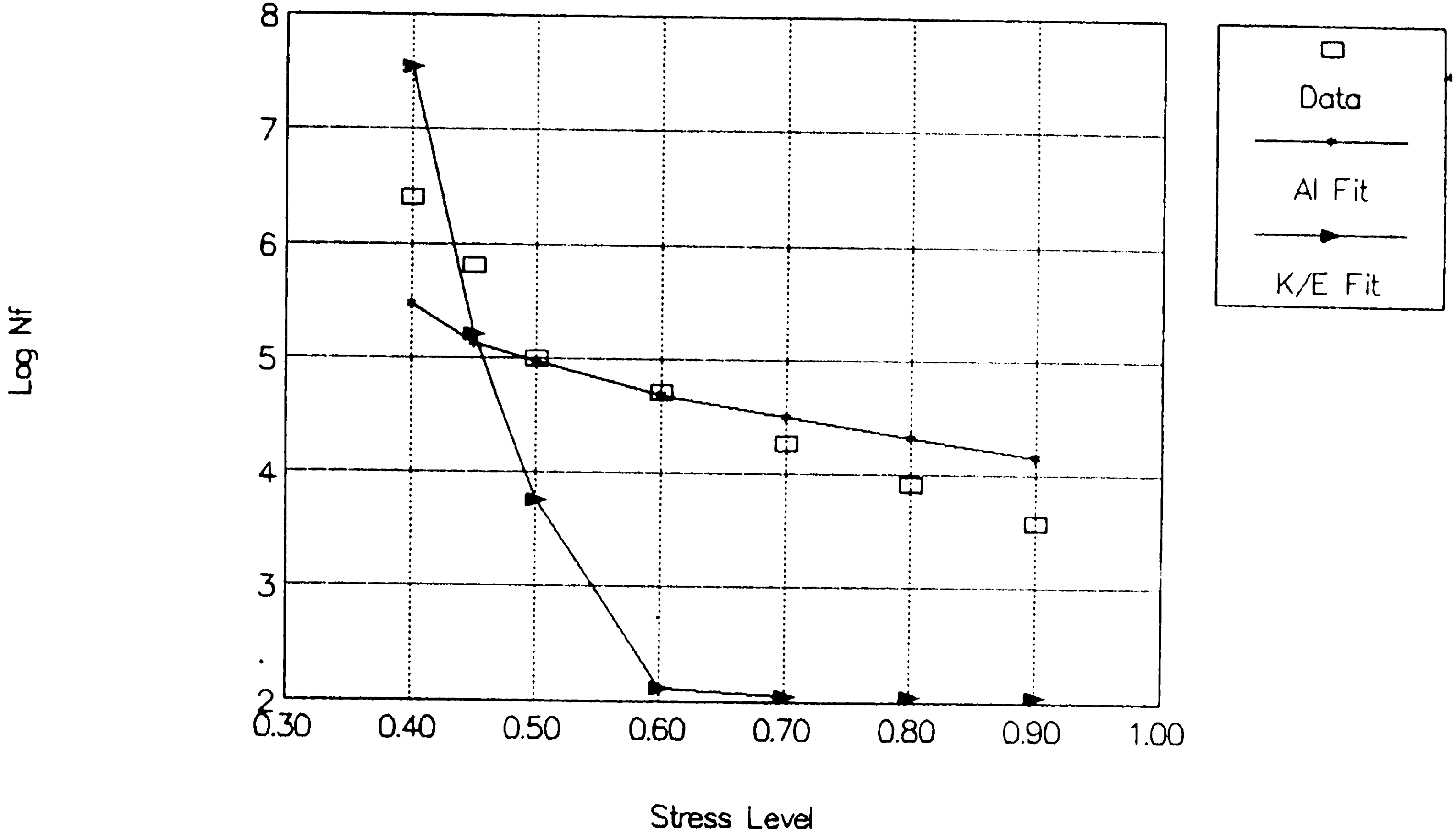

Figure 47. Aluminum and K/E Evaluated Fatigue Performance Superimposed on Arall-2 Data

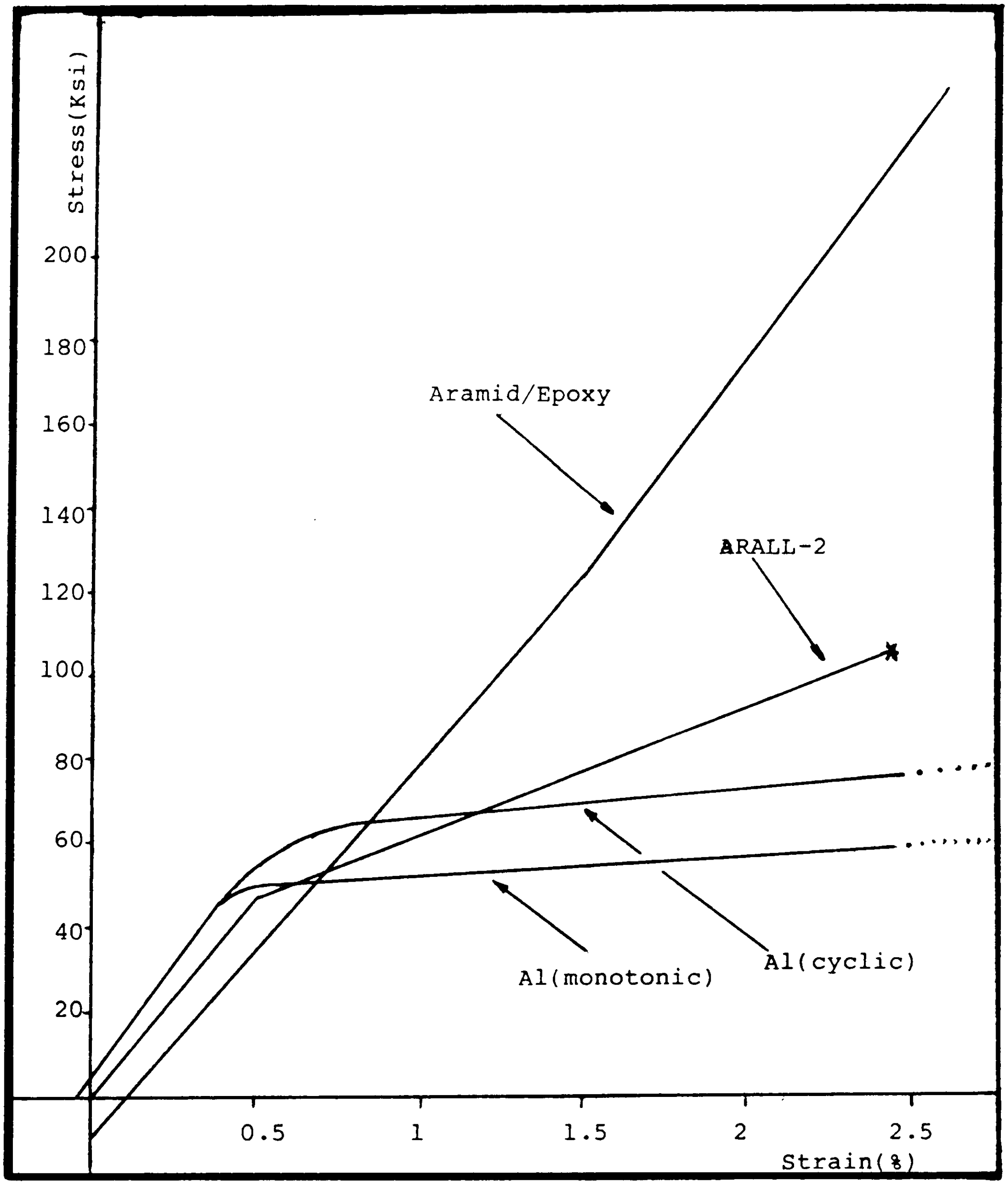

Figure 48. Stress-strain curves for Arall-2, Aluminum and K/E, accounting for Residual Stresses

Table 18. Normalized Stresses for All Plies in Fatigue Specimens of Arall 2

	Aluminum		Aramid/Epoxy		Max. Load Divided by K/E area (Ksi)	
S	σ^{b}max (Ksi)	σ^{b}min (Ksi)	σ^{a}max (Ksi)	σ^{a}min (Ksi)		SR^{c}
0.9	56.8	-29.8	175	97.5	302.9	1.51
0.8	55.0	-22.2	145	77	268.8	1.34
0.7	54.1	-13.9	114	55	235.8	1.18
0.6	54.8	-3.6	78	28	201.2	1.01
0.5	52.8	4.0	50	8	168.8	0.84
0.45	52.7	8.6	33.5	-4	152.1	0.76
0.4	46.9	8.6	29	-6	134.6	0.67

(a) Calculated from maximum and minimum strain of first cycle.

(b) Calculated by substracting (a) from the global loads.

(c) Assuming $\sigma^{ult}_{K/E}$ = 200 Ksi.

comprise the theoretical range of stress being transfered to the fiber layers. In reality, the stress in the fiber layers cannot exceed their ultimate strength.

4.2.2 STIFFNESS REDUCTION

Stiffness is perhaps the most significant observable monitored during cyclic loading. Its importance resides in the fact that it is a easily mesurable quantity and can be directly correlated to damage if the unloading modulus is used, as suggested by Johnson [55] for metal matrix composites.

Stiffness changes could be correlated with crack development, crack growth (see figures 25 to 30 of crack patterns at different stiffnesses) or delaminations (see C-scans on figures 31 to 33). But this study is concerned with the performance aspects of the fatigue response, i.e. how stiffness reduction is related to loading conditions, life and eventually residual strength.

Stiffness reduction data may be fitted using a general evolutionary equation of the form,

$$E_{n+1} = E_n * \mu \; (1 - E_n) \qquad (11)$$

Although a reasonable fit can be achieved and the evolutionary form lends itself to numerical procedures easily, no particular meaning or trend could be found for the parameters - μ and E_o - that determine the shape of the curve.

A polynomial of adequate order could be fit easily,

$$E_n = E_o * (1 + A*n + B*n^2 + C*n^3 + D*n^4 +...) \qquad (12)$$

but again the coeffients are meaningless.

Instead, the reduced stiffness vs. life fraction curves were fitted with a modified power law of the form

$$E(n) = E_o + \frac{E_s - E_o}{(1 + \tau/\lambda)^{\mu}} \qquad (13)$$

where E_o is the initial stiffness, E_s is the secondary stiffness and two parameters define the curve. The first one - τ - moves the curve in the time ordinate and the second - μ - determines the slope. λ, the time ordinate was transformed using the following relationship,

$$\lambda = 10 \hat{} (10 * n) \qquad (14)$$

The values of these parameters for S=0.6 to 0.4 are listed in table 19 and were fitted as functions of stress level S as,

$$\mu(S) = 0.3687 + 9.1279E\text{-}5*(S)^{-11.56} \qquad (15)$$

and,

$$\tau(S) = 10 \,\hat{}\, \left[\frac{10}{(1+10\hat{}(4.75-10\hat{}S))^{1.25}} \right] \qquad (16)$$

The fitted curves for S=0.4 to 0.6 are presented in figure 49.a. Using (15) and (16) in the reduced stiffness equation (13), a three dimensional surface may be obtained, as shown in figure 49.b. The reduced stiffness is a function of stress level and life fraction.

4.2.3 TIME DEPENDENT EFFECTS

The non linear viscoelastic behavior of the Kevlar fibers and the K/E composite add another dimension to the already complex fatigue response of Arall 2 laminates.

As previously shown, the stress levels sustained by the K/E layers are large and increase as the damage in the aluminum develops and load is transfered to the fiber layers. Ho and Schapery [52] conclude that the creep compliance of the K/E unidirectional composite is dominated by the viscoelastic response of the fibers. Summarizing their experimental investigation, the creep compliance at 75°F was best fitted by,

$$D = 10.6 \; (\; 1 + 0.11 * t^{.06} \;) * 10e\text{-}8 \;\; psi^{-1} \qquad (17)$$

where t is in minutes.

Table 19. Curve Fitting Parameters for Modified Power Law

$$E(n) = E_o + \frac{E_s - E_o}{(1 + \tau/\lambda)^{\mu}} \quad , \lambda = 10\hat{\ }(10*n)$$

S	τ	μ
0.4	10^0.9	4
0.45	10^3.1	1.2
0.5	10^8.3	0.7
0.6	10^9.2	0.4

$$\tau(S) = 10\ \hat{\ } \left[\frac{10}{(1 + 10\hat{\ }(4.75-10*S))^{1.25}} \right]$$

$$\mu(S) = 0.3687 + 9.1279E\text{-}5*(S)^{-11.56}$$

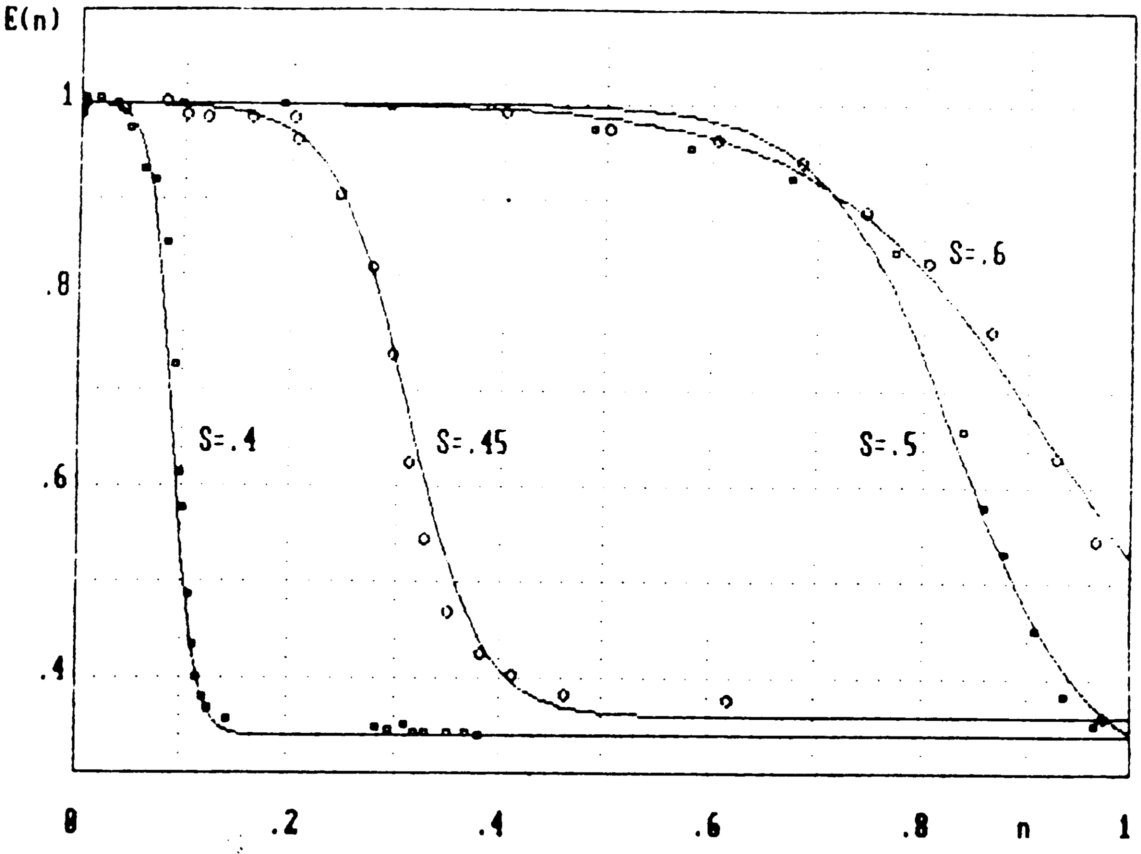

Figure 49.a. Generalized Power Law Fit for Reduced Stiffness vs. Life Fraction Data, S = 0.4 to S = 0.6

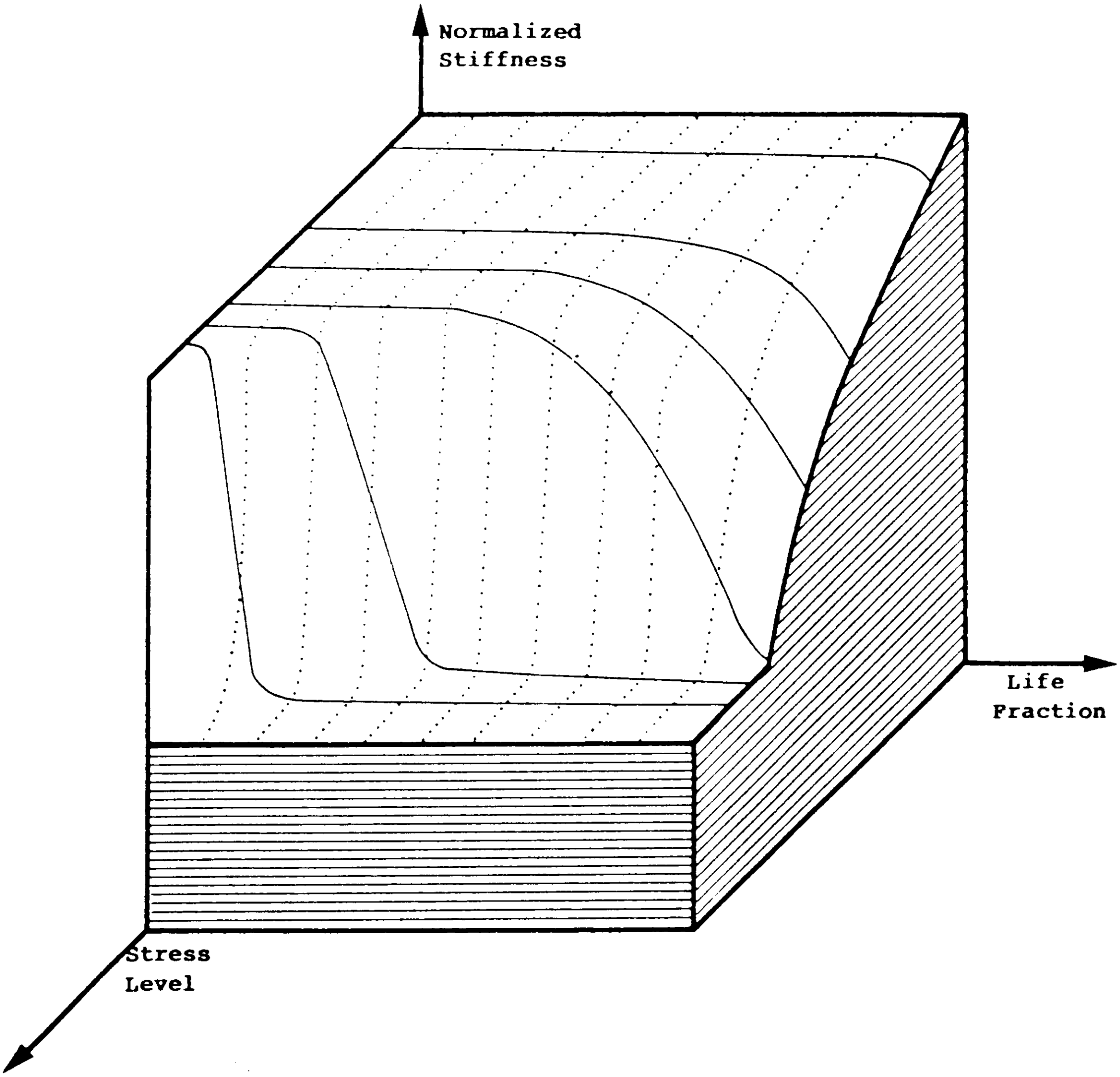

Figure 49.b. Normalized Stiffness Three-dimensional Surface as a Function of Life Fraction and Stress Level

Gramoll [50] fits the non linear viscoelastic compliance of unidirectional K/E in the fiber direction as

$$S_{11} = 10.667*(1-4.448*10^{-8}\sigma_1^2) + 2.515*t^{0.04} \quad \mathrm{TPa}^{-1} \qquad (18)$$

where t is in seconds and σ_1 is the applied stress in MPa.

Assuming that the stress in the fiber plies at the mean cyclic load is a comparable creep stress, the total creep strain after N cycles, $\varepsilon(t)$, may be evaluated using several methods.

Equation (19) is the hereditary Volterra integral,

$$\varepsilon(\sigma(t),t) = \sigma(0)*S(t) + \int_0^t S(t-\tau)\,\frac{\partial\sigma(\tau)}{\partial\tau}d\tau \qquad (19)$$

where S is the time dependent compliance and σ is the applied stress. Equation (19) reduces to equation (20) for creep at constant load, σ_0.

$$\varepsilon(\sigma_0,t) = \sigma_0*S(t) + \sigma_0*\int_c^t \frac{\partial\, S(t)}{\partial\,\tau}\, d\tau \qquad (20)$$

In the present case, the first term that represents the initial elastic compliance has to be modified to include the plastic deformation. Using the code VCAP developed by Gramoll, equation (20) is numerically integrated where S(t) is given by (18). This approximation yields the lower curve in figures 50 to 52.

This first approximation does not take into account the damage sustained by the aluminum layers. The actual mean stress in the K/E layers is continually increasing, accelerating the viscoelastic process. The measured reduced stiffness can be used to evaluate the this effect in the following way,

$$\varepsilon(t) = \frac{\sigma_o}{E_o - E(t)} * D(t) \qquad (21)$$

where the stiffness E(t) is given by (13) and D(t) is given by (17). The results of this approximation are also shown in figures 50 to 52 as the intermediate curve.

The numerical integration of (20) yields a larger strain than measured for the initial part of life but fails to follow the general behavior of the time dependent strain once damage starts.

The approximate values calculated using equation (21) also yield a higher initial strain. The general shape of the curve does fit the measured behavior. The initial discrepancy is attributed to the constraint of the aluminum plies on the fiber plies. The actual stress in the fiber plies may relax, transfering load to the aluminum plies. Once damage starts this trend is reversed and creep is accelerated. The measured strains are larger than predicted. One possible explanation is the rise of temperature of the specimen due to hysteresis heating and dissipation.

The effects of stress nonlinearity are not included in (17) and obviously (18) is a better approximation. Regretfully, the capability

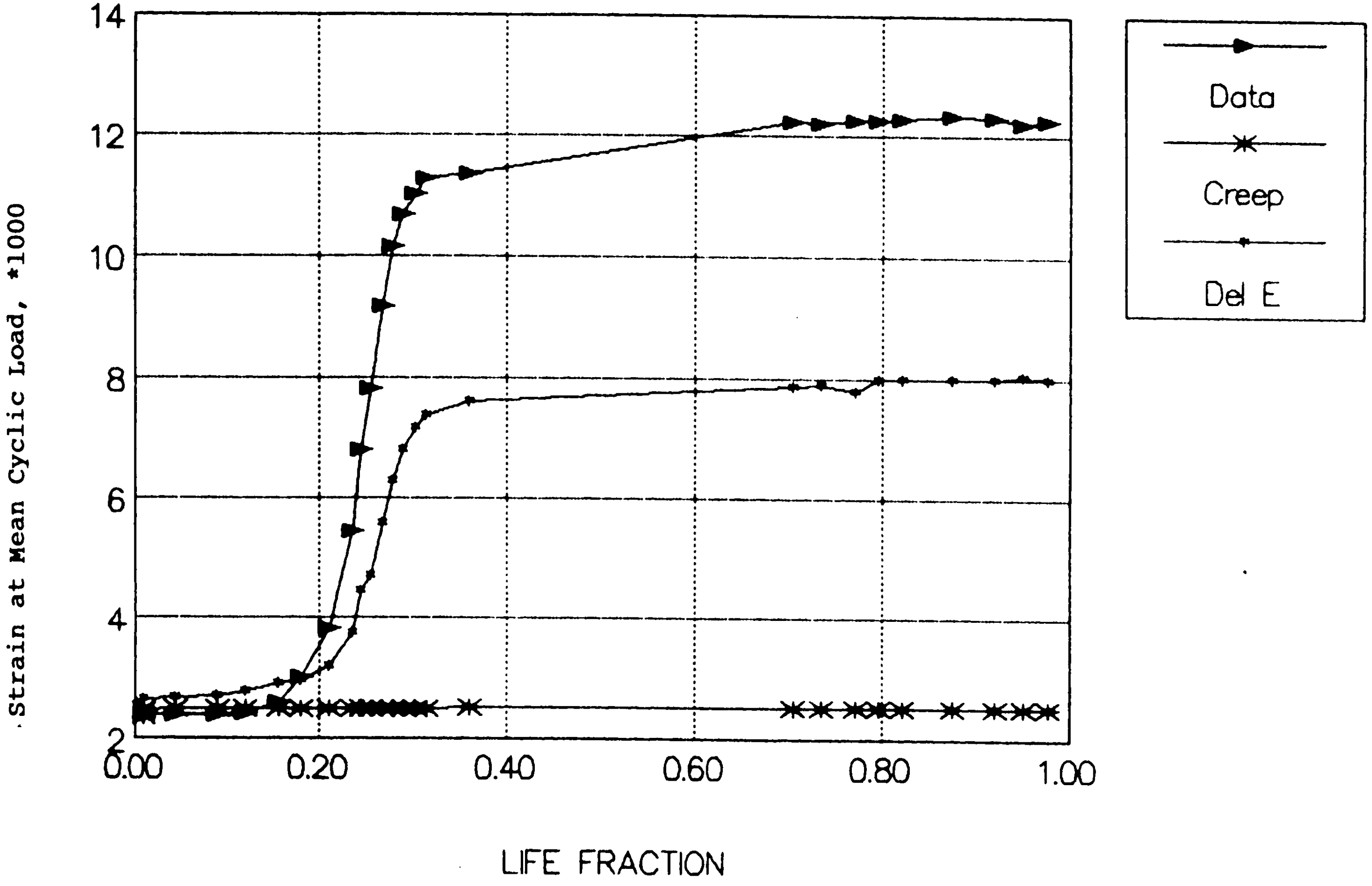

Figure 50. Measured and Predicted Creep Strain for S = 0.4

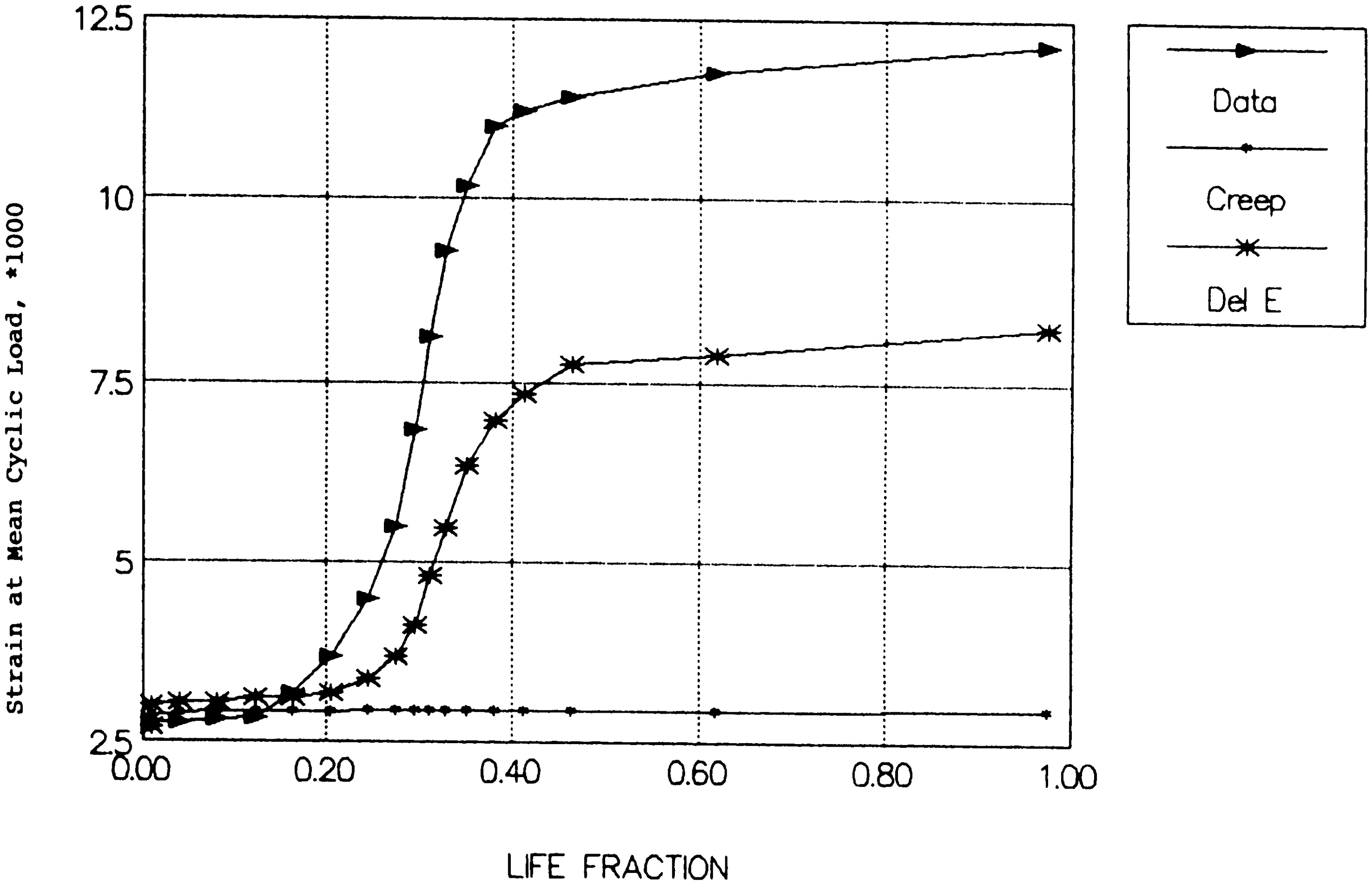

Figure 51. Measured and Predicted Creep Strain, S = 0.45

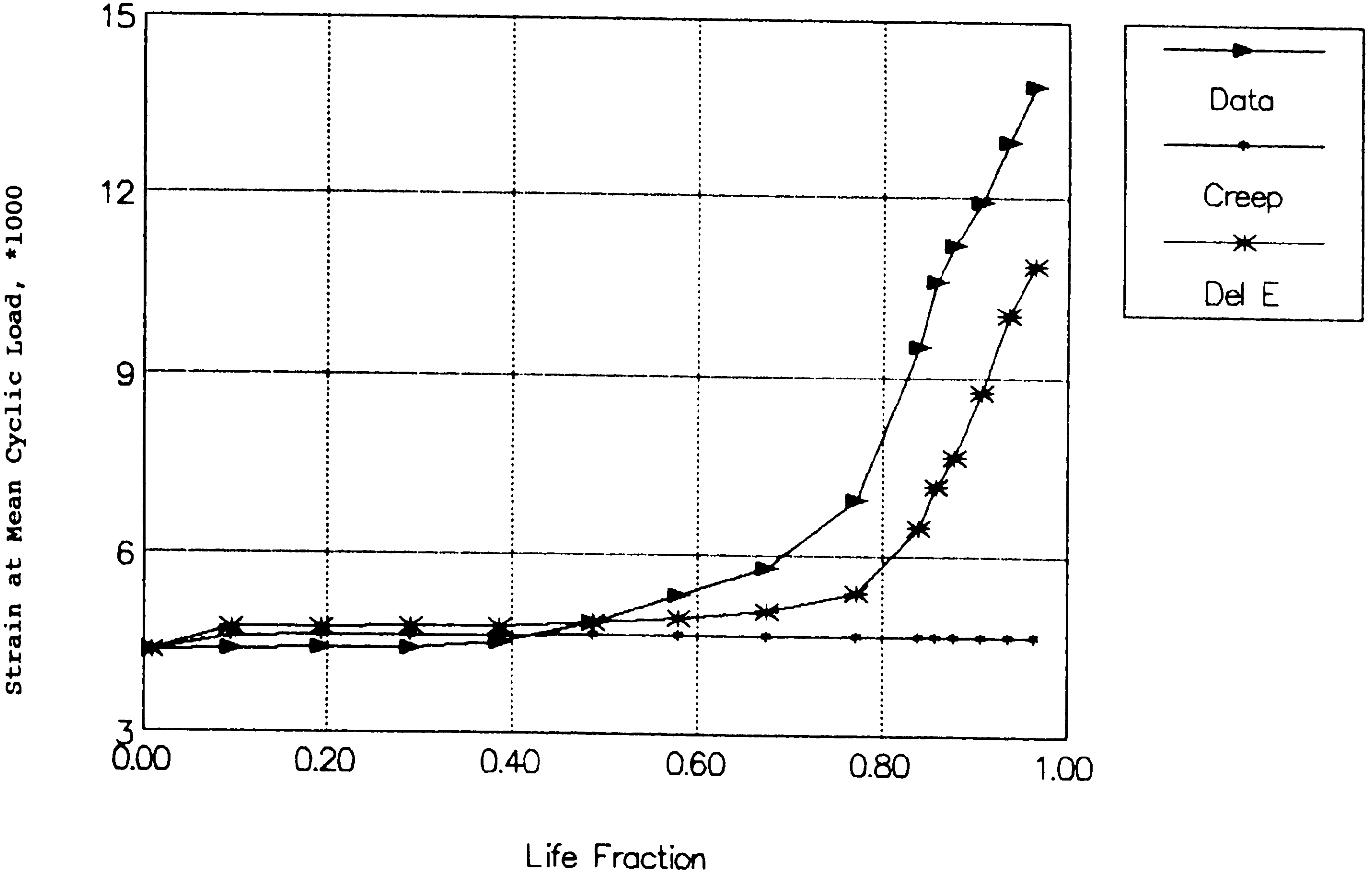

Figure 52. Measured and Predicted Creep Strain for S = 0.5

of numerically integrating (21) with the aid of VCAP is not available at this time.

4.3 EDGE STRESSES

Edge stresses were calculated using the approximate solution of Pipes and Pagano [24] and the order of singularity was estimated using the more sophisticated approach of Shalev [27].

The Pipes-Pagano solution was incorporated into a classical lamination program. The results for an in-plane load of 2000 lb/in are shown in table 20. This load is within the elastic response of the laminate, where classical lamination theory is valid. The stress free temperature of the laminate is assumed to be 200°F. The inner aluminum layer was modelled as two plies of half thickness.

The Shalev approach accounts for the fact that there exists a stress singularity at the edge of an interface. EDGESTRESS, a computer code developed by Shalev, calculates the order of singularity at a certain interface, which in turn is a criterion for the probability of delamination. All four interfaces in Arall 2 are identical. Using the information on the plies presented in chapter 2, the calculated order of singularity is -0.01008. This is a weak singularity and the fact that the normal interlaminar stresses are compressive suggest that edge delaminations will not be dominant. Thus it is assumed that the

Table 20. Pipes-Pagano Approximation of Normal Interlaminar Stresses at the Edge of Arall 2 Laminates, $N_x = 2000$ lb/in

Interface	Ply	Material	In-plane Stress[a] in Load Direction @ K^{th} Ply (psi)	Normal Interlaminar Stress (psi) @ Interface
0 - 1				0
	1	Aluminum	-868	
1 - 2				-297
	2	Ar/Ep	1951	
2 - 3				-396
	3	Aluminum	-868	
3 - 4				-322
	4	Aluminum	-868	
4 - 5				-396
	5	Ar/Ep	1951	
5 - 6				-297
	6	Aluminum	-868	
6 - 7				0

(a) Includes thermal residual stresses and the applied loads delaminations observed in the C-scans are a consequence of the cracks in the aluminum plies.

4.4 DAMAGE SEQUENCE

The sequence of events leading to the eventual failure of Arall 2 laminates in tension-tension fatigue are summarized and examined in the following paragraphs. An effort is made to include the findings of all experimental techniques. The focus is on S values of 0.5, 0.45 and 0.4 because of the more complete investigation performed at this stress levels.

Five main stages are recognized in the damage sequence.

Stage 1 will be called the initiation stage. During this stage the following observations were made.

- A strain hardening effect takes place in the aluminum layers and in the fiber layers (fiber straightening).
- A similar and small residual strength reduction is measured at all tested stress levels, approximately 4 to 5 percent.
- No damage is evident in the C-scans and no cracks are detected on the surface.
- No changes in unloading stiffness are measured.

Obviously, some form of undetected microscopic level damage occurs as it is reflected in the reduced residual strength.

Stage 2 will be called the damage development stage, the following observations were made.

- This stage begins with the appearance of cracks at the edges of the aluminum layers and is completed when a saturated or characteristic damage state is reached in the aluminum layers.
- Crack spacing slightly decreases with increasing stress level.
- Delaminations develop at all cracks.
- Stiffness is reduced gradually. Small cracks at the edges do not influence the strain measured by the extensometer, hence a stiffness reduction is noticed only after the cracks have advanced inward by some distance, dependent on location.
- At E(n)=0.7 stage 2 is completed.

Stage 3 will be called the crack growth stage, the following events take place.

- Cracks from the edges continue to grow perpendicular to the load direction. Two cracks growing in opposite directions may interact and join. Cracks originating away from the edges also appear. These seem to join cracks growing from the edges.
- Delaminations (cohesive debonding) between the outer aluminum and the fiber layers grow parallel to the load direction and may join with those of neighboring cracks.
- At lower stress levels cracks grow longer and delaminations are

larger.

- Stiffness is reduced significantly. The rate of reduction is dependent on the stress level. At S values of 0.45 and below, the stiffness will level off at $E(n) \cong 0.34$.
- There is a significant reduction in residual strength that accompanies the stiffness drop. This reduction is also dependent on stress level. Lower S values result in larger strength degradation at a given stiffness reduction.

Stage 4 will be called the fiber ply degradation stage. The extent of this stage is highly dependent on stress level and it will be adressed separately for each S value and the correspondent SR value.

- S=0.5. For this stress level SR=0.84. Though the reduced stiffness begins to level off, the fiber layers are unable to carry the total load for a significant number of cycles. Failure occurs shortly after the aluminum layers are cracked across the width of the specimen. Because of the difficulty in monitoring the events in the last few cycles, not enough data is available to comment on the process of fiber ply degradation.
- S=0.45. The value of SR=0.76. Stage 4 becomes a significant part (greater than 50 percent) of the total life of the specimens. After the reduced stiffness levels off at approximately 0.34, the measured normalized residual strength is 0.57. During stage 4 the stiffness and residual strength decrease slowly. Failure occurs when the normalized

residual strength reaches the level of applied load of 0.45. Assuming that no load (or very little load) is reintroduced to the aluminum plies due to extensive cracking and delaminations, at the corresponding stress level in the fiber plies, life is predicted to be 169000 cycles. This estimate is in reasonable agreement with the measured average value of 387000 cycles.

- S=0.4. The value of SR is relatively low, SR=0.67. The predicted life of a unidirectional K/E laminate at this stress level is 3.5E+7 cycles, well over the 1E+6 limit of this investigation. The reduced stiffness levels off at 0.34 and remains nearly constant up to the end of the test. The normalized residual strength at the beginning of stage 4 is 0.5.

Stage 5 is the final fracture. Under tensile loading, the final failure event is controlled by the unidirectional fiber layers. Fibers break and cause the rapid growth of a crack across the width of the specimen as in quasi static tests. Unlike quasi static tests, this final crack in the fiber layers may occur at some distance from the large cracks on the outer aluminum layers that grew across the width of the specimen in stage 3. In most cases, the inner aluminum layer and the fiber layers pull away from the outer aluminum layers exposing delaminated areas of varying length.

The sequence of events described above summarizes the damage development observations made during this investigation. Though the actual life fraction spent at each stage varies with stress level, the order is maintained. The value of SR emerges as the single most important parameter in determining the tension-tension fatigue behavior of Arall 2 laminates. At values above one, life ends shortly after the aluminum layers crack. Stage 3 through 5 collapse into one single event. At values below one, life is controlled by the fiber plies although there is a great degradation in performance, i.e. stiffness and residual strength. A failure mode transition range exists at SR values close to one.

CHAPTER 5

PRELIMINARY CONSIDERATIONS FOR MODELLING

The modelling approach in this investigation reflects the philosophy, previous efforts, and concepts developed by many others at VPI&SU. In a sense, it is a step in a new direction, where several ideas are integrated, updated and modified, in an attempt to address with the challenges presented by Arall laminates.

Two candidate analytical models concerning the fatigue behavior of Arall 2 laminates are presented in this chapter. The first one describes the characteristic damage state attained during stages 1 and 2 of the cyclic loading, as defined in chapter 4. The second attempts to predict residual strength and evaluate fatigue life under general cyclic loading conditions.

The viscoelastic behavior of composite laminates is discussed. A constitutive model, based on four time dependent material properties for an orthotropic lamina, describing the nonlinear viscoelastic properties is presented.

Preliminary results and conclusions are drawn on the basis of the present state of the models.

5.1 THE CHARACTERISTIC DAMAGE STATE

Reifsnider et al. [17] announced in 1977 the existence of a unique characteristic damage state (CDS) for laminated composites (i.e. material and stacking sequence), consisting of a specific array of matrix cracks parallel to the fibers in each off-axis ply of a composite laminate. The CDS is attained when each ply becomes saturated with cracks that appear at regularly spaced intervals. This equilibrium spacing is identical for quasi static and tensile fatigue loading, and is controlled by the constraint of the laminate on the cracked plies.

The CDS of a laminate has the following properties.

- It depends only on the material strengths and stiffnesses of each ply, ply thicknesses, stacking sequence and laminate properties.
- It is independent of load history, initial stress and global geometry.
- It is independent of environmental effects such as moisture and temperature as long as these do not change the elastic moduli. The changes in CDS can be predicted from knowledge of those changes [56].
- It is a unique, well defined physical situation which can be described and modeled analyticaly.
- A stable CDS forms prior to failure (unless the off-axis ply cracking is life limiting), and can be regarded as the composite counterpart of the single crack in homogeneous materials.

The formation of a CDS, first reported to exist in graphite-epoxy composites has been observed and confirmed in widely differing material systems such as aramid-epoxy, glass-epoxy, metal-matrix composites, etc.

A brief description of the shear lag mathematical model and a discussion of how the presence of a CDS affects the stiffness, residual strength, and implicitely, the fatigue life of the laminate follows.

5.1.1 EQUILIBRIUM ELEMENT ANALYSIS

Reifsnider [17] and later Reifsnider and Highsmith [18] have postulated a model used to predict the CDS. The one dimensional case is depicted in figure 53. In the equilibrium approach, the cracked, uncracked, and remainder of the laminate are each represented by one element respectively. In each element, the average displacement is the dependent variable. Axial and shear forces are summed resulting in a system of coupled equations with their respective boundary conditions. The solution yields an estimate of the stresses in the neighborhood of the crack in the x-z plane. The closest distance from the crack over which the stress in the cracked ply reaches its undisturbed value, is a lower bound on crack spacing. CDS results when that spacing is attained along the length of the laminate.

In figure 53, the α plies are the constraint layers, and the 90°

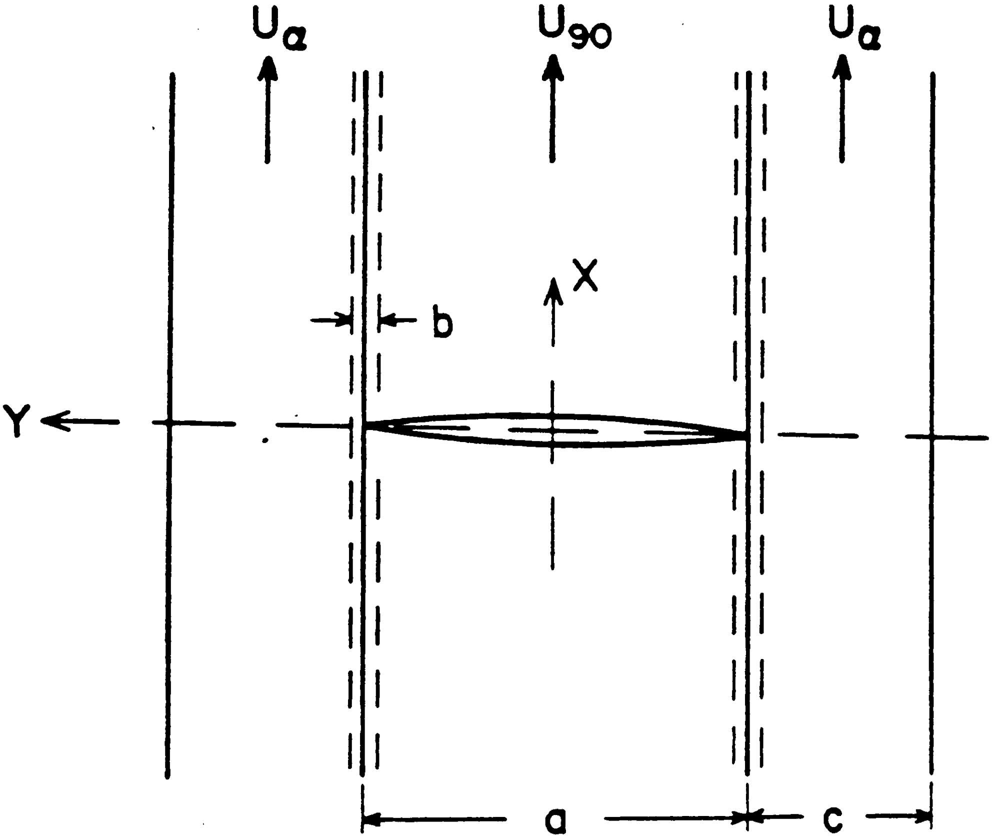

Figure 53. Equilibrium Element for One-dimensional Model of Characteristic Damage State [33]

plies are cracked. Gradients in response between plies occur in an interface of thickness b; whose properties need to be evaluated. A force balance over the cracked and constraint elements is done (see details in [18]). The boundary conditions require that the disturbance must die out at large distances from the crack and that all stresses with normal components vanish at the crack face. The solutions that satisfy the boundary and auxilliary conditions provide a complete approximate solution to the problem.

Material properties, stacking sequence, free surfaces, etc, may change the specific form of the equations or boundary conditions, but a CDS can be predicted for all laminates. The spacing is calculated by solving for the strains in the 90° plies and determining the minimum distance required for the normalized stress to reach a value of 1. Since the function is asymptotic, a value of 0.999 is commonly used.

A full three dimensional analysis is required in order to evaluate the complex stress field in the neighborhood of a crack. This stress field will determine whether a crack will grow into the next ply, cause delamination, couple with other cracks or cause laminate fracture. A quasi-three dimensional finite diference treatment is given in references [22,74]. In a complete analysis, interlaminar shear and normal stresses must be included. These are of enormous importance because of their contribution to the final fracture event.

After the CDS has formed, other damage modes may play an important role in the response of the laminate. As cyclic loading continues, cracks may grow from one ply to another accompanied by longitudinal cracking and delamination, continuous non-planar cracks form through the thickness of all off-axis plies. The manner in which the CDS evolves into the final fracture event is not yet fully understood.

5.1.2 THE EFFECT ON STIFFNESS, STRENGHT AND LIFE

Reifsnider and Highsmith [21] comment on the effects of a stable array of cracks forming in the off-axis plies of a laminate.

The cracks that develop in the off-axis plies cause a transfer of load to a neighboring unbroken region. The redistribution of stress causes the unbroken plies to extend an additional increment with no additional load being introduced. The laminate becomes less stiff with each increment in crack length or appearance of a new crack. If the cracked layers have a low stiffness, then the additional load introduced into the unbroken plies is small, causing a small stiffness reduction. Each crack will result in a specific stiffness change. Stiffness changes can be directly related to stresses through measured strains and displacements.

The CDS formation results in a corresponding stiffness reduction which can be predicted. Since the CDS is a unique laminate property, this stiffness reduction is independent of the path, i.e. load history, temperature, moisture, residual stresses, etc.

As mentioned previously, at large life fractions, damage develops beyond the CDS. Coupling of cracks, delaminations and other events will be reflected in a secondary or tertiary stiffness reduction indicating progressive damage development and inpending failure. Though the precise chain of events leading from the CDS to the final failure, controlled by the 0° plies, has not yet been identified; it is apparent that it is influenced by the states of stress and strength defined by the CDS.

The most basic approach to evaluate the effect of the CDS on stiffness is a simple rule of mixtures, establishing the relationship between the CDS and stress redistribution. Assuming that all stresses are uniaxial, for k plies of E_i stiffness in the load direction and volume fraction v_i, the laminate stiffness, E_c, would be,

$$E_C = \sum_{i=1}^{k} v_i E_i \qquad (22)$$

The modulus E_i of a cracked ply is reduced to zero and the load is redistributed among the uncracked plies, increasing their load by the amount carried by the broken plies and causing a specific stiffness reduction.

In reality, the stress field is strongly two and even three dimensional. Load is reintroduced into the cracked plies by shear stresses between cracks. Average two dimensional stresses may be evaluated with the aid of lamination theory. These stresses can be used to approximate remaining strength based on a phenomenological failure theory, such as the Tsai-Hill criterion.

A complete three dimensional approach such as the one presented by Highsmith [74] is required to account for the interlaminar stresses (stacking sequence effects) and local stress fields surrounding every crack. Summarizing, residual strength depends on the way the CDS reduces the effective stiffness tensor and redistributes the internal stresses.

Accepting the definition of fatigue life as the number of cycles to failure by fracture, residual strength controls the fatigue behavior. Reifsnider and Highsmith [21] make the following remarks.

- The stiffness change due to the CDS is similar to the total stiffness change in a quasi static test (secant modulus at fracture). This total stiffness reduction is a lower bound below which no fatigue failure is expected. The secant modulus concept (SMC), first postulated by Hahn [36], is useful as a nondestructive indicator of remaining life.
- Under fatigue loading, the transverse cracks in adjacent plies have a tendency to couple through short delaminations. The process of crack coupling and related stiffness change destroy the CDS and precede final failure. Generally, the stability of the CDS leads to expectations of no fatigue failure.
- The characteristic array of transverse cracks in the off-axis plies is believed to initiate delaminations in the interior of laminates under tensile loading.

5.1.3 PRELIMINARY RESULTS

A computer code available at VPI&SU was used to perform a preliminary characterization of the CDS of Arall 2 laminates. Assumptions were made in order to accomodate for the hybrid nature of Arall laminates in the code developed for orthotropic laminated materials.

The characteristic crack spacing in the surface plies of aluminum was predicted on the basis of information measured in the context of this investigation where possible. Data available from other sources was introduced where necessary.

The nature of the assumptions and the unavailability of a complete set of data at this point in time, result in first order approximations. At best, these show the qualitative validity of the proposed model.

The computer code calculates the stress state in cracked and uncracked layers of general laminates. It performs a semi-infinite analysis for the case of one crack or a finite analysis between two cracks. From the stress state, the effective stiffness is calculated. The formulation is similar to a finite difference problem, but it is solved exactly.

The input to the program includes the elastic properties of the laminae, geometry, applied strain and boundary conditions (crack(s) location). The interface between layers is characterized by the value of G/b, the ratio of shear modulus and thickness of the interface. This value is generally unknown. The two common assumptions are,

- G is taken as the shear modulus of the resin and, b is the thickness of the resin rich area between layers.
- G is taken as G_{23} of the ply, and b is half of the ply thickness.

All of the above assumptions correspond to fiber reinforced composites, where all the laminae are of the same material or at least the same kind of interface. The load-transfering interface is a part of both adjacent layers and its properties are evaluated on this basis. This certainly is not the case in Arall 2 laminates and the following assumptions were made.

-The aluminum layers crack through their whole thickness and are not a part of the interface. This assumption is supported by the evidence that delaminations originating at the cracked aluminum layers, grow inside the resin rich area within the K/E plies.

- Since there is no information regarding the interface, G is taken to be G_{23} of the K/E plies, and b is taken to be half the K/E ply thickness, yielding a value of G/b = 54.25 E6 psi/in.

A semi infinite analysis was performed for the case of one crack in the outer aluminum ply. The upper bound on the distance between cracks is evaluated by determining the distance away from the introduced crack where the strain reaches 0.999 of the ply level strain that caused the first crack, see figure 54. The strains in the uncracked aluminum ply and fiber ply are depicted in figures 55 and 56 respectively.

The strain distribution in the K/E ply for a combinations of cracks in both aluminum layers is shown in figure 57.

The available information on the characteristic crack spacing is used to perform a finite stress analysis between two adjacent cracks in the outer aluminum ply. The strain distributions between the two cracks in the aluminum plies and K/E ply between them are shown in figure 58.

The value obtained for the lower bound on the crack spacing from the semi infinite analysis is 0.22 inch. The actual average crack spacing, as given in Table 14, is 0.345 inch. A reasonably good correlation taking into account the approximate nature of the assumptions and the presence of large delaminations.

The calculated local stress concentrations in the fiber plies in the vicinity of cracks range from 2.3 for the case of a single crack in the outer aluminum plies to 3.7 for parallel cracks in the inner and outer aluminum plies.

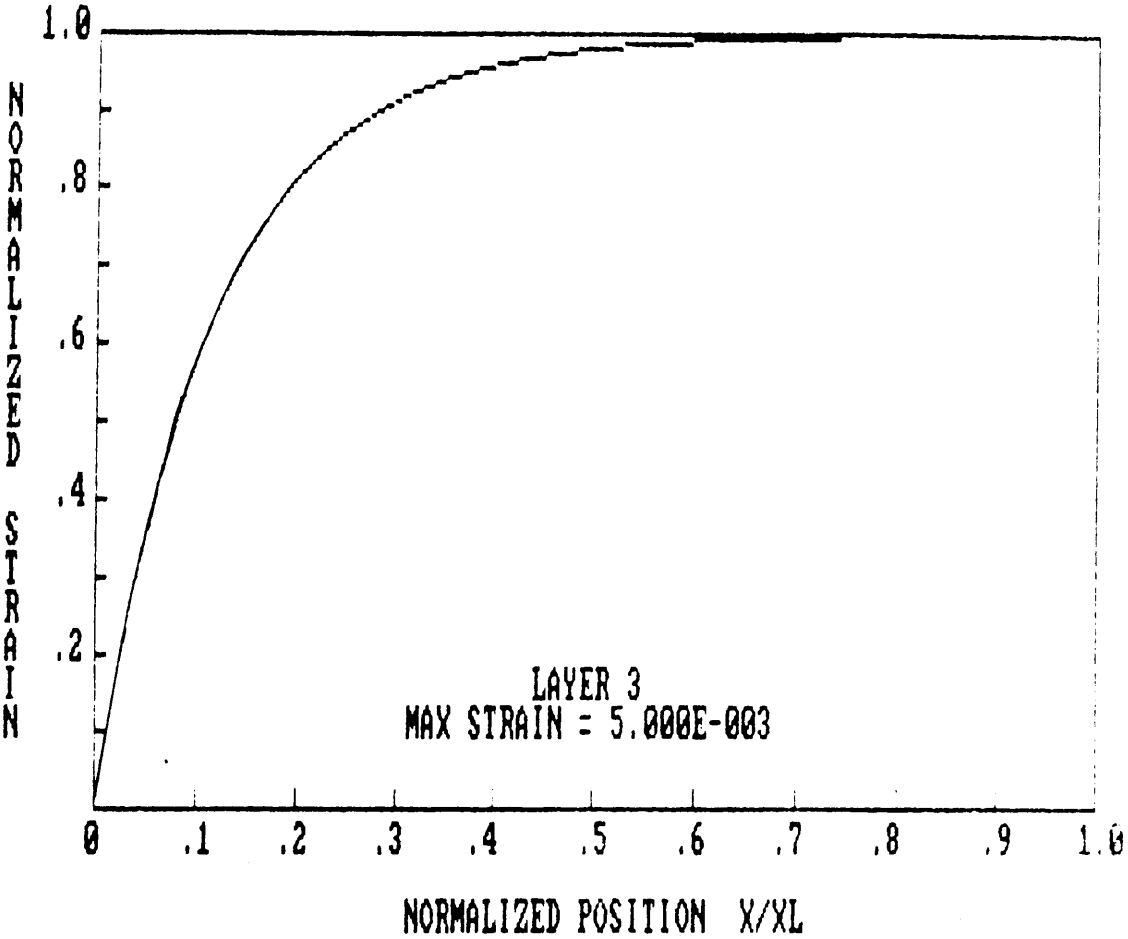

Figure 54. Semi-infinite CDS Analysis, Outer Aluminum Ply

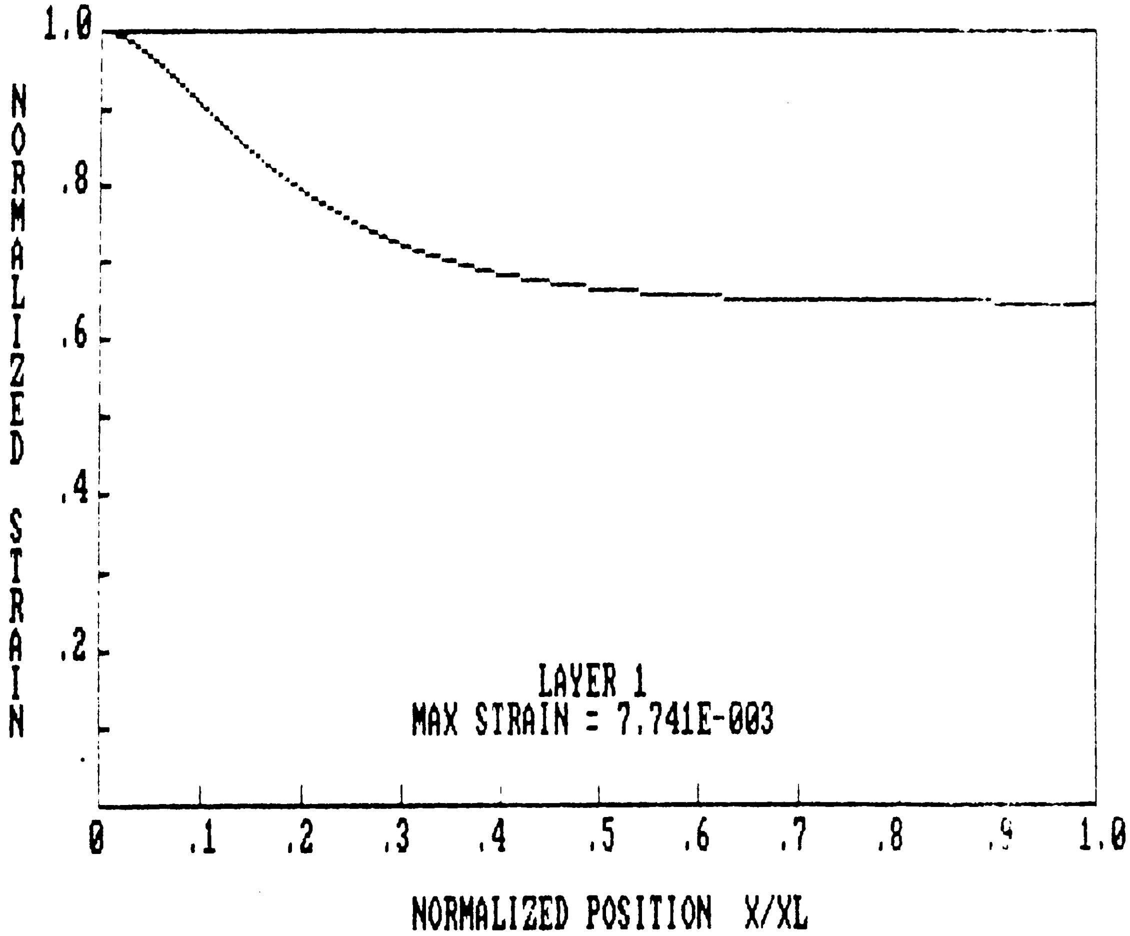

Figure 55. Semi-infinite CDS Analysis, Inner Aluminum Ply for One Crack in the Outer Aluminum Ply

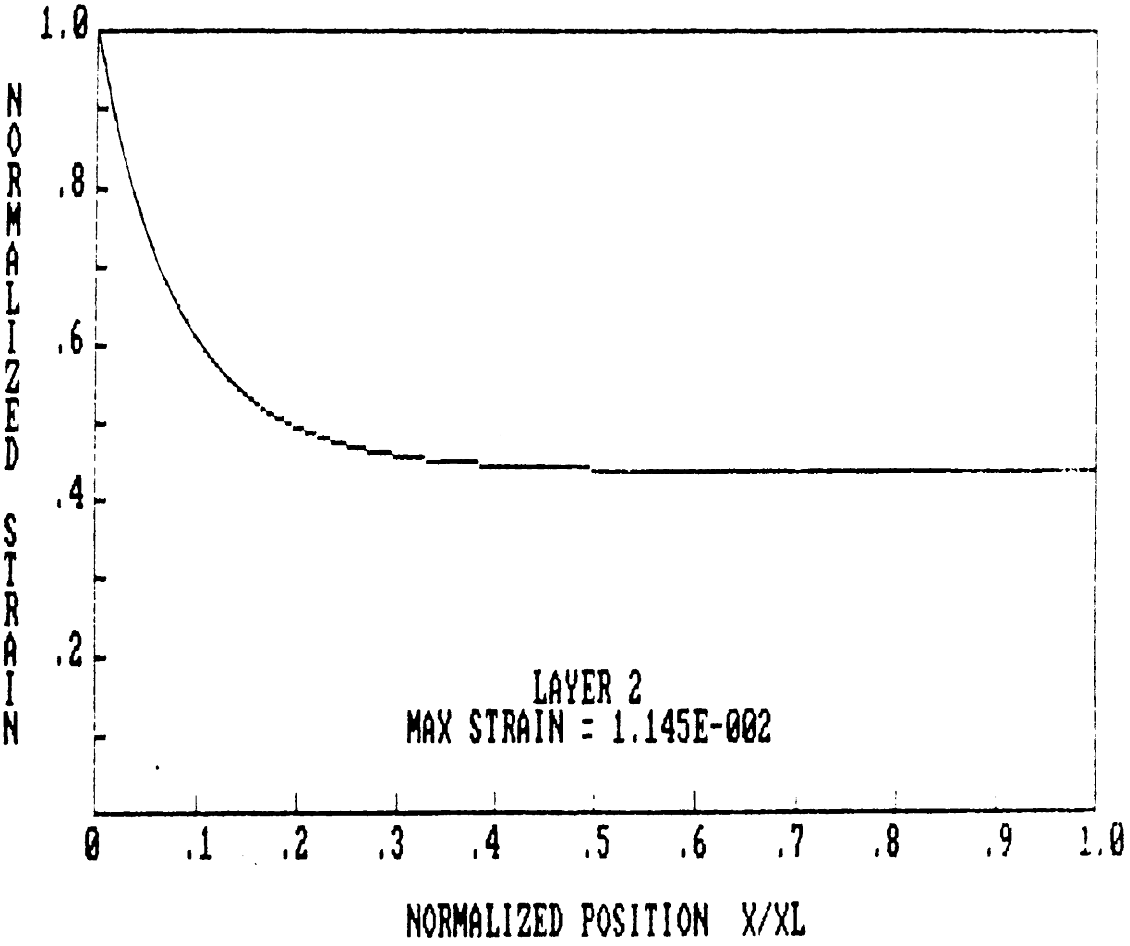

Figure 56. Semi-infinite CDS Analysis, K/E Ply for One Crack in the Outer Aluminum Ply

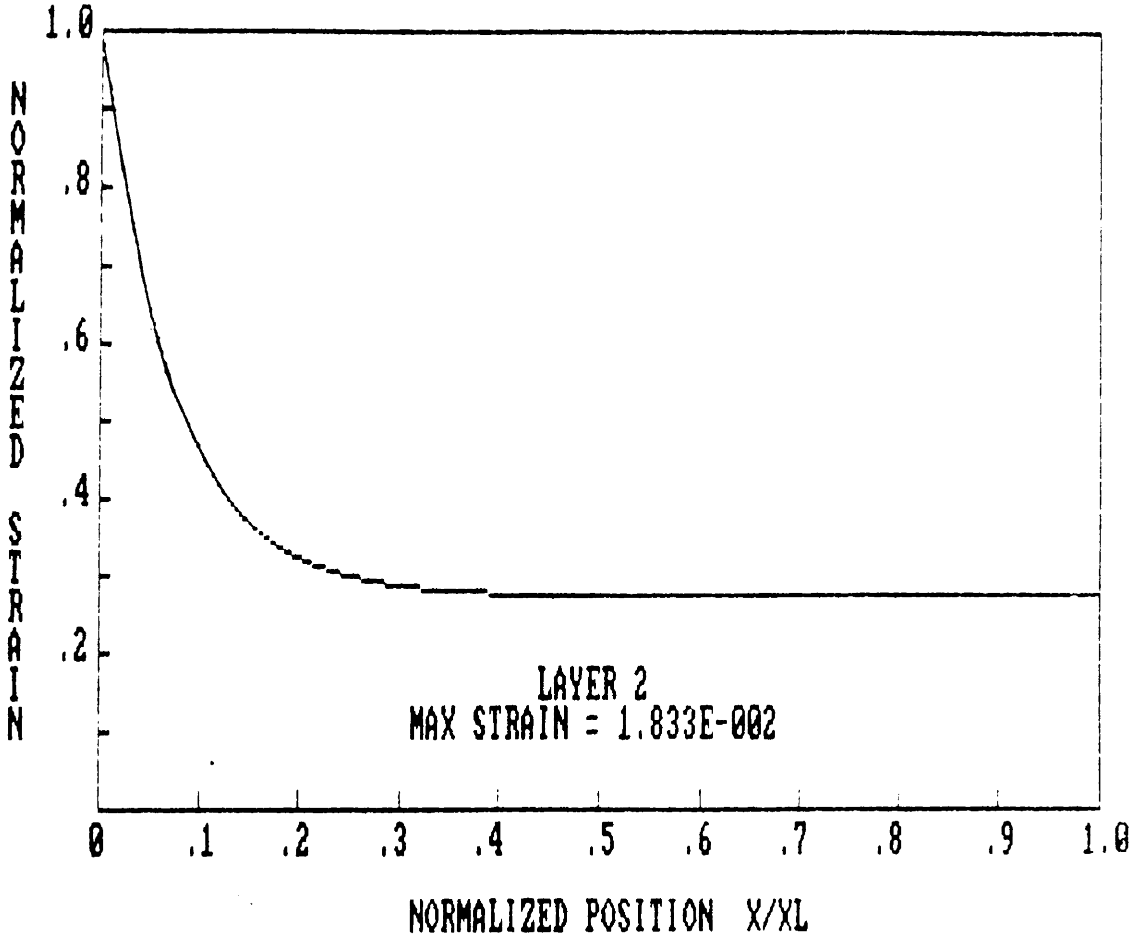

Figure 57. Semi-infinite CDS Analysis, K/E Ply for One Crack in Each Aluminum Ply

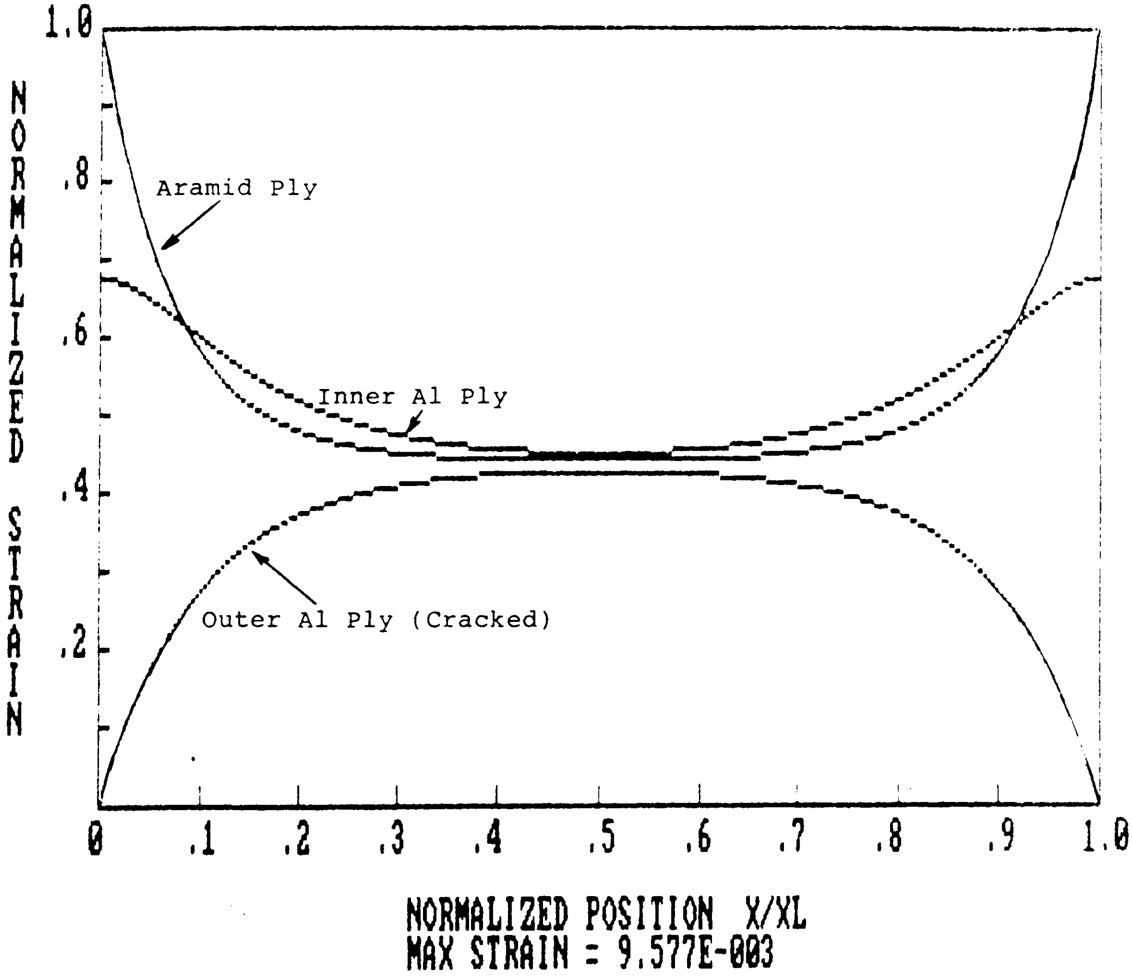

Figure 58. Finite CDS Analysis Between Two Cracks in the Outer Aluminum Ply for All Layers

5.2 THE CRITICAL ELEMENT MODEL

The Critical Element Model (CEM) is a mechanistic cumulative damage model for damage development in high modulus fiber reinforced composite laminates subjected to arbitrary cyclic loading. The model is developed on the concepts of equivalent damage based on equivalent residual strength. Details of the objectives, approach, formulation and results are found in references [29,32,44,57].

The development of an understanding of the behavior of laminates under cyclic loading is still incomplete. The CEM represents an effort to build a framework into which precise physical and analytical observations, such as those made in this study, can to be included in the future.

This engineering model has the following features.

- A minimum amount of phenomenological characterization of materials systems is needed to predict various laminate configurations under arbitrary loading conditions.
- It is based on measurable parameters which describe the current state of damage and its development, which in turn are used to evaluate the present condition and anticipated behavior.
- A definition of "equivalent damage state" is established so that cumulative damage under arbitrary load spectra can be assesed.
- The model provides a framework into which the physical and analytical interpretations of particular events can be introduced or

removed by modifying the codes, thus allowing for design and inspection interpretations.

5.2.1 PROBLEM DEFINITION

This investigation is concerned with the residual strength and life of unnotched coupons subjected to tension-tension cyclic loading. A short presentation of the fundamental CEM approach is presented in the following paragraphs, then a more detailed presentation of the pertinent case follows.

The nature of damage in composite laminates is extremely complicated. The representation of the complex damage state and the formulation of the appropriate mechanics problem become difficult in the presence of numerous combinations of matrix and fiber damage, delaminations and debonding.

A large body of information is available in the literature, describing the many complex ways damage develops in numerous composite laminates. Because these details are distinct, essential, and vary according to load history; the approach of the CEM is to choose a representative volume such that its mechanical response is the same as the total volume.

A process of progressive localization of damage has been identified around primary cracks, near the interface between plies.

Consequently, that is the choice of representative volume. The process includes local delamination at the intersection of primary and secondary cracks, which is believed to lead to local fracture initiation and unstable propagation, causing specimen failure.

The representative volume is then divided into critical and subcritical elements, based on their contribution to the response. Each is handled differently and separately. A laminate consisting of zero-degree and off-axis plies is considered.

The subcritical elements are those whose failure does not cause laminate failure. Damage to these elemnts causes changes in internal stress states that comprise the major part of the cumulative damage process. These elements represent the internal stress redistribution defined by local geometry changes in the representative volume.

Stiffness is chosen as the measurable parameter since it is related to microdamage and reduction of strength, and indicates internal stress redistribution. In this discussion, the off-axis plies are the subcritical elements, their internal state of stress is calculated according to the amount of damage as evaluated from measured stiffness changes, as a function of applied cycles.

The critical elements are defined to be those which control fracture directly. Their state defines the state of the material. In this case, the zero-degree plies are chosen to be the critical elements. The state of the material is characterized by a physical constitutive characteristic. The simplest example is a phenomenological representation of the critical element life as a function of normal stress range in the fiber direction and the number of applied cycles (S/N curve). A conceptual chart detailing the CEM approach is shown in figure 59.

5.2.2 FUNDAMENTAL FORMULATION

The life of the laminate is defined as the coincidence of residual strength and the applied load level, as schematically depicted in figure 60. Equation (23) is a generalized normalized three dimensional equation which computes the residual strength as a function of increments of applied cyclic loading.

$$1-F^{r}(n) = \int_{0}^{\gamma} [1-F_{L}(n)]\, i \left[\frac{n}{N(n)} \right]^{i-1} d\left[\frac{n}{N(n)} \right] \qquad (23)$$

$1-F^{r}(n)$, is the normalized change in residual strength as a function of cycles n.

$F_L(n)$, is a local, desirably three dimensional failure function, that represents the tendency for the internal stress state in the critical elements to cause their failure.

$1-F_L(n)$, is the total allowable amplitude of strength reduction.

i, is a parameter introduced to accomodate nonlinearity in the residual strength reduction curve, it is obtained from curve fitting of data.

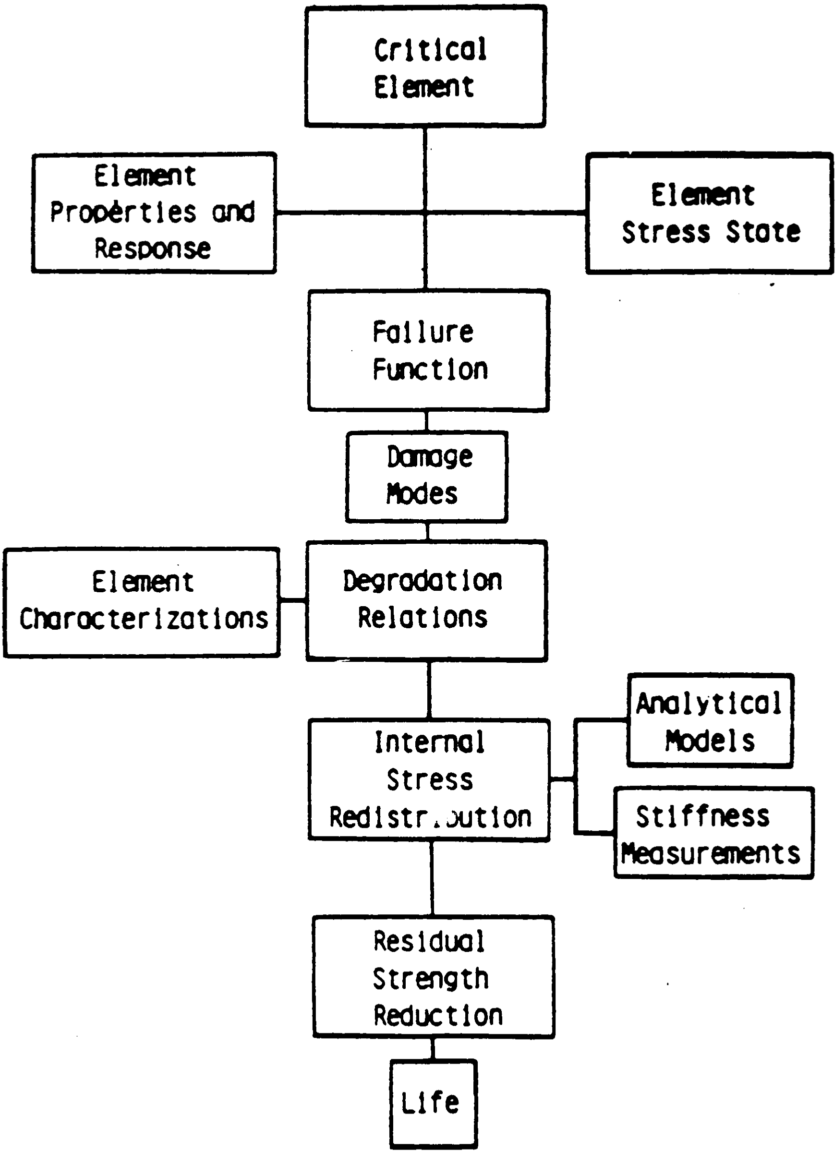

Figure 59. Conceptual Flow Chart of the Damage Accumulation Model [44]

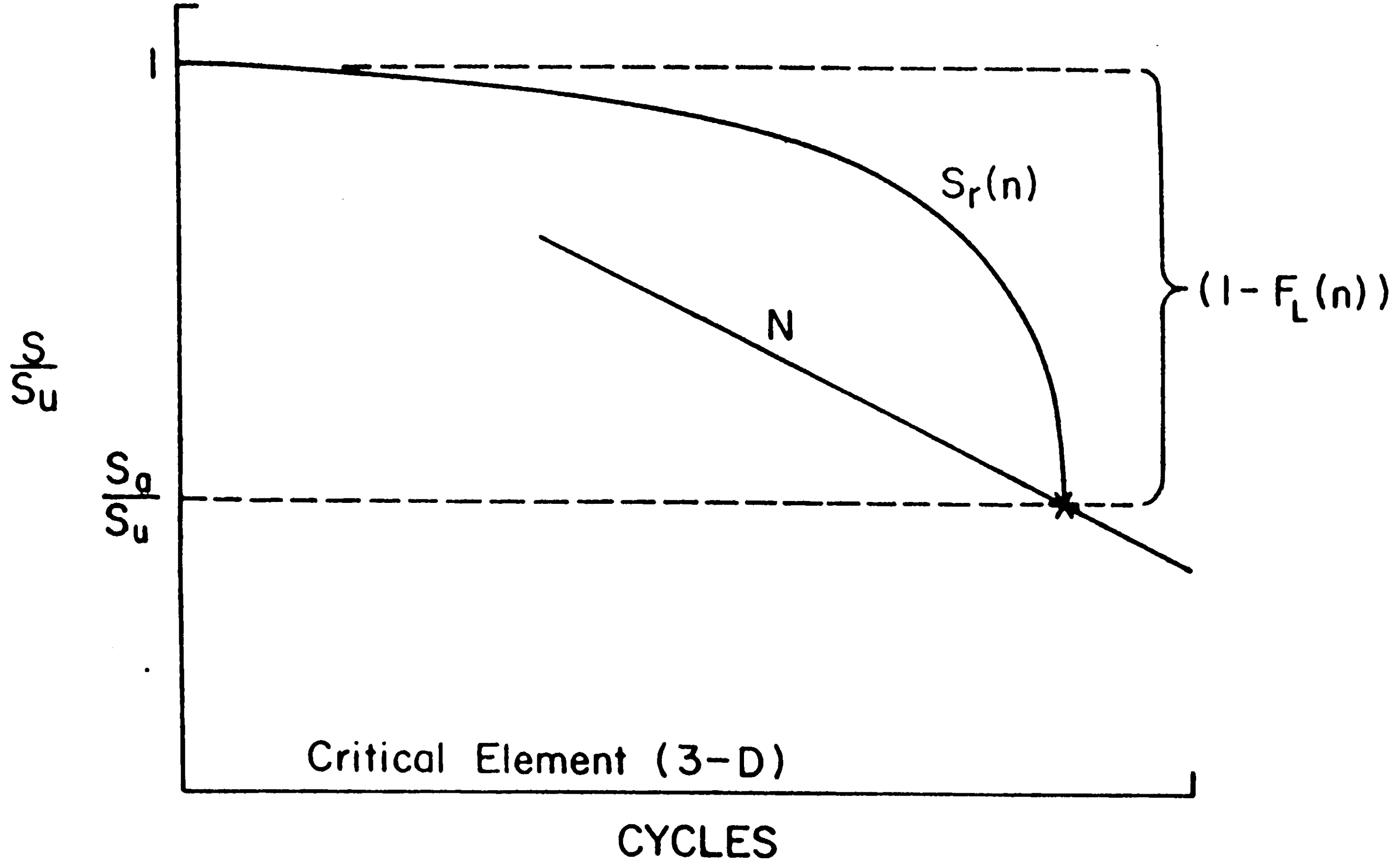

Figure 60. Schematic Diagram of the Critical Element Strength-life Relationship for 3-D Formulation [44]

γ, is a specific value of the life fraction n/N.

$N(n)$, is the phenomenological life data for the critical element. It is also a function of n because the applied stress varies due to stress redistribution.

The variable of integration n/N, is a continuous function and includes the effect of cumulative damage under arbitrary loading conditions.

Equation (23) produces a continuous estimate of the normalized residual strength by integrating the damage in subcritical elements (redistribution of internal stress and geometry changes) and critical elements (control final fracture).

5.2.3 TENSION-TENSION SCENARIO

The Tsai-Hill failure function for the critical element, shown in equation (24), is chosen in such a way that the stresses are a function of n, since stress redistribution will change the local stresses that cause failure of the critical element.

$$F(n) = \frac{\sigma_1^2(n)}{X^2} + \frac{\sigma_2^2(n)}{Y^2} - \frac{\sigma_1(n)\sigma_2(n)}{X^2} + \frac{\tau^2(n)}{S^2} \qquad (24)$$

where X, Y and S are the allowable stresses in the fiber, transverse and shear directions.

The life relationship for the zero degree plies is of the form,

$$N = \log^{-1}\left[\frac{B}{\frac{S(n)}{S_u} - A}\right]^{1/x} \qquad (25)$$

where A, B and x are the material constants of the zero degree plies obtained from the fatigue data of unidirectional laminates of the same material. S(n) is the applied unidirectional stress in the critical element normalized by S_u, the ultimate strength of the element. S(n) is determined from the measured change in laminate stiffness.

It is worthwhile noticing that the above treatment is limited to laminates with no significant edge delaminations, and for the case where failure does not involve buckling.

5.2.4 THE CEM REQUIREMENTS

Residual strength and life predictions for notched and unnotched coupons subjected to tension-tension cyclic loading and many other loading conditions were performed using a computer code developed by Reifsnider and co-workers [44]. The code, available at VPI&SU, performs a numerical intergration routine that predicts residual strength and life at prescribed intervals, based on phenomenological data for the chosen critical element.

The input to the program includes:

- Elastic properties for all materials.
- Allowable stresses for all materials.

- Geometrical stacking sequence and thicknesses.
- Stiffness reduction data for the laminae.
- Strength reduction data for the laminae.
- S/N curve for the critical element.
- Prescribed in-plane loads.
- Integrating parameters such as time increment, direction with respect to axis and number of integration points.

Arall 2 could be modelled as a symmetric laminate, where the aluminum plies fill the role of the off axis - subcritical - elements, as was assumed for the CDS model. Denoting the aluminum plies as I (for isotropic), the stacking sequence would be $(I/0/\bar{I})_s$.

Elastic and allowable properties for both components are found in chapter 2 and elsewhere in the literature. Stacking sequence and prescribed loads are known, integrated parameters can be determined.

At this stage, the stiffness and strength reduction curves for the laminae are yet undetermined. Data for the S/N curve of the critical element, the K/E plies, is not available. The only comparable material data, presented in equation (9) [58] pertains to unidirectional K/E composites with a higher fiber content and an unspecified epoxy resin matrix. Obtaining the essential data to implement the CEM is the next step in this investigation.

5.3 VISCOELASTIC CHARACTERIZATION

The long term behavior characterization of Arall 2 laminates could not be complete without presenting a preliminary approach to the thermoviscoelastic treatment. The viscoelastic nature of the Kevlar fibers and epoxy matrix, combined with the elastic-plastic behavior of the aluminum, makes this a uniquely challenging task.

Most recently Gramoll [50], and others at VPI&SU have addressed the problem of accelerated viscoelastic characterization of fiber reinforced materials. Gramoll also offers an excellent review of previous efforts in the area of isotropic and composite linear and non-linear viscoelasticity.

The effort at VPI&SU revolves around the use of the Time-Temperature Superposition principle (TTSP) to obtain creep compliance master curves for unidirectional materials. Then, classical lamination theory is modified to account for time dependent properties and proper failure criteria are proposed. Ample data and discussions are found in references by Brinson and Yeow [45], Griffith [46], Dillard [47], Heil [48] and Tuttle [49]. A diagram of the procedure is depicted in figure 61.

The original simple statement of the TTSP relates time and temperature effects on the behavior of thermorheologically simple materials, Leaderman [59]. Based on experimental data at different temperatures, an accelerated characterization of the time dependent

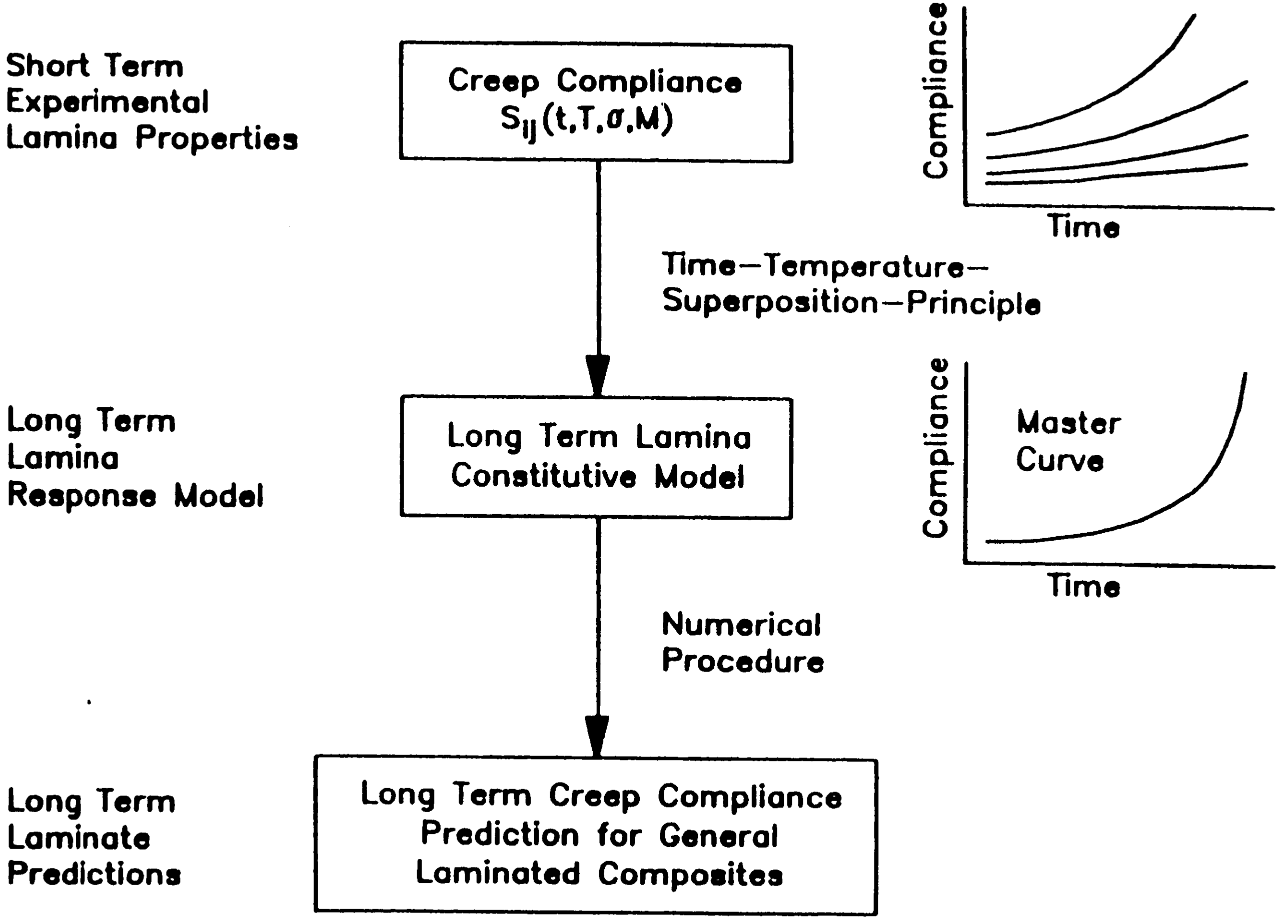

Figure 61. Long Term Characterization of Viscoelastic Composite Materials [50]

process is performed empirically. Time is horizontally "shifted" or reduced, to rapidly obtain a master compliance curve applicable for all temperatures, as shown by Rosen [60] and illustrated in figure 62.

Thermorheologically complex materials, such as fibrous composites, have different viscoelastic components relating stress and strain. The constitutive equation for an orthotropic material is,

$$\begin{Bmatrix} \varepsilon_1 \\ \varepsilon_2 \\ \gamma_{12} \end{Bmatrix} = \begin{bmatrix} S_{11}(t,T,\sigma_1) & S_{12}(t,T,\sigma_1) & 0 \\ S_{12}(t,T,\sigma_1) & S_{22}(t,T,\sigma_2) & 0 \\ 0 & 0 & S_{66}(t,T,\tau_{12}) \end{bmatrix} \begin{Bmatrix} \sigma_1 \\ \sigma_2 \\ \tau_{12} \end{Bmatrix}_o \qquad (26)$$

where ε_i are the in plane strains and $(\sigma_i)_o$ are the applied stresses. S_{ij} is the time and temperature dependent compliance matrix. Four components completely describe an orthotropic viscoelstic material.

The fibers have been found to dominate the fiber direction compliance, S_{11}, and the fiber/transverse coupling compliance, S_{12}. The matrix dominates the transverse direction compliance, S_{22} and shear compliance, S_{66}. Gramoll employs the following quadratic expression to account for nonlinear stress effects,

$$S_{ij}(t,T,\sigma) = S_{ij_o}(1+g_{ij}\sigma^2) + m_{ij}(1+ f_{ij}\sigma^2)\, t^{n_{ij}} \qquad (27)$$

where $(S_{ij})_o$, g_{ij}, m_{ij}, f_{ij} and n_{ij} are material constants.

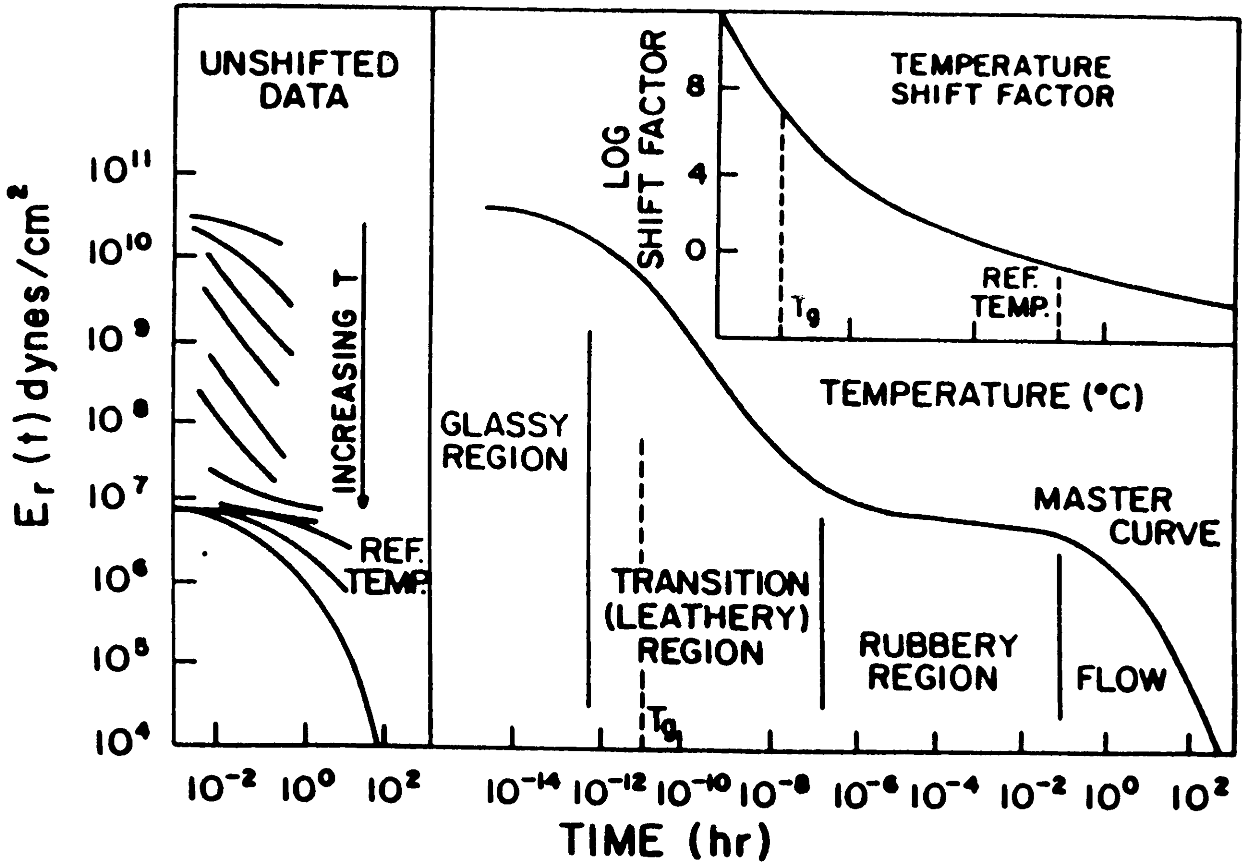

Figure 62. Time Temperature Superposition Principle [60]

Results of Gramoll's investigation and the previously mentioned work by Ho and Schapery, conclude that while the fiber direction has almost linear behavior (stress independent); the coupling, transverse and shear components are increasingly nonlinear. Once the lamina response is complete, Gramoll employs a numerical procedure to predict the viscoelastic response of any arbitrary laminate based on a nonlinear differential equation method. Simply stated, stresses and strains are calculated based on the value of the laminate compliance matrix at time t; then the compliance of all laminae are adjusted for the next increment in time, Δt. An updated compliance matrix for the laminate is evaluated, resulting in new stresses and strains. The problems of convergence and numerical stability are extensively discussed in reference [50].

No specific work has been done within this investigation regarding the viscoelastic characterization of Arall 2 laminates. The accumulated strains reported in chapter 3 and the large stresses to which the K/E plies are subjected following the damage of the aluminum layers, suggest that viscoelastic effects could have significant role in the long term behavior of the hybrid laminate.

The damage occuring during cyclic loading, as it is reflected in the reduction of stiffness and strain accumulation, may represent the synergistic combination of cracks, delaminations, temperature changes time dependent behavior.

CHAPTER 6

SUMMARY, CONCLUSIONS AND RECOMMENDATIONS

Conclusions based on the work and preliminary modelling considerations performed during this investigation are presented below, in the order in which they were discussed in this report. Comments and recommendations are made regarding future experimental and analytical efforts.

6.1 MATERIALS AND METHODS

Materials

The mechanical characterization of the components that form Arall laminates is incomplete. While data for all aluminum grades is readily available, similar data for the epoxy resin and aramid/epoxy laminate is partial. Of particular importance are:

- Accurate data on the fatigue response of the unidirectional aramid/epoxy composite subjected to cyclic loading.

- Thermoviscoelastic characterization of the aramid/epoxy composite.
- The effect of the number of aramid/epoxy plies on the strength of the unidirectional composite.
- Adequate characterization of the resin rich interface between the fiber rich composite and the aluminum plies.
- The content and distribution of voids within the fiber plies.

The as-received panels have a small curvature in the fiber direction due to the residual thermal bending moments caused by a thickness difference in the aramid/epoxy plies. This situation may change from panel to panel and in any case, a remedy should be found.

Although the panels in their entirety were pronounced acceptable by the manufacturer, the ultrasonic C-scans revealed gross defects such as delaminations, porosity and seams in the aramid/epoxy plies. All the specimens were cut from defect-free areas, discarding 20% to 30% of the panel. Preliminary measurements of the damaged areas show a reduction of 3% in ultimate tensile strength and initial elastic modulus.

Mechanical Testing

The use of strain gages was discontinued after several adhesive failures due to the large strains. The development of cracks across the face of the specimen during cyclic loading makes the use of strain gages impractical. One inch gage extensometers and v-notched tabs were used to measure strains. A measuring device with a larger gage length is recommended to obtain a better measure of the overall axial strain in the test section. This will have an effect on values of stiffness reduction due to fatigue damage.

Sandpaper between the specimen and gripping areas and low gripping pressure, 300 psi for monotonic loading and 800 psi for cyclic loading were used to minimize grip-induced damage with success.

Strain measurements were recorded manually, requiring numerous interruptions of every test. The procedure is not only tedious but also fails to record the important events taking place close to the specimen's failure. An automated data acquisition system would improve the situation significantly.

The MTS servo-hydraulic control is not able to keep the prescribed load levels when changes in the specimen's compliance occur. The mean value and amplitude of the sinusoidal signal were adjusted periodically. Again, a computerized feed back control would be welcomed.

Nondestructive Evaluation

Microscopy proved a valuable tool while looking at the crossection of the laminate, easily detecting the thickness asymmetry and providing evidence of the existence of a resin rich interface next to the aluminum plies. Combining microscopy with a suitable deplying technique may lead, in the future, to better understanding of the damage mechanisms in the fiber plies, inaccesible by other means.

Enhanced photography was used to document the crack patterns that develop in the outer aluminum plies. It offers less information than surface replication techniques but it is easier to implement and has enough resolution for the purposes of this study.

Surface analysis using electron spectroscopy is an excellent complimentary technique, easily providing information regarding the chemical nature of the surface. Preliminary and limited results indicate that the in plane delaminations occur within the resin rich interface. The adhesive failure is cohesive and not adhesive.

Ultrasonic C-scans were performed to determine the extent of damage in residual strength specimens. The integrative nature of this technique does not permit the examination of individual defects. Regretfully, X-ray radiography is not feasible due to the relative transparency of the fiber plies compared with respectthe large attenuation of the aluminum plies. Acoustic microscopy might prove in the future an invaluable nondestructive technique, able to discern damage in each of the plies.

Stiffness monitoring appears to be the single most important nondestructive evaluation method available. It was found to truly reflect the damage state of the material. A simple power law with a spring correlates stiffness and residual strength. Even so, several problems exist in the present configuration:

- Damage occuring at the edges, away from the extensometer, is not detected until it grows some distance away from the edges. The measured stiffness lags behind the actual global value.
- Large delaminations under the tabs may alter the results.
- Cracks growing under the tabs completely disrupt the stiffness masurement.

Two devices with a larger gage length, one on each side of the specimen may help alleviate these problems.

The unloading modulus was found to be unaffected by the cyclic stiffening of the secant modulus, it only changes as a function of damage. It is recommended to use the unloading modulus to monitor damage in future experiments.

A preliminary method to evaluate time dependent effects was deviced.Strains at 0, minimum, mean and maximum load were recorded manually. These measurements were used to evaluate the strain accumulated during cyclic loading.

It is recommended to monitor the specimen's temperature in every test. The stress-strain curves (hysteresis loops) show that stiffness reduction is accompanied by large amounts of energy dissipation and, (from preliminary measurements) temperature rises significantly, accelerating the viscoelastic effects and other damage mechanisms.

6.2 EXPERIMENTAL RESULTS

Quasi static tests

The quasi static tests results of virgin specimens yield a great deal of information, showing how the components contribute to the behavior of the hybrid laminate.

- The ultimate tensile strength is 103.6 Ksi. It reflects the sum of the stress in the fiber plies and the aluminum plies at the ultimate strain within experimental error.
- The stress strain curve is bilinear. A sharp knee at 46 Ksi corresponds to the yielding strain of the aluminum plies.

- The initial axial modulus is 9.3 Msi, lower than anticipated by classical lamination theory. The secondary stiffness - 3 Msi - reflects the contribution of the fiber plies to the post yielding stiffness.
- The fracture strain of the Arall @ laminate is 2.43%, slightly lower than the ultimate strain of the aramid fibers, 2.64% [52].

Residual tensile strength tests at three stages in fatigue life, as determined from the reduced stiffness, lead to the following conclusions:

- Tensile strength decreases monotonically
- Tensile strength reduction correlates well with the reduction in stiffness using a simple power law, given by equation (6).
- Based on the information available for all three stress levels at E(n)=0.7, it appears that the strength reduction rate is slightly stress level dependent. Equation (6) could be modified to account for this effect, but not enough data is available at this time.
- Reduced stiffness is a true indicator of the damage state as evidenced by the excellent repetition shown in the results.

Fatigue tests

The results of the cyclic loading program show that:

- Lives of $8x10^3$ to over $1x10^6$ cycles were measured for stress levels ranging from S=0.9 to 0.4.

- A ratio SR was defined. It relates the maximum applied load to the ultimate tensile load capability of the fiber plies. The SR ratio descrobes the mechanisms which control the fatigue behavior of the Arall laminate.
- At high stress levels, SR>1 (S≥0.6), life is influenced by the initiation of damage in the aluminum plies.
- At low stress levels, SR<1 (S≤0.45), life is determined by the fatigue behavior of the fiber plies.
- At intermediate stress levels, 0.6>S>0.45, a transition occurs between the two life controlling damage modes.
- The normalized stiffness was fitted with a modified power law containing two parameters. In turn, these were correlated with the stress level, S. A three dimensional Stiffness-Stress Level-Life Fraction surface is thus obtained.
- The initial small, and rapid drop in stiffness observed in all-fiber reinforced composites is replaced by a large (and sometimes slow) process of degradation in the aluminum plies.

The amount of secant modulus stiffening was found to be dependent on the extent of the plastic deformation in the first cycle. There is a combined effect, the well characterized cyclic strain hardening of the aluminum and a much less characterized aramid fiber straightening process, that may depend on any number of parameters.

Time dependent effects

Significant viscoelastic effects take place during cyclic loading. The initial approach of using the mean load as a comparable creep load yields qualitatively matching results if the stiffness degradation is taken into account. The larger measured strains may be the result of a temperature rise within the specimen (causing accelerated creep), plastic deformation in the resin rich interfaces, etc.

The sum of the accumulated strain and fracture strain of residual strength specimens approaches the value of the fracture strain for virgin specimens, except for intermediate life specimens. At this stage in life, the cracks in the aluminum plies cause local stress concentrations that reduce the total strain.

Cyclic loading is very different from creep or relaxation tests, the common techniques used by experimental researchers in the field of viscoelasticity. The difference is especially important because the damaged aluminum plies may interact with the viscoelastic fiber plies in many complex ways. Caution is of the essence.

Damage sequence

Five stages were recognized in the damage sequence:

1. Initiation of damage in the aluminum plies. Stiffness remains constant, strength decreases by less than 5%.
2. A characteristic damage state develops, achieving a regularly spaced array of cracks originating at the edges. A large decrease in stiffness and strength occurs.
3. Crack growth across the width of the specimen accompanied by delaminations of elliptical shape. There is an additional decrease in strength and the stiffness reaches a secondary value.
4. Degradation of the fiber plies.
5. Final fracture.

The duration of each stage is stress-level dependent. At high stress levels stages 3 through 5 collapse into one event. No specific information was gathered regarding the sequence of events leading to failure during stages 4 and 5.

6.3 INITIAL MODELLING CONSIDERATIONS

In general terms the hybrid laminate is analogous to a symmetric composite laminate. In some ways the aluminum layers play the role of the "off-axis" plies, for example, transverse cracks developing during cyclic loading to form a characteristic damage state and it serves as the subcritical element in the critical element model. The aluminum also plays a role in the elastic portion of the laminate's response when analysing the viscoelastic behavior. But the analogy is not complete; the aluminum differs greatly from transverse fiber reinforced plies in some respects. It is isotropic, it carries a large portion of the load, it contributes significantly to the laminate's stiffness, cracks may grow in any direction and/or at different rates and it undergoes plastic deformation.

Characteristic Damage State

A shear lag model was used with reasonable success to predict a lower bound on the characteristic crack spacing that develops during cyclic loading, 0.22 inch. The measured average value is 0.345 inch. The calculated stress concentrations in the fiber plies as a result of cracks developing in the aluminum plies are large, 2.3 for one crack in the outer aluminum ply and 3.7 for cracks in both aluminum plies.

The analysis is as good as the underlying assumptions. The nature of the hybrid laminate presents many unanswered questions such as:

- The nature, geometry and properties of the resin rich interface.
- The effect of the large delaminations in the wake of the crack tip.
- Time (rate) and temeprature effects.
- Crack growth rate.

Critical Element Model

The critical element model, a mechanistic cumulative damage model was proposed as a framework into which the observations made during this study could be introduced. The model is capable of predicting the residual strength and life of a laminate subjected to long term cyclic loading. The aluminum plies and the resin rich interface were identified as the subcritical element, where damage develops but does not cause laminate failure. Damage in the subcritical elements results in the redistribution of stress. The fiber plies were identified as the critical element in that their failure causes the laminate to fracture.

The next step in this investigation should be the damage and fatigue behavior characterization of the critical element which is necessary to obtain predictions using the available codes.

Time Dependent Behavior

The strains accumulated during cyclic loading were compared to creep strain at an analogous constant load using two approaches, both of which discounted the constraint imposed by the aluminum plies. Since the thermoviscoelastic characteristics of the fiber plies are unavailable, data collected by other investigators were used.

The simplest approach was the numerical integration of the hereditary integral assuming a constant load and nonlinear viscoelastic properties. This approach yielded larger strains at low life fractions but failed completely as soon as damage appeared.

The more successful approach took into account the stiffness degradation but used linear viscoelastic properties. Again, at low life fractions the predicted strain is larger than measured; and it is smaller than measured after the stiffness is reduced. A qualiatative agreement was obtained.

The situtation may improve by considering the time dependent bahavior of the whole laminate. Although the analysis is not available at this point in time, the following explanations should be considered. At low life fractions, the aluminum plies act as a constraint, the fiber plies relax, and load is transfered to the metal plies resulting in lower strains. Once damage begins load is transfered to the fiber plies, the dissipation of energy causes the temperature to rise thereby accelerating the viscoelastic response. Large plastic deformations of the resin rich interfaces should also be considered.

It is recommended that the effects of time dependent elastic constraints and varying temperature be considered in to the present analytical procedures.

The potentially synergistic effects of cyclic loading and the presence of local stress concentration due to damage remain unknown and present a unique challenge.

REFERENCES

1. Vogelesang, L.B., Marissen, R., Schijve J.,"A new fatigue resistant material: aramid reinforced aluminum laminate (Arall)", 11th Symposium, International Committee on Aeronautical Fatigue", 1981.

2. van Veggel, L.H.,"Arall applications in Fokker aircraft wing structures", Arall laminates technical conference, Seven Springs, Pennsylvania, 1987.

3. Mohaghegh, M.,"Preliminary evaluation of Arall laminates", Arall laminates technical conference, Seven Springs, Pennsylvania, 1987.

4. Bucci, R.J., Mueller, L.N., Vogelesang, L.B., Gunnick, J.W.,"Arall laminates properties and design update", 33rd International SAMPE Synposium and Exhibition "Materials - Pathway to the future", Anaheim, California, 1988.

5. Teply, J.L.,"Analytical modeling of Arall laminates", Arall laminates technical conference, Seven Springs, Pennsylvania, 1987

6. Yeh, J.R.,"Fracture mechanics of delamination in Arall laminates", Arall laminates technical conference, Seven Springs, PA, 1987.

7. Phillips, M.A.,"Damage tolerance evaluation of Arall laminates under the Air Force phase I program", Arall laminates technical conference, Seven Springs, Pennsylvania, 1987.

8. Marissen, R.,"Fatigue crack growth in aramid reinforced aluminum

laminates (Arall) - mechanisms and predictions", DFVLR Institute fur Werkstoff-Forschung, DFVLR-FB 84-37, 1984.

9. Petit, R.,"Arall technology at Douglas Aircraft Corporation", Arall laminates technical conference, Seven Springs, Pennsylvania, 1987.

10 Ritchie, R.O., Weikang, Y., Bucci, R.J.,"Fatigue crack propagation in Arall laminates: measurement of the effect of crack-tip shielding from crack bridging", to be published.

11. Stiffler, R.C.,"Fatigue tests of narrow (3/4 in. wide) Arall specimens", Alcoa internal report, 1987.

12. Reifsnider, K.L., Henneke, E.G., Stinchcomb, W.W., Duke, J.C.,"Damage mechanics and NDE of composite laminates", Proceedings, IUTAM Symposium on Mechanics of Composite Materials, Virginia Polytechnic Institute and State University, Pergamon Press, 1982.

13. Stinchcomb, W.W.,"Fatigue damage mechanisms in composite materials: a review", Fatigue Mechanisms, ASTM STP 675, J.F. Fong, Ed., American Society for Testing and Materials, 1979, pp.762-787.

14. Schapery, R.A.,"Models for damage growth and fracture in nonlinear viscoelastic particulate composites",MM3168-82-5, Mechanics and Materials Center, Texas A&M University, 1982.

15. Christensen, R.M., Theory of Viscoelasticity - An Introduction, Second Edition, Academic Press, New York, 1982.

16. Jones, R.M., Mechanics of Composite Materials, Hemisphere Publishing Corporation, New York, 1975.

17. Reifsnider, K.L.,"Some fundamental aspects of the fatigue and fracture response of composite materials",Proceedings, 14th Annual Conference, Lehigh University, Bethlehem, PA, 1977, pp. 373-384.

18. Reifsnider, K.L., Highsmith, A.,"Charactristic damage states: a new approach to representing fatigue damage in composite laminates", Materials, Experimentation and Design in Fatigue, Westbury House, Guilford, U.K.,1981, pp. 246-260.

19. Jamison, R.D.,"Advanced fatigue damage development in graphite epoxy laminates", Ph.D. dissertation, College of Engineering, Virginia Polytechnic Institute and State University, Blacksburg, VA, 1982.

20. Rosen, B.W.,"Tensile failure of fibrous composites", AIAA Journal, vol. 2, no.11, 1964, pp.294-309.

21. Hihgsmith, A.L., Reifsnider, K.L.,"Internal load distribution effects during fatigue loading of composite laminates", Composite Materials:Fatigue and Fracture, ASTM STP 907, H.T. Hahn, Ed., American Society for Testing and Materials, 1986, pp.233-252.

22. Talug, A.,"Analysis of stress fields in composite laminates with interior cracks", Ph.D. dissertation, College of Engineering, Virginia Polytechnic Institute and State University, 1978.

23. O'Brien, T.K.,"Characterization of delamination onset and growth in a composite laminate", Damage in Composite Materials, ASTM STP 775, K.L. Reifsnider, Ed., American Society for Testing and Materials, 1982, pp. 140-167.

24. Pagano, N.J., Byron Pipes, R.,"Some observations on the interlaminar strength of composite laminates", Int. J. Mech. Sci., Pergamon Press, 1973, Vol. 15, pp. 679-688.

25. Wang, S.S.,"Elasticity solutions for a class of composite laminate problems with stress singularities", Mechanics of Composite Materials: Recent Advances, Hashin, Z. and Herakovitch, C.T., Eds., Pergamon Press, New York, 1983, pp. 259-281.

26. Reifsnider, K.L., Henneke, E.G., Stinchcomb, W.W., "Delamination in quasi isotropic graphite epoxy laminates", Composite Materials: Testing and Design (Fourth Conference), ASTM STP 617, American Society for Testing and Materials, 1977, pp. 93-105.

27. Shalev, D., Reifsnider, K.L.,"Analysis of the edge effect for a circular hole embedded in a composite laminate", to be published.

28. Lekhnitskii, S.G.,Theory of Elasticity of an Anisotropic Elastic Body, Holden-Day, San Francisco, CA, 1963.

29. Reifsnider, K.L., Stinchcomb, W.W.,"Stiffness change as a fatigue damage parameter for composite laminates", Advances in Aerospace Structures, Materials and Dynamics, Yuceoglu, U., Sierakowski, R.L., Glasgow, D.A., Editors, American Society of Mechanical Engineers, New York, 1983.

30. Highsmith, A.L., Reifsnider, K.L.,"Stiffness reduction mechanisms in composite laminates", Damage in Composite Materials, ASTM STP 775, K.L. Reifsnider, Ed., American Society for Testing and Materials, 1982, pp. 103-117.

31. Batdorf, S.B.,"Tensile failure of unidirectionally reinforced composites", J. of Reinforced Plastics and Composites, 1982, 1, pp. 153-164.

32. Highsmith, A.L., Stinchcomb, W.W., Reifsnider, K.L.,"Effect of fatigue-induced defects on the residual response of composite laminates", Effects of Defects in Composite Materials, ASTM STP 836, American Society for Testing and Materials, 1984, pp.194-216.

33. Reifsnider K.L., Henneke, E.G., Stinchcomb, W.W., "Defect-property relationships in composite materials", AFML-TR-76-81, Part IV, Virginia Polytechnic Institute and State University, Blacksburg, VA, 1979.

34. O'Brien, T.K.,"Stiffness change as a nondestructive damage measurement", Mechanics of Nondestructive Testing, W.W. Stinchcomb, Ed.,Plenum Press, New York, 1980, pp. 101-122.

35. Reifsnider, K.L., Highsmith, A.L.,"The relationship of stiffness changes in composite laminates to fracture-related damage mechanisms", Proceedings, 2nd US-USSR Symposium on Fracture of Composite Materials, Lehigh University, 1981, pp. 9-12.

36. Hahn, H.T., Kim, R.Y.,"Fatigue behavior of composite laminates", J. Composite Materials, Vol. 10, 1976, pp. 156-179.

37. Rotem, A., Mechanics of Composite Materials, Recent Advances, Z. Hashin, C.T. Herakovitch, Eds., Pergamon Press, New York, 1983, pp. 421-436.

38. Wilkins, D.J., Eisenman, J.R., Camin, R.A., Margolis, W.S., Bensom, R.A., Damage in Composite Materials, ASTM STP 775, American Society of Testing and Materials, 1982, pp. 168-183.

39. Chou, P.C., Wang, A.S.D., Miller, H.,"Cumulative damage model for advanced composite materials", TR-82-4083, Air Force Wright Aeronautical Laboratories, Dayton, OH, 1982.

40. Wang, A.S.D., Slomiana, M.,"Fracture mechanics of delamination initiation and growth", NADC-TR-79056-60, Naval Air Development Center, 1982.

41. Hashin, Z., Rotem, A., Materials Science and Engineering, Elsevier-Sequoia, Lausanne, Switzerland, 1978, pp. 147-160.

42. Poursartip, A., Ashby, M.F., Beaumont, P.R., Fatigue and Creep of Composite Materials, H. Lilholt, R. Talreja, Eds., Denmark, 1982, pp. 279-284.

43. Charewicz, A., Daniel, I.M.,"Damage mechanisms and accumulation in graphite epoxy laminates", Composite Materials: Fatigue and Fracture, ASTM STP 907, H.T. Hahn, Ed., American Society for Testing and Materials, 1986, pp. 274-297.

44. Reifsnider, K.L., Miller, H.R., Stinchcomb, W.W., Ulman, D.A., Bruner, R.D., Liechti, K.M.,"Cumulative damage model for advanced composite materials", AFWAL-TR-84-4007, Air Force Wright Aeronautical Laboratories, Dayton, OH, 1984.

45. Brinson, H.F., Morris, D.H., Yeow, Y.T.,"The viscoelastic behavior of the principle compliance matrix of a unidirectional graphite/epoxy composite", Virginia Polytechnic Institute and State University, VPI-E-79-9, Blacksburg, VA, 1979.

46. Griffith, W.I., Morris, D.H., Brinson, H.F.,"The accelerated characterization of viscoelastic composite materials", Virginia Polytechnic Institute and State University, VPI-E-80-15, Blacksburg, VA, 1980.

47. Dillard, D.A., Morris, D.H., Brinson, H.F.,"Creep and creep rupture of laminated graphite/epoxy composites", Virginia Polytechnic Institute and State University, VPI-E-81-3, Blacksburg, VA, 1981.

48. Hiel, C., Cardon, A.H., Brinson, H.F.,"The nonlinear viscoelastic response of resin matrix composite laminates", Virginia Polytechnic Institute and State University, VPI-E-83-6, Blacksburg, VA, 1983.

49. Tuttle, M.E., Brinson, H.F.,"Accelerated viscoelastic characterization of T300/5208 graphite/epoxy laminates", Virginia Polytechnic Institute and State University, VPI-E-84-9, Blacksburg, VA, 1984.

50. Gramoll, K.C.,"Thermoviscoelastic characterization and predictions of Kevlar/epoxy composite laminates", Ph.D. dissertation, College of Engineering, Virginia Polytechnic Institute and State University, Blacksburg, VA, 1988.

51. Military Std. Handbook, MIL-HDBK-5D,"Metallic Materials and Elements for Aerospace Vehicle Structures", U.S.D.o.D., Rev. May 1, 1985, pp. 3-73 - 3-139.

52. Ho, T., Schapery, R.A., Harbert, B.C.,"The viscoelastic behavior of Kevlar/epoxy materials", LTV Aerospace report, Contract no. DAAG46-83-C-0032, US Army Materials Technology Laboratory, Watertown, MA, 1985.

53. Cooper, J.N.,"The effect of residual thermal stresses on the viscoelastic behavior of adhesively bonded joints", M.Sc. thesis, Virginia Polytechnic Institute and State University, Blacksburg, VA, 1987.

54. Pindera, M.J., Gurdal, Z., Hidde, J.S., Herakovitch, C.T.," Mechanical and thermal characterization of unidirectional aramid epoxy", Virginia Polytechnic Institute and State University, VPI-E-86-29, Blacksburg, VA, 1987.

55. Johnson, W.S.,"Mechanisms of fatigue damage in boron/aluminum composites", Damage in Composite Materials, ASTM STP 775, K.L. Reifsnider, Ed., American Society for Testing and Materials, 1982, pp. 83-102.

56. Kriz, R.D., Stinchcomb, W.W.,"Effects of moisture, residual thermal curing stresses, and mechanical load on the damage development in quasi-isotropic laminates", Damage in Composite Materials, ASTM STP 775, K.L. Reifsnider, Ed., American Society for Testing and Materials, 1982, pp. 63-80.

57. Reifsnider, K.L., Stinchcomb, W.W.,"A critical element model of the residual strength and life of fatigue loaded composite coupons", Composite Materials: Fatigue and Fracture, ASTM STP 907, H.T. Hahn, Ed., American Society for Testing and Materials, 1986, pp. 298-313.

58. Dupont, Data manual for Kevlar 49 aramid, E.I. DuPont de Nemours & Co., Inc., 1986.

59. Leaderman, H.,"Elastic and creep properties of filamentous materials and other high polymers", The Textile Foundation, Washington, 1943, p. 175.

60. Rosen, S.L., Fundamental Principles of Polymeric Materials, John Wiley, New York, 1982.

61. Bucci, R.J., Mueller, L.N., Schultz, R.W., Prohaska, J.L,"Arall laminates Mechanical Behavior", Alcoa Laboratories Report at ASM Materials Week, Orlando, Florida, 1986

62. 3M, Structural Adhesive Film AF-163-2, Scotch-Weld Aerospace Technical Data, Issue No. 1, 1986

63. Wagnecz, L.,"Thermal behavior and damage mechanisms of woven graphite-polyimide composite materials", M.Sc. thesis, College of Engineering, Virginia Polytechnic Institute and State University, 1987.

64. Sun, C.T., Jen, K.C.,"On the effect of matrix cracks on laminate strength", Journal of Reinforced Plastics and Composites, Vol. 6, July 1987, pp. 208-222

65. Jamison, R.D.,"Fiber fracture in composite laminates", ICCM-VI, Vol. 3, July 1987, pp. 185-199.

66. Goree, J.G., Gross, R.S.,"Analysis of a unidirectional composite containing broken fibers and matrix damage", Engr. Frac. Mech., 1979, Vol. 13, 563-578.

67. Goree, J.G., Gross, R.S.,"Stresses in three-dimensional composites containing broken fibers", Engr. Frac. Mech., 1979, Vol. 13, pp. 395-405.

68. Harlow, D.G., Phoenix, S.L.,"The chain of bundles probability model for the strength of fibrous materials I: analysis ans conjecture", J. Comp. Mat., 1978, Vol. 12, pp. 195-214.

69. Harlow, D.G., Phoenix, S.L.,"The chain of bundles probability model for the strength of fibrous materials II: A numerical study of convergence", J. Comp. Mat., 1978, Vol. 12, pp. 314-334.

70. Harlow, D.G., Phoenix, S.L.,"Bounds on the probability of failure in composite materials", Int. J. of Fracture, 1979, Vol. 15, pp. 321-336.

71. Zweben, C., Rosen, B.W.,"A statistical theory of material strength with application to composite materials", J. mech. and Phys. of Solids, 1970, Vol. 18, pp. 189-206.

72. Batdorf, S.B.,"Failure statistics of unidirectional long-fiber composites", Probabilistic Methods in Mechanics of Solids and Structures, IUTAM Symposium, 1984, pp. 299-305.

73. Sundaresan, M.J., Henneke II, E.G.,"SEM observations of failure process in unidirectional composite materials", 9th Symposium on Composite Materials: Testing and Design, April 1988.

74. Highsmith, A. L., "Stiffness reduction from transverse cracking in fiber reinforced composite laminates", M.Sc. Thesis, College of Engineering, VPI & Su, 1981.